View metadata, citation and similar papers at core.ac.uk
brought to you by CORE
provided by ScholarBank@NUS

WIRELESS INFORMATION AND POWER TRANSFER: SYSTEM MODELING, PERFORMANCE ANALYSIS AND RESOURCE ALLOCATION OPTIMIZATION

ZHOU XUN

NATIONAL UNIVERSITY OF SINGAPORE

2015

WIRELESS INFORMATION AND POWER TRANSFER: SYSTEM MODELING, PERFORMANCE ANALYSIS AND RESOURCE ALLOCATION OPTIMIZATION

ZHOU XUN

(*B. Eng. University of Electronic Science and Technology of China*)

A THESIS SUBMITTED
FOR THE DEGREE OF DOCTOR OF PHILOSOPHY
DEPARTMENT OF ELECTRICAL AND COMPUTER ENGINEERING
NATIONAL UNIVERSITY OF SINGAPORE

2015

Declaration

I hereby declare that this thesis is my original work and it has been written by me in its entirety.

I have duly acknowledged all the sources of information which have been used in the thesis.

This thesis has also not been submitted for any degree in any university previously.

Zhou Xun

31 July 2015

To my dear parents and sister

Acknowledgements

I feel very fortunate to have the opportunity to work with and learn from so many outstanding people during my Ph.D. study in National University of Singapore. Foremost, I would like to thank my main supervisor Dr. Zhang Rui for his tremendous guidance, invaluable advices and intensive training during the past four years. Without him, this thesis would definitely not be possible. I have benefited enormously from his unique blend of solid knowledge on optimization, expertise on communications, technical insights, profound thinking and broad vision. Especially I want to thank him for his constructive criticism, which has helped me to improve exponentially on my research. His passion for doing great research inspires me to be a lifelong learner for pursuing the truth and beauty within the universe. I thank Dr. Ho Chin Keong for being a great co-supervisor as well as a sincere friend. I have benefited tremendously from his expertise on communication system, practical sensitivity and broad vision. I have learned a lot from the fruitful discussions with him. Especially I want to thank him for his encouragement and support.

I thank all the current and past group members, Liu Liang, Xu Jie, Zeng Yong, Bi Suzhi, Hyungsik Ju, Katayoun Rahbar, Mohammad Reza, Luo Shixin, Guo Yinghao, Seunghyun Lee, Zhang Shuowen, Reuben Stephen, Che Yueling, Nguyen Duy Hieu, Yang Gang, Yang Lu, Huang Chuan, and Xing Hong, for the stimulating discussions and sincere help. I also thank my colleagues in the communication lab, for all the happy tea-hours we spent together. I thank all my friends, for their love and support.

Last but most importantly, I would like to express my deepest gratefulness to my family: my parents, Zhang Jianglian and Zhou Jiawen, and my dear sister, Zhou Yun. They are the best hybrid access point, providing me unconditional love, emotional support and endless energy.

Table of Contents

Summary . . . . . **iv**

List of Tables . . . . . **vi**

List of Figures . . . . . **vii**

List of Abbreviations . . . . . **ix**

List of Symbols . . . . . **xi**

Chapter 1 Introduction **1**
1.1 Overview of Wireless Power Transfer 2
1.2 Simultaneous Wireless Information and Power Transfer (SWIPT) . . 3
1.2.1 Ideal Receiver 3
1.2.2 Practical Receivers 5
1.3 Wireless Powered Communication (WPC) 6
1.3.1 Basic Models 6
1.3.2 Harvest-then-transmit Protocol 7
1.4 Challenges and Motivations 9
1.5 Thesis Outline and Contributions 11
1.5.1 Thesis Outline 11
1.5.2 Major Contributions 12

Chapter 2 SWIPT: System Modeling and Performance Analysis . **15**
2.1 Introduction 15
2.2 System Modeling 16
2.2.1 Channel Model 16
2.2.2 Information Receiver 17
2.2.3 Energy Receiver 18
2.2.4 Performance Upper Bound 20
2.3 Receiver Architecture for SWIPT 21
2.3.1 Dynamic Power Splitting 21
2.3.2 Separated vs. Integrated Receivers 23
2.4 Performance Analysis for Separated Receiver 25
2.5 Performance Analysis for Integrated Receiver 28

2.6 Performance Analysis with Receiver Circuit Power Consumption . . . 35
2.6.1 Separated Receiver . . . 36
2.6.2 Integrated Receiver . . . 39
2.7 Practical Modulation . . . 41
2.8 Chapter Summary . . . 47

Chapter 3 SWIPT in Multiuser OFDM System . . . 48
3.1 Introduction . . . 48
3.2 Literature Review . . . 49
3.3 System Model and Problem Formulation . . . 50
3.3.1 Time Switching . . . 51
3.3.2 Power Splitting . . . 54
3.3.3 Performance Upper Bound . . . 56
3.4 Resource Allocation in Single-User System . . . 57
3.5 Resource Allocation in Multiuser System . . . 63
3.5.1 Time Switching . . . 63
3.5.2 Power Splitting . . . 70
3.5.3 Performance Comparison . . . 74
3.6 Chapter Summary . . . 78

Chapter 4 WPC in OFDM System . . . 79
4.1 Introduction . . . 79
4.2 Literature Review . . . 80
4.2.1 Protocol Design and Resource Allocation for WPC . . . 80
4.2.2 Wireless Communication Powered by Opportunistic Energy Harvesting . . . 81
4.3 System Model . . . 81
4.4 Problem Formulation . . . 84
4.5 Offline Algorithm for Joint Power and Sub-Channel Allocation . . . 86
4.5.1 Joint Power Allocation . . . 87
4.5.2 Sub-Channel Allocation . . . 95
4.6 Online Algorithm for Sub-Channel Allocation . . . 96
4.7 Numerical Example . . . 100
4.7.1 Offline Algorithms . . . 100
4.7.2 Online Algorithms . . . 103
4.8 Chapter Summary . . . 104

Chapter 5 Conclusion and Future Work . . . 106
5.1 Conclusion . . . 106
5.2 Future Work . . . 108

Appendix A Proof of Proposition 2.4.1 . . . 110

Appendix B Proof of Proposition 2.6.1 . . . 111

Appendix C Proof of Lemma 2.6.1 . . . 112

Appendix D Proof of Proposition 2.7.1 . . . . . **113**

Appendix E Proof of Lemma 3.5.1 . . . . . **114**

Appendix F Proof of Proposition 3.5.1 . . . . . **115**

Appendix G Proof of Proposition 4.5.1 . . . . . **116**

Appendix H Proof of Proposition 4.5.2 . . . . . **117**

Appendix I Proof of Proposition 4.5.3 . . . . . **118**

Appendix J Proof of Lemma 4.5.1 . . . . . **120**

Appendix K Proof of Lemma 4.5.2 . . . . . **121**

Appendix L Proof of Proposition 4.5.4 . . . . . **123**

Appendix M Proof of Lemma 4.5.3 . . . . . **125**

References **126**

List of Publications **131**

Summary

Radio frequency (RF) signals have been utilized as a vehicle for information transmission or wireless communication for decades. Meanwhile, the energy carried by RF signals can also be used to transfer power wirelessly. Wireless information and power transfer, with the aim to provide energy supply and data access to wireless users at the same time, has recently drawn significant interests. This thesis pursues a unified study on wireless information and power transfer, by investigating two main models for applications, namely, simultaneous wireless information and power transfer (SWIPT) using the same RF signals, as well as wireless powered communications (WPC) via RF energy harvesting (EH).

First, we present practical receiver designs for a point-to-point link, and analyze their various rate-energy performance trade-offs for SWIPT. We model the EH and information decoding (ID) processing at the receiver, and propose a novel integrated information and energy receiver for SWIPT, in which part of the EH and ID circuits are integrated. We characterize the performance and derive optimal operation strategies for the proposed receivers under both ideal assumption and practical consideration on circuit power consumption. Furthermore, the performance is evaluated for a system using practical modulation schemes.

Next, we study SWIPT in a multiuser broadcast channel using orthogonal frequency division multiplexing (OFDM), and design radio resource allocation schemes to achieve multiuser optimal rate-energy trade-offs. To coordinate the wireless information and energy transmissions to the multiple users and their receiver operations, we propose two schemes, namely, time division multiple access (TDMA) with time switching (TS) receivers and orthogonal frequency division multiple access

(OFDMA) with power splitting (PS) receivers. For both schemes, we study the problem of maximizing the weighted sum-rate over all users subject to the minimum harvested power constraint for each receiver as well as the peak and/or average power constraint at the transmitter.

Last, we study the optimal resource allocation for an OFDM-based WPC system, where wireless information and energy transmissions over finite time slots are jointly designed to maximize the throughput. The problem is investigated under two different assumptions on the availability of channel state information (CSI), namely, full CSI, with the knowledge of CSI for the past, present and future slots, and causal CSI, with the knowledge of CSI only for the past and present slots. With full CSI, the structure of the optimal resource allocation solution is derived and a close-to-optimal offline algorithm is proposed to obtain the performance. With causal CSI, we propose a low-complexity online algorithm for real-time implementation and compare its performance against that by the offline optimization.

List of Tables

3.1 Algorithm for solving Problem (P-TS). 69
3.2 Iterative algorithm for solving Problem (P-PS). 74

4.1 Algorithm for solving Problem (4.8) with given $\Pi(k), k \in \mathcal{K}$. 94

List of Figures

1.1 Energy receiver. 3
1.2 Architecture for SWIPT system. 4
1.3 Information receiver. 5
1.4 Separated information and energy receiver that employs TS and PS, respectively. 6
1.5 Architecture for WPC system: separated EAP/DAP and co-located EAP/DAP. 7
1.6 Harvest-then-transmit protocol. 8

2.1 A point-to-point SWIPT system. 16
2.2 Architecture for the separated information and energy receiver. 23
2.3 Architecture for the integrated information and energy receiver. . . . 24
2.4 Rate-energy trade-off for TS vs. PS based separated receiver with $h = 1, P = 100, \zeta = 1$ and $\sigma_{\mathrm{A}}^2 = 1$. 27
2.5 Capacity bounds for the channels (2.25), (2.26) and (2.29) with $h = 1, \sigma_{\mathrm{A}}^2 = 10^{-4}$ and $\sigma_{\mathrm{rec}} = 1$. 31
2.6 Rate-energy trade-off for separated receiver (SepRx) vs. integrated receiver (IntRx) with $h = 1, P = 100, \zeta = 0.6$, $\sigma_{\mathrm{A}}^2 = 1$ and $\sigma_{\mathrm{ADC}}^2 = 0$. . 33
2.7 Rate-energy trade-off for separated receiver (SepRx) vs. integrated receiver (IntRx) with $h = 1, P = 100, \zeta = 0.6$ and $\sigma_{\mathrm{A}}^2 = \sigma_{\mathrm{ADC}}^2 = 1$. . . 34
2.8 Rate-energy trade-off for the separated receiver with receiver circuit power consumption. It is assumed that $h = 1, P = 100, \zeta = 0.6, \sigma_{\mathrm{A}}^2 = 1, \sigma_{\mathrm{cov}}^2 = 10$ and $P_{\mathrm{S}} = 25$. 38
2.9 Rate-energy trade-off for separated receiver (SepRx) vs. integrated receiver (IntRx) with receiver circuit power consumption. It is assumed that $h = 1, P = 100, \zeta = 0.6, \sigma_{\mathrm{A}}^2 = 0.01, \sigma_{\mathrm{cov}}^2 = 1$ and $\sigma_{\mathrm{rec}} = 10$. 40
2.10 Maximum achievable rate for separated receiver (SepRx) and integrated receiver (IntRx) over different transmission distance. . . . 45
2.11 Optimal modulation size (M) and information receiver off-time percentage (α) for separated receiver (SepRx) and integrated receiver (IntRx). 46

3.1 Energy utilization at receivers for a two-user OFDM-based SWIPT system: TDMA-based information transmission with TS applied at each receiver. 53
3.2 Energy utilization at receivers for a two-user OFDM-based SWIPT system: OFDMA-based information transmission with PS applied at each receiver. 55
3.3 Achievable rate versus minimum required harvested energy in a single-user OFDM-based SWIPT system, where $N = 64$. 62
3.4 Achievable rate versus minimum required harvested energy in a single-carrier point-to-point SWIPT system, i.e., $N = 1$. 63
3.5 Achievable rates versus minimum required harvested energy in a multiuser OFDM-based SWIPT system, where $K = 4$, $N = 64$, and $P_{\text{peak}} \to \infty$. 75
3.6 Achievable rates versus minimum required harvested energy in a multiuser OFDM-based SWIPT system, where $K = 4$, $N = 64$, and $P_{\text{peak}} = 4P/N$. 76
3.7 Time ratio of the EH slot versus minimum required harvested energy for the TS scheme in Fig. 3.6. 77
3.8 Achievable rates versus number of users, where $P_{\text{peak}} = 4P/N$ and $\overline{E}_k = \overline{E} = 150\mu$W. 77

4.1 A WPC system with one user. 82
4.2 Energy utilization for the scheme of dynamic SC with OTT, where $K = 16, N = 4$ and $L = 5$. 99
4.3 Performance comparison for offline algorithms when full CSI is available. 101
4.4 Performance comparison for online algorithms when casual CSI is available, where $L = 15$. 102
4.5 Performance comparison for online algorithms when casual CSI is available, where $Q = 60$mW. 103

List of Abbreviations

ADC	Analog-to-Digital Converter
AWGN	Additive White Gaussian Noise
CSCG	Circularly Symmetric Complex Gaussian
CSI	Channel State Information
DAP	Data Access Point
DC	Direct Current
DL	Downlink
DPS	Dynamic Power Splitting
EAP	Energy Access Point
EH	Energy Harvesting
EM	Electromagnetic
HAP	Hybrid Access Point
ID	Information Decoding
KKT	Karush-Kuhn-Tucker
LP	Linear Programming
LPF	Low Pass Filter
LTE	Long Term Evolution
MCS	Modulation and Coding Scheme
OFDM	Orthogonal Frequency Division Multiplexing
OFDMA	Orthogonal Frequency Division Multiple Access
OPS	On-off Power Splitting
OTT	Observe-Then-Transmit
PEM	Pulse Energy Modulation

PS	Power Splitting
QAM	Quadrature Amplitude Modulation
R-E	Rate-Energy
RF	Radio Frequency
SC	Sub-Channel
SDMA	Space Division Multiple Access
SER	Symbol Error Rate
SNR	Signal-to-Noise Ratio
SQNR	Signal-to-Quantization-Noise Ratio
SWF	Staircase Water-Filling
SWIPT	Simultaneous Wireless Information and Power Transfer
TDMA	Time Division Multiple Access
TS	Time Switching
UL	Uplink
WF	Water-Filling
WIT	Wireless Information Transfer
WL	Water-Level
WPC	Wireless Powered Communication
WPT	Wireless Power Transfer

List of Symbols

$\lvert x \rvert$	the Absolute Value of x
$\mathbb{E}[x]$	the Statistical Expectation of Random Variable x
$\mathcal{N}(x, y)$	the Distribution of a Gaussian Random Variable with Mean x and Variance y
$\mathcal{CN}(x, y)$	the Distribution of a Circularly Symmetric Complex Gaussian (CSCG) Random Variable with Mean x and Variance y
$\sim$	"Distributed As"
$\Re\{x\}$	the Real Part of a Complex Number x
$\lvert \mathcal{A} \rvert$	the Cardinality of the Set $\mathcal{A}$
$\mathcal{A} \backslash \mathcal{B}$	the Set $\{x \lvert x \in \mathcal{A} \text{ and } x \notin \mathcal{B}\}$
$\mathcal{A}^{\mathrm{c}}$	the Complementary Set of Set $\mathcal{A}$
$\lfloor x \rfloor$	$\mathrm{floor}(x)$
$(x)^+$	$\max(0, x)$

Chapter 1

Introduction

Radio frequency (RF) signals have been widely used as a vehicle for wireless information transmission (WIT) since the first radio transmission demonstrated by Marconi in 1895. Recently, the advances in energy harvesting (EH) circuit design enable RF signals as a viable source for powering devices wirelessly. In contrast to conventional wireless networks, where nodes are powered by fixed energy sources, e.g., batteries, which have to be replaced or replenished manually after depletion, RF-enabled wireless power transfer (WPT) avoids the nuisance of battery replacement by providing perpetual energy supply. Accordingly, WPT is especially appealing for applications where wireless nodes are deployed in conditions that replacement of batteries is inconvenient (e.g., for numerous sensors in large-scale sensor networks, and for Internet of Things) or even infeasible (e.g., for implanted devices in human body).

Realizing both useful utilizations of RF signals, to provide both energy supply and data access to wireless devices could potentially provide great convenience to users. This thesis provides the unified study of the emerging field of joint wireless information and power transfer.

In this chapter, we first give an overview of WPT in Section 1.1. We then introduce SWIPT and WPC in Section 1.2 and Section 1.3, respectively. The challenges and motivations are presented in Section 1.4. Finally, we present the outline and contributions of this thesis in Section 1.5.

1.1 Overview of Wireless Power Transfer

WPT refers to the transmission of electrical power from an energy source to electrical loads without wire connections. In general, WPT technologies can be realized based on three different mechanisms, i.e., inductive coupling, magnetic resonant coupling, and electromagnetic (EM) radiation [1]. Both inductive coupling and magnetic resonant coupling are based on near-field coupling, where power is transfered via the magnetic field flow through coils that are located within close proximity of each other [2, 3]. In particular, magnetic resonant coupling achieves resonance between the coils by adding compensation capacitors in the system. The two near-field technologies enjoy high energy transmission efficiency. However, the operation distances are small. The inductive coupling operates within a few centimeters, while the magnetic coupling in general operates from several centimeters to a couple of meters. Therefore, the two technologies are limited to short-distance applications. In addition, it is challenging for the two technologies to supply power to an arbitrary number of distributed loads located over a large space simultaneously.

In contrast, WPT based on EM radiation, or RF-enabled WPT, exploits the far-field radiation property of EM wave, by which the EM field along with the RF signals is propagated through space where the energy can be harvested by remote devices by capturing the RF signals. In general, the RF-enabled WPT can support larger operation distances, from a few meters to tens of meters, depending on different receiver sensitivities. As reported by the Powercast Company, with transmission power of 3Watt (W), the receiver is able to harvest power of 159μW at distance of 5meters (m) [4]. In [5], with transmission power of 1.78W, the receiver harvests 2μW of power at distance of 27m. Furthermore, the broadcasting nature of RF signal enables powering a large number of distributed devices simultaneously, which makes it particularly suitable for applications such as wireless sensor networks or Internet of Things. We focus on the RF-enabled WPT in this thesis.

In RF-enabled WPT system, an energy transmitter, or energy access point (EAP), is deployed to broadcast RF signals to distributed users. In order to harvest

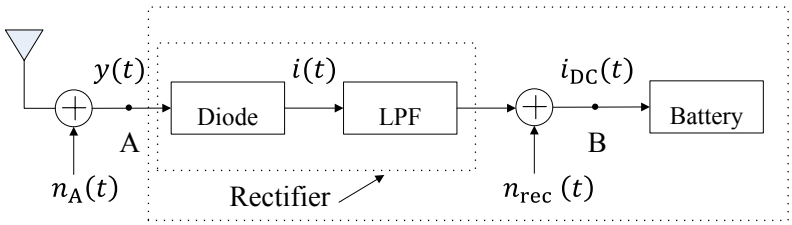

Figure 1.1: Energy receiver.

the energy carried by the RF signals, each user contains an energy receiver to perform EH, by which the received RF signals are converted to electrical power. Fig. 1.1 illustrates a typical RF energy receiver. As shown in Fig. 1.1, the received RF signal is converted to a direct current (DC) signal by a rectifier, which consists of a diode and a passive low-pass filter (LPF). The diode is typically a Schotty diode with low turn-on voltage. The DC signal is then used to charge the battery to store the energy.

1.2 Simultaneous Wireless Information and Power Transfer (SWIPT)

As RF signals can be utilized for both energy and information transmission, an interesting application is simultaneous wireless information and power transfer (SWIPT), which aims to provide WPT and WIT from the same RF signals. Fig. 1.2 illustrates the architecture for SWIPT system. As shown in Fig. 1.2, a hybrid access point (HAP) broadcasts RF signals to transfer both power and information to users. For SWIPT, both WPT and WIT is performed in the downlink (DL), i.e., in the transmission from the HAP to the users.

1.2.1 Ideal Receiver

In general, WPT and WIT pursue different objectives, which are to maximize the harvested energy and the information rate, respectively. This raises a

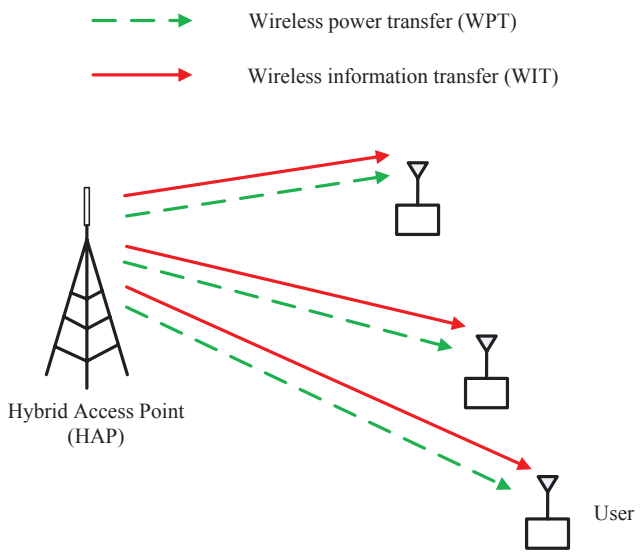

Figure 1.2: Architecture for SWIPT system.

fundamental question for SWIPT: Is there a trade-off between the energy and information transmissions?

The question is investigated by Varshney in his seminal work [6], where the idea of transmitting information and energy simultaneously is first proposed. In [6], a rate-energy (R-E) function is defined to characterize the fundamental performance trade-off for simultaneous information and power transfer. It is shown by [6] that for a point-to-point additive white Gaussian noise (AWGN) channel with amplitude-constrained input, there exists a non-trivial trade-off between the harvested energy and the achievable rate by optimizing the input distribution.

In [7], Grover and Sahai extend the work in [6] to frequency-selective channels with AWGN. Given total transmission power over all frequencies, the optimal transmission strategy for WPT is to "concentrate" all power to the frequency which achieves the maximum power efficiency; whereas the optimal strategy for WIT is to "spread" the power over frequency spectrum according to the water-filling (WF) function [8]. Clearly, a non-trivial trade-off exists for information transfer versus energy transfer via the power allocation over frequencies.

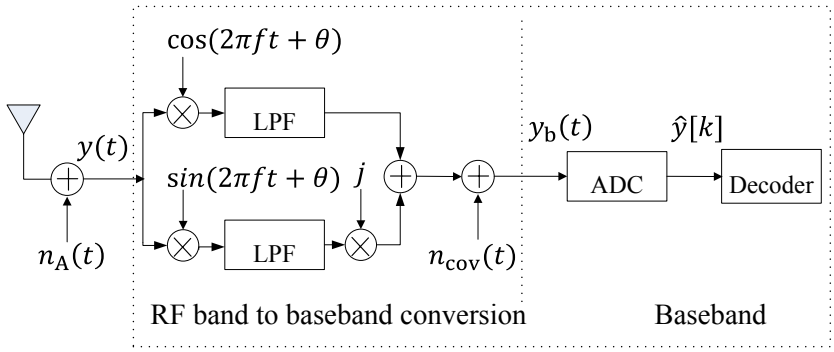

Figure 1.3: Information receiver.

1.2.2 Practical Receivers

One underlying assumption by the two works [6, 7] is that the receivers are able to observe and extract power simultaneously from the same received signal. However, this assumption may not hold in practice, as practical circuits for harvesting energy from radio signals are not yet able to decode the carried information directly. More precisely, consider Fig. 1.3 which illustrates the basic functional blocks of a typical information receiver. As shown in Fig. 1.3, the received RF signal is first converted to a baseband signal and then sampled and digitalized by an analog-to-digital converter (ADC) for further decoding. These operations for information decoding (ID) at the information receiver is very different from the operations for EH at the energy receiver shown in Fig. 1.1, which clearly is not able to decode the carried information by the signal directly. Due to this potential limitation, the results in [6, 7] actually provide only optimistic performance bounds.

In the pioneering work [9], Zhang and Ho propose a separated information and energy receiver for SWIPT based on two practical receiver operations, namely, time switching (TS) and power splitting (PS). For the TS scheme (see Fig. 1.4(a)), at any time the received signal is either connected to the information receiver or to the energy receiver. Hence, EH and ID are performed orthogonally in time. For the PS scheme (see Fig. 1.4(b)), the received signal is split into two streams with a fixed power ratio, which are used for EH and ID, respectively. By coordinating WIT and

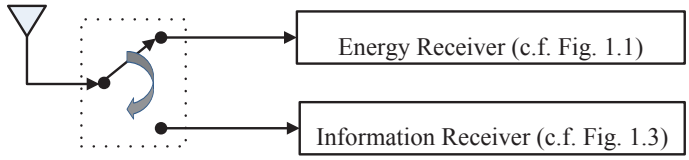

(a) Time switching (TS)

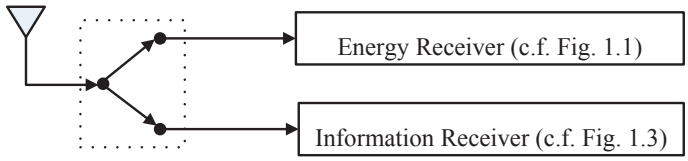

(b) Power splitting (PS)

Figure 1.4: Separated information and energy receiver that employs TS and PS, respectively.

WPT at the receiver side, the two schemes make SWIPT possible and feasible from an engineering perspective.

1.3 Wireless Powered Communication (WPC)

1.3.1 Basic Models

Fig. 1.5 illustrates the architecture for WPC system. As shown in Fig. 1.5, wireless users transmit information to a data access points (DAP) using the energy harvested from an EAP. Hence, WPT is performed at DL from EAP to users, whereas WIT is performed at uplink (UL) from users to DAP. In general, the DAP and EAP can be separately located in the network, referred to as the *separated EAP/DAP* case (see Fig. 1.5(a)). A pair of DAP and EAP also can be co-located as a HAP, providing the dual function of energy transfer and data access, which is referred to as the *co-located EAP/DAP* case (see Fig. 1.5(b)). In both cases, the channel state information (CSI) of WPT/WIT links is estimated at users and DAP, respectively, which are then sent to a central controller (located at EAP or DAP for example) for coordination of energy/information transmission. Separated EAP/DAP enjoys

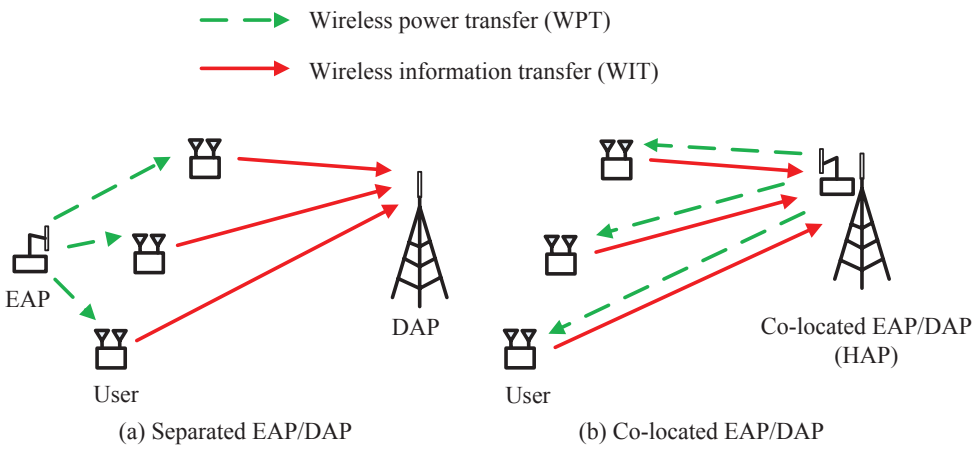

Figure 1.5: Architecture for WPC system: separated EAP/DAP and co-located EAP/DAP.

more flexibility in deployment of EAP/DAP; however, additional coordination and synchronization between the EAP and DAP is necessary. Co-located EAP/DAP is advantageous in information sharing (e.g., the channel estimation is simplified when UL/DL channel reciprocity applies) and hardware reuse (e.g., computational units). However, due to the same operation distance of WPT and WIT for the co-located EAP/DAP case, the users far away from the HAP achieve low throughput, since higher transmission power needs to be consumed at these users yet with lower harvested energy, which is observed as a *doubly near-far* phenomenon in [10].

1.3.2 Harvest-then-transmit Protocol

For WPC systems, the DL WPT and UL WIT are coupled together due to the energy constraint that the transmission energy available for UL WIT is constrained by the amount of harvested energy from DL WPT. Therefore, a major challenge for WPC is how to jointly design the transmission strategy for DL WPT and UL WIT.

To coordinate the DL WPT and UL WIT, a harvest-then-transmit protocol is proposed in [10] for the WPC system with co-located EAP/DAP as shown in Fig. 1.5(b), where a single-antenna HAP provides both energy transmission and data

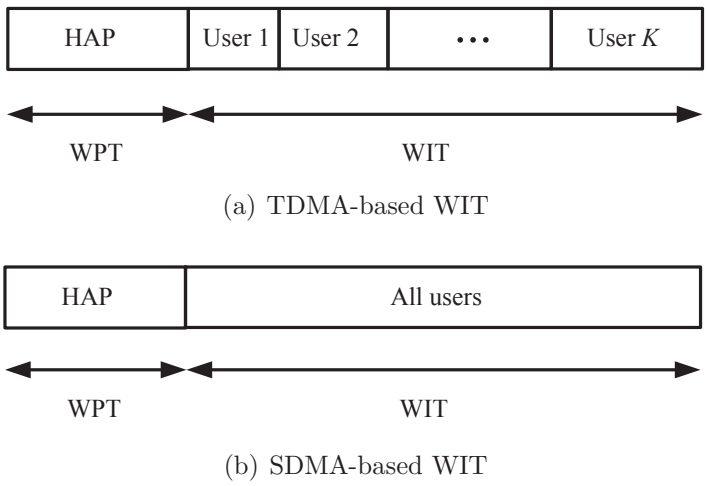

Figure 1.6: Harvest-then-transmit protocol.

access to multiple users. As shown in Fig. 1.6(a), the harvest-then-transmit protocol divides the transmission into two phases: the DL WPT is performed during the first phase, where all users harvest energy from the received signal broadcasted by the HAP; the UL WIT is performed during the second phase, where each user transmits independent information to the HAP using the energy harvested during the first phase. In particular, the time division multiple access (TDMA) scheme is assumed in [10] for the UL WIT among multiple users. Clearly, the transmission time allocated for the DL WPT and UL WIT at each user needs to be jointly optimized to maximize the sum-throughput for the UL WIT. To tackle the doubly near-far phenomenon, [10] further introduces an additional constraint that all users are allocated with the same rate, by which the fairness among all users are guaranteed.

The work [10] is extended in [11] by employing a multi-antenna HAP. In contrast to [10], during the second phase for uplink WIT, all users simultaneously transmit independent information to the HAP by the space division multiple access (SDMA) scheme (see Fig. 1.6(b)). To overcome the doubly near-far phenomenon, [11] proposes to use the minimum throughput of all users as the performance metric, with which the transmission time allocated for DL WPT and UL WIT, the energy beamforming for DL WPT, the power allocation and receive beamforming for UL

WIT are jointly optimized.

1.4 Challenges and Motivations

1. Receiver Design for SWIPT

For the SWIPT system in Fig. 1.2, one major challenge is the receiver design to trade-off between WIT and WPT. The separated receiver in Fig. 1.4 uses the conventional information receiver and energy receiver, which are designed for solely WIT and WPT, respectively. Under the context of SWIPT, the design may not be optimal due to the following reasons.

- WIT and WPT operate with very different power sensitivity at the receiver (e.g., -10dBm for energy receivers versus -60dBm for information receivers). Thus, for SWIPT systems that involve both WIT and WPT, the receiver design should be optimized for WPT as a first priority.
- Circuit power consumed by ID is a significant design issue for SWIPT, since the circuit power reduces the net harvested energy that can be stored in the battery for future use. In particular, the active mixers used in conventional information receiver for RF to baseband conversion are substantially power-consuming. The receiver will consume less power by avoiding the use of active devices.

It thus motivates us to consider a new receiver design for SWIPT system that considers WPT as a first priority and avoids the use of energy-hungry active components as much as possible.

2. Resource Allocation for SWIPT and WPC in OFDM System

In practice, wireless transmissions typically experience multipath propagation, especially in indoor environments, which results in frequency-selective channels. The inter-symbol interference caused by the frequency-selective fading becomes a severe issue. Based on multi-carrier modulation, the orthogonal frequency division

multiplexing (OFDM) technique breaks the data stream into lower-rate substreams modulated onto narrowband flat-fading sub-channels (SCs). As a result, the inter-symbol interference on each SC is less severe. Besides robustness against frequency-selective fading, OFDM is appealing for its efficient implementation by fast Fourier transform. Enjoying these key advantages, OFDM is suitable for high-rate wireless communications, and has been adopted in various standards, e.g., IEEE 802.11n and Long Term Evolution (LTE) Advanced. Nevertheless, the performance may be limited by the availability of energy in the devices for some energy-constrained application scenarios, e.g., sensor networks. Employing WPT to supply OFDM users thus becomes appealing.

Moreover, in wireless communication systems, multiple users co-exist to share the wireless medium. Since the broadcast nature of wireless power allows multiple users to harvest the energy concurrently, it is critical to consider the problem of how users share the wireless resources for WPT as well as for WIT.

To be concrete, consider for illustration the OFDM-based multiuser SWIPT system in Fig. 1.2, where the HAP broadcasts RF signals that carry both information and energy to multiple OFDM users. In addition to the coordination for the information transmission between multiple users as considered in conventional wireless communication system, the receiver operations need to be designed to coordinate the EH and ID processing to fulfill the requirements on both data rate and harvested energy. The two-fold coordination inevitably introduces a non-trivial trade-off for the R-E performance that is not yet studied. It is thus important to study jointly optimal resource allocation and receiver strategies to achieve the optimal system performance.

To shed further light on the interesting trade-off for R-E peformance, consider the OFDM-based WPC system in Fig. 1.5, where one OFDM user harvests energy from the EAP to supply its information transmission to the DAP within finite time slots. Since the information transmission is supplied by the harvested energy via energy transmission, the total energy consumed for information transmission until

any given time cannot be greater than the total harvested energy at the same time, which is referred to as the energy causality constraint. This inevitably introduces a trade-off for the energy and information scheduling by resource allocation for the WPT and WIT links.

1.5 Thesis Outline and Contributions

1.5.1 Thesis Outline

The rest of the thesis is organized as follows.

Chapter 2 investigates practical receiver designs for the SWIPT system. We first mathematically model the EH and ID processing at the receiver based on circuit analysis. We then propose a receiver operation, as a generalization of the TS and PS schemes, based on which we further propose a new receiver architecture, namely, the integrated information and energy receiver, in which we integrate part of the EH and ID circuits. We derive the equivalent information channel model for the proposed receiver. The performance of the proposed receiver is analyzed and compared to the separated ID/EH receiver under both ideal and practical circuit power consumption. In addition, the performance is analyzed under a realistic system setup that employs practical modulation.

Chapter 3 studies the optimal resource allocation for SWIPT in a multiuser OFDM system. We propose two schemes to coordinate the wireless information and energy transmissions, namely, TDMA with TS receivers and orthogonal frequency division multiple access (OFDMA) with PS receivers. For both TS and PS schemes, we solve the problem of maximizing the weighted sum-rate over all users by jointly optimizing the time/frequency power allocation and either TS or PS ratio, subject to a minimum harvested energy constraint on each user as well as a peak and/or total transmission power constraint. The performance of the two schemes are analyzed and compared.

Chapter 4 studies the optimal scheduling and resource allocation for WPC

for a single user OFDM system. The DL WPT and UL WIT are performed simultaneously in time but orthogonally over separate SCs to avoid interference to the WIT. With the objective of maximizing the achievable rate for the UL WIT, we jointly optimize the SC allocation over time and the power allocation over time and SCs for both WPT/WIT links. Offline and online algorithms are proposed to solve the problem assuming availability of full CSI and causal CSI, respectively.

1.5.2 Major Contributions

The major contributions of this thesis are summarized as follows.

1. In-depth System Modeling for SWIPT (Chapter 2)

In Chapter 2, we systematically model the EH and ID processing at the receiver deeply rooted on circuit analysis. Our modeling bridges the information theoretical analysis and RF circuit design, and provides a fundamental basis for practical receiver designs for SWIPT.

2. A Novel Receiver Design for SWIPT (Chapter 2)

In Chapter 2, we propose a novel receiver for SWIPT, namely, the integrated information and energy receiver, in which part of the front-end components of conventional information and energy receivers are integrated. In this architecture, the active RF band to baseband conversion in conventional ID circuits is replaced by a passive rectifier operation, which is conventionally used only for EH. By providing a dual use of the rectifier, the energy cost for ID is reduced significantly. We demonstrate that under practical setups, the integrated receiver is superior as compared to the conventional separated ID/EH receiver at short transmission distances, which is the range that SWIPT systems usually operate in.

3. Useful Insights to the Design of Multiuser SWIPT System

For the resource allocation in multiuser OFDM-based SWIPT system, both TS and PS schemes lead to non-convex optimization problems, which are difficult

to solve directly. However, the two problems are efficiently solved by appropriate problem reformulation and iterative optimization, respectively. Our results provide useful insights to the design of practical OFDM-based SWIPT system.

- Joint design for the resource allocation (power, bandwidth, time, etc.) and receiver strategy (TS/PS ratios) is essential to achieve near-optimal performance in SWIPT system.
- The peak power constraint imposed on each OFDM SC as well as the number of users in the system play key roles in the R-E performance comparison.
- The TS receiver outperforms the PS receiver for a moderate EH requirement at users.

4. Key Principles to the Design of WPC System

For the OFDM-based WPC system, we derive the optimal structure of the resource allocation given full CSI, based on which offline and online algorithms are proposed. We demonstrate the superiority of WPC with dedicated wireless power over the conventional EH wireless communication. Our results provide key principles to the design of OFDM-based WPC system.

- Joint resource allocation (power, bandwidth, time, etc.) for both WPT and WIT links is necessary to achieve optimal performance by balancing the energy supply and consumption at users. This is in contrast to conventional EH wireless communication, where the design principle is to adapt the information transmission to the EH dynamics and the channel of the WIT links.
- Energy transmission should occur sparsely in frequency on certain SCs, and in time on certain slots. First, if energy transmission is performed on one slot, then the power should be concentrated on one SC. Second, when full CSI is available, energy transmissions may occur only during the so-called causally dominating slots. We say a slot is causally dominating if the slot has a larger channel power gain on the allocated SC than any of its previous slots.

- For optimal performance, higher priority is placed for WPT link as compared to WIT link. For the orthogonal SC allocation to WPT and WIT, more priority should be given to WPT. When only causal CSI is available, even utilizing partial information of the channels for the WPT link can be much beneficial to the communication performance.

Chapter 2

SWIPT: System Modeling and Performance Analysis

2.1 Introduction

In this chapter, we study practical receiver designs for a point-to-point wireless link with SWIPT. We generalize the TS and PS schemes proposed in [9] to a general receiver operation scheme, namely, *dynamic power splitting* (DPS), by which the signal is dynamically split into two streams with arbitrary power ratio over time. Besides TS and PS, another special case of the DPS scheme, namely, *on-off power splitting* (OPS) is also investigated. Employing DPS, we propose an *integrated* receiver architecture, in which we integrate the ID and the EH circuits. In this architecture, the active RF band to baseband conversion in conventional ID is replaced by a passive rectifier operation, which is conventionally used only for EH. By providing a dual use of the rectifier, the energy cost for ID is reduced significantly. The R-E performances for both conventional separated receiver in Fig. 1.4 and the proposed integrated receiver are further characterized. With receiver circuit power consumption taken into account, it is shown that the OPS scheme is optimal for both receivers. For the ideal case when the consumed power at the receiver is negligible, the PS scheme is optimal for both receivers. Finally, the performance for the two receivers are compared under a realistic system setup that employs practical modulation. The results show that for a self-sustainable system with zero-net-energy consumption, the integrated receiver achieves more rate than separated receiver at sufficiently short transmission distance.

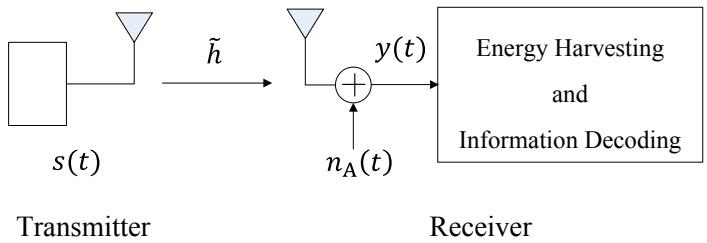

Figure 2.1: A point-to-point SWIPT system.

The rest of this chapter is organized as follows. Section 2.2 presents the system modeling. Section 2.3 presents the two receiver architectures. Section 2.4 and Section 2.5 study the rate-energy performance for the separated and integrated receivers, respectively. Section 2.6 extends the results in Sections 2.4 and 2.5 to the case with receiver circuit power taken into consideration. Section 2.7 studies the performance for the two types of receivers under a realistic system setup. Finally, Section 2.8 summarizes the conclusion.

2.2 System Modeling

2.2.1 Channel Model

As shown in Fig. 2.1, in this chapter we study a point-to-point wireless link with simultaneous information and power transfer. Both the transmitter and receiver are equipped with one antenna. At the transmitter, the complex baseband signal is expressed as $x(t) = A(t)e^{j\phi(t)}$, where $A(t)$ and $\phi(t)$ denote the amplitude and the phase of $x(t)$, respectively. It is assumed that $x(t)$ is a narrow-band signal with bandwidth of B Hz, and $\mathbb{E}[|x(t)|^2] = 1$, where $\mathbb{E}[\cdot]$ and $|\cdot|$ denote the statistical expectation and the absolute value, respectively. The transmitted RF band signal is then given by $s(t) = \sqrt{2P}A(t)\cos(2\pi ft + \phi(t)) = \sqrt{2P}\Re\{x(t)e^{j2\pi ft}\}$, where P is the average transmit power, i.e., $\mathbb{E}[s^2(t)] = P$, f is the carrier frequency, and $\Re\{\cdot\}$ denotes the real part of a complex number. It is assumed that $B \ll f$.

The transmitted signal propagates through a wireless channel with channel

gain $h > 0$ and phase shift $\theta \in [0, 2\pi)$. The equivalent complex channel is denoted by $\tilde{h} = \sqrt{h}e^{j\theta}$. The noise $n_{\mathrm{A}}(t)$ after the receiving antenna[1] can be modeled as a narrow-band Gaussian noise (with bandwidth B and center frequency f), i.e., $n_{\mathrm{A}}(t) = \sqrt{2}\Re\{\tilde{n}_{\mathrm{A}}(t)e^{j2\pi ft}\}$, where $\tilde{n}_{\mathrm{A}}(t) = n_{\mathrm{I}}(t) + jn_{\mathrm{Q}}(t)$ with $n_{\mathrm{I}}(t)$ and $n_{\mathrm{Q}}(t)$ denoting the in-phase and quadrature noise components, respectively. We assume that $n_{\mathrm{I}}(t)$ and $n_{\mathrm{Q}}(t)$ are independent Gaussian random variables with zero mean and variance $\sigma_{\mathrm{A}}^2/2$, denoted by $\mathcal{N}(0, \sigma_{\mathrm{A}}^2/2)$, where $\sigma_{\mathrm{A}}^2 = N_0 B$, and N_0 is the one-sided noise power spectral density. Thus, we have $\tilde{n}_{\mathrm{A}}(t) \sim \mathcal{CN}(0, \sigma_{\mathrm{A}}^2)$, i.e., $\tilde{n}_{\mathrm{A}}(t)$ is a circularly symmetric complex Gaussian (CSCG) random variable with zero mean and variance σ_{A}^2. Corrupted by the antenna noise, the received signal $y(t)$ is given by $y(t) = \sqrt{2}\Re\{\tilde{y}(t)\}$, where the complex signal $\tilde{y}(t)$ is

$$\tilde{y}(t) = \sqrt{hP}x(t)e^{j(2\pi ft+\theta)} + \tilde{n}_{\mathrm{A}}(t)e^{j2\pi ft}. \tag{2.1}$$

2.2.2 Information Receiver

First, we consider the case where the receiver shown in Fig. 2.1 is solely an information receiver (see Fig. 1.3). We assume coherent demodulation (assuming that the channel phase shift θ is perfectly known at the receiver) at the information receiver. The received RF band signal $y(t)$ is first converted to a complex baseband signal $y_{\mathrm{b}}(t)$ and then sampled and digitalized by an ADC for further decoding. The noise introduced by the RF band to baseband signal conversion is denoted by $n_{\mathrm{cov}}(t)$ with $n_{\mathrm{cov}}(t) \sim \mathcal{CN}(0, \sigma_{\mathrm{cov}}^2)$. For simplicity, we assume an ideal ADC with zero noise[2]. The discrete-time ADC output is then given by

$$\hat{y}[k] = \sqrt{hP}x[k] + \tilde{n}_{\mathrm{A}}[k] + n_{\mathrm{cov}}[k] \tag{2.2}$$

where $k = 1, 2, \ldots$, denotes the symbol index.

It follows from (2.2) that the equivalent baseband channel for wireless

[1]The antenna noise may include thermal noise from the transmitter and receiver chains.
[2]The general case with nonzero ADC noise is considered in Remark 2.5.1.

information transmission is the well-known AWGN channel:

$$Y = \sqrt{hP}X + Z \tag{2.3}$$

where X and Y denote the channel input and output, respectively, and $Z \sim \mathcal{CN}(0, \sigma_{\mathrm{A}}^2 + \sigma_{\mathrm{cov}}^2)$ denotes the complex Gaussian noise (assuming independent $\tilde{n}_{\mathrm{A}}(t)$ and $n_{\mathrm{cov}}(t)$). When the channel input is distributed as $X \sim \mathcal{CN}(0, 1)$, the maximum achievable information rate (in bps/Hz) or the capacity of the AWGN channel is given by [12]

$$R = \log_2 \left(1 + \frac{hP}{\sigma_{\mathrm{A}}^2 + \sigma_{\mathrm{cov}}^2} \right). \tag{2.4}$$

2.2.3 Energy Receiver

Next, we consider the case where the receiver in Fig. 2.1 is solely an energy receiver (see Fig. 1.1), and derive the average wireless power that can be harvested from the received signal. The energy receiver in Fig. 1.1 converts RF energy directly via a *rectenna* architecture [13]. In the rectenna, the received RF band signal $y(t)$ is converted to a DC signal $i_{\mathrm{DC}}(t)$ by a rectifier, which consists of a Schottky diode and a LPF. The DC signal $i_{\mathrm{DC}}(t)$ is then used to charge the battery to store the energy. With an input voltage proportional to $y(t)$, the output current $i(t)$ of a Schottky diode is given by [14]:

$$i(t) = I_s \left(e^{\gamma y(t)} - 1 \right) = a_1 y(t) + a_2 y^2(t) + a_3 y^3(t) + \cdots \tag{2.5}$$

where I_s denotes the saturation current, γ denotes the reciprocal of the thermal voltage of the Schottky diode, and the coefficients a_n's are given by $a_n = I_s \gamma^n / n!, n = 1, 2, \ldots$, due to the Taylor series expansion of the exponential function.

From (2.1), for convenience we re-express $y(t)$ as follows:

$$\begin{aligned} y(t) &= \sqrt{2}\Re\{\sqrt{hP}x(t)e^{j(2\pi ft+\theta)} + \tilde{n}_{\mathrm{A}}(t)e^{j2\pi ft}\} \\ &= \sqrt{2}\mu_{\mathrm{Y}}(t)\cos\left(2\pi ft + \phi_{\mathrm{Y}}(t)\right) \end{aligned} \tag{2.6}$$

where $\phi_{\mathrm{Y}}(t) = \arctan\frac{\mu_{\mathrm{Q}}(t)}{\mu_{\mathrm{I}}(t)}$ and

$$\mu_{\mathrm{Y}}(t) = \sqrt{\mu_{\mathrm{I}}^2(t) + \mu_{\mathrm{Q}}^2(t)} \tag{2.7}$$

with

$$\mu_{\mathrm{I}}(t) = \sqrt{hP}A(t)\cos\left(\phi(t)+\theta\right) + n_{\mathrm{I}}(t) \tag{2.8}$$

$$\mu_{\mathrm{Q}}(t) = \sqrt{hP}A(t)\sin\left(\phi(t)+\theta\right) + n_{\mathrm{Q}}(t). \tag{2.9}$$

By substituting (2.6) into (2.5) and ignoring the higher-order (larger than two) terms of $y(t)$, since $\gamma y(t)$ is practically a small number close to zero, we obtain

$$\begin{aligned} i(t) &\approx \sqrt{2}a_1\mu_{\mathrm{Y}}(t)\cos\left(2\pi ft + \phi_{\mathrm{Y}}(t)\right) + 2a_2\mu_{\mathrm{Y}}^2(t)\cos^2\left(2\pi ft + \phi_{\mathrm{Y}}(t)\right) \\ &= a_2\mu_{\mathrm{Y}}^2(t) + \sqrt{2}a_1\mu_{\mathrm{Y}}(t)\cos\left(2\pi ft + \phi_{\mathrm{Y}}(t)\right) + a_2\mu_{\mathrm{Y}}^2(t)\cos\left(4\pi ft + 2\phi_{\mathrm{Y}}(t)\right). \end{aligned} \tag{2.10}$$

The output current $i(t)$ of the diode is processed by a LPF, through which the high-frequency harmonic components at both f and $2f$ in $i(t)$ are removed and a DC signal $i_{\mathrm{DC}}(t)$ appears as the output of the rectifier. Assuming that the additive noise introduced by the rectifier is $n_{\mathrm{rec}}(t)$, the filtered output $i_{\mathrm{DC}}(t)$ is thus given by

$$i_{\mathrm{DC}}(t) = a_2\mu_{\mathrm{Y}}^2(t) + n_{\mathrm{rec}}(t). \tag{2.11}$$

Since a_2 is a constant specified by the diode, for convenience we assume in the sequel that $a_2 = 1$ (with $n_{\mathrm{rec}}(t)$ normalized accordingly to maintain the signal-to-noise ratio (SNR)). Note that in (2.11), a_2 involves unit conversion from a power signal to a

current signal, thus by normalization $n_{\rm rec}(t)$ can be equivalently viewed as a power signal. Assume $n_{\rm rec}(t) \sim \mathcal{N}(0, \sigma_{\rm rec}^2)$, where $\sigma_{\rm rec}$ is in watt. Substituting (2.7), (2.8) and (2.9) into (2.11) yields

$$\begin{aligned} i_{\rm DC}(t) =& \Big(\sqrt{hP}A(t)\cos\left(\phi(t)+\theta\right) + n_{\rm I}(t)\Big)^2 \\ &+ \Big(\sqrt{hP}A(t)\sin\left(\phi(t)+\theta\right) + n_{\rm Q}(t)\Big)^2 + n_{\rm rec}(t). \end{aligned} \tag{2.12}$$

We assume that the converted energy to be stored in the battery is linearly proportional to $i_{\rm DC}(t)$ [15], with a conversion efficiency $0 < \zeta \leq 1$. We also assume that the harvested energy due to the noise (including both the antenna noise and the rectifier noise) is a small constant and thus ignored. Hence, the harvested energy (assuming the symbol period to be one) stored in the battery, denoted by Q in joule, is given by[3]

$$Q = \zeta \mathbb{E}[i_{\rm DC}(t)] = \zeta hP. \tag{2.13}$$

2.2.4 Performance Upper Bound

Now consider the general case of interest where both information decoding and energy harvesting are jointly implemented at the receiver, as shown in Fig. 2.1. Our main objective is to maximize both the decoded information rate R and harvested energy Q from the same received signal $y(t)$. Based on the results in the previous two subsections, we derive an upper bound for the performance of any practical receiver with the joint operation of information decoding and energy harvesting, as follows. For information transfer, according to the data-processing inequality [12], with a given antenna noise $\tilde{n}_{\rm A}(t) \sim \mathcal{CN}(0, \sigma_{\rm A}^2)$, the maximum information rate R that can be reliably decoded at the receiver is upper-bounded by $R \leq \log_2(1 + hP/\sigma_{\rm A}^2)$. Note that state-of-the-art wireless information receivers are not yet able to achieve this rate upper bound due to additional processing noise such as the RF band to baseband

[3]For convenience, in the sequel, the two terms "energy" and "power" may be used interchangeably by assuming the symbol period to be one.

conversion noise $n_{\text{cov}}(t)$, as shown in (2.4). On the other hand, for energy transfer, according to the law of energy conservation, the maximum harvested energy Q to be stored in the battery cannot be larger than that received by the receiving antenna, i.e., $Q \leq hP$. Note that practical energy receivers cannot achieve this upper bound unless the energy conversion efficiency ζ is made ideally equal to unity, as suggested by (2.13). Following the definition of R-E region given in [6, 7, 9] to characterize all the achievable rate (in bps/Hz for information transfer) and energy (in joules/sec for energy transfer) pairs under a given transmit power constraint P, we obtain a performance upper bound on the achievable R-E region for the system in Fig. 2.1 as

$$\mathcal{C}_{\text{R-E}}^{\text{UB}}(P) \triangleq \left\{(R, Q) : R \leq \log_2\left(1 + \frac{hP}{\sigma_{\text{A}}^2}\right), Q \leq hP\right\} \tag{2.14}$$

which is a box specified by the origin and the three vertices $(0, Q_{\max})$, $(R_{\max}, 0)$ and $(R_{\max}, Q_{\max})$, with $Q_{\max} = hP$ and $R_{\max} = \log_2(1 + hP/\sigma_{\text{A}}^2)$. This performance bound is valid for all receiver architectures, some of which will be studied next.

2.3 Receiver Architecture for SWIPT

This section considers practical receiver designs for simultaneous wireless information and power transfer. We propose a general receiver operation called *dynamic power splitting* (DPS), from which we propose the *integrated* information and energy receiver.

2.3.1 Dynamic Power Splitting

Currently, practical circuits for harvesting energy from radio signals are not yet able to decode the carried information directly. In other words, the signal that is used for harvesting energy cannot be reused for decoding information. Due to this potential limitation, we propose a practical DPS scheme to enable the receiver to harvest energy and decode information from the same received signal at any time t, by dynamically splitting the signal into two streams with the power ratio

$\rho(t) : 1 - \rho(t)$, which are used for harvesting energy and decoding information, respectively, where $0 \leq \rho(t) \leq 1$.

Consider a block-based transmission of duration T with $T = NT_{\mathrm{s}}$, where N denotes the number of transmitted symbols per block and T_{s} denotes the symbol period. We assume that $\rho(t) = \rho_k$ for any symbol interval $t \in [(k-1)T_{\mathrm{s}}, kT_{\mathrm{s}}), k = 1, \ldots, N$. For convenience, we define a power splitting vector as $\boldsymbol{\rho} = [\rho_1, \ldots, \rho_N]^T$. In addition, we assume an ideal power splitter [16, 17] at the receiver without any power loss or noise introduced, and that the receiver can perfectly synchronize its operations with the transmitter based on a given vector $\boldsymbol{\rho}$. During the transmission block time T, it is assumed that the information receiver may operate in two modes: switch off (off mode) for a time duration T_{off} to save power, or switch on (on mode) for a time duration $T_{\mathrm{on}} = T - T_{\mathrm{off}}$ to decode information. The percentage of time that the information decoder operates in off mode is denoted by α with $0 \leq \alpha \leq 1$, thus we have $T_{\mathrm{off}} = \alpha T$ and $T_{\mathrm{on}} = (1-\alpha)T$. Without loss of generality, we assume that the information receiver operates in off mode during the first $\lfloor \alpha N \rfloor$ symbols during each block with $k = 1, \ldots, \lfloor \alpha N \rfloor$, where $\lfloor \cdot \rfloor$ denotes the floor operation, while in on mode during the remaining symbols with $k = \lfloor \alpha N \rfloor + 1, \ldots, N$. For convenience, we also assume in the sequel that αN is a positive integer regardless of the value of α, which is approximately true if N is chosen to be a very large number in practice.

Next, we investigate three special cases of DPS, namely TS, PS and *on-off power splitting* (OPS) given in [9]:

- *TS*: With TS, for the first αN symbols when the information receiver operates in off mode, all signal power is used for energy harvesting. For the remaining $(1-\alpha)N$ symbols when the information receiver operates in on mode, all signal power is used for information decoding. Thus for TS, we have

$$\rho_k = \begin{cases} 1, & k = 1, \ldots, \alpha N \\ 0, & k = \alpha N + 1, \ldots, N. \end{cases} \tag{2.15}$$

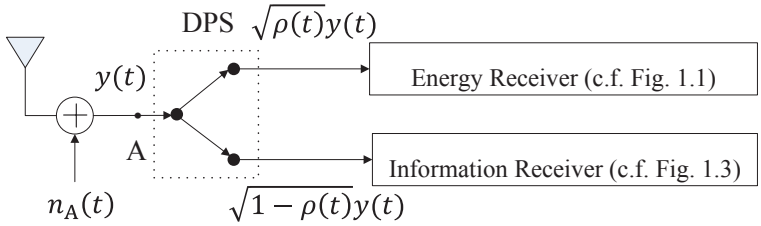

Figure 2.2: Architecture for the separated information and energy receiver.

- *PS*: With PS, the information receiver operates in on mode for all N symbols, i.e., $\alpha = 0$. Moreover, the ratio of the split signal power for harvesting energy and decoding information is set to be a constant ρ for all N symbols. Thus for PS, we have

$$\rho_k = \rho, \ k = 1, \ldots, N. \tag{2.16}$$

- *On-off power splitting (OPS)*: With OPS, for the first αN symbols all signal power is used for energy harvesting. For the remaining $(1-\alpha)N$ symbols, the ratio of the split signal power for harvesting energy and decoding information is set to be a constant ρ, with $0 \leq \rho < 1$. Thus, for a given power splitting pair (α, ρ), we have

$$\rho_k = \begin{cases} 1, & k = 1, \ldots, \alpha N \\ \rho, & k = \alpha N + 1, \ldots, N. \end{cases} \tag{2.17}$$

  Note that TS and PS are two special cases of OPS by letting $\rho = 0$ (for TS) or $\alpha = 0$ (for PS) in (2.17).

2.3.2 Separated vs. Integrated Receivers

In this subsection, we investigate two types of receivers that exploit the DPS scheme in different ways. The first type of receivers is called *separated* information and energy receiver [9], as shown in Fig. 2.2, while the second type is called *integrated*

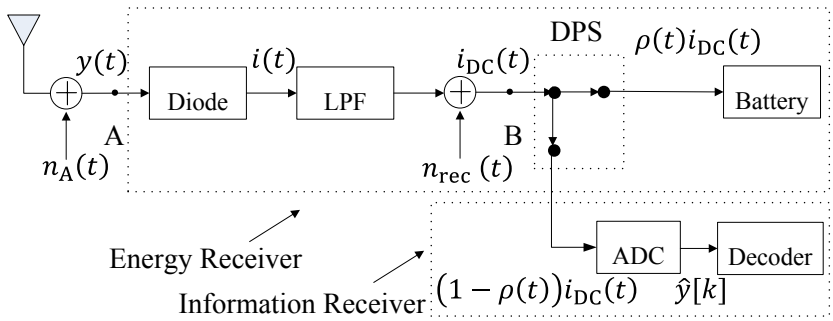

Figure 2.3: Architecture for the integrated information and energy receiver.

information and energy receiver, as shown in Fig. 2.3. These two types of receivers both use the energy receiver in Fig. 1.1 for energy harvesting. Their difference lies in that for the case of separated receiver, the power splitter for DPS is inserted at point 'A' in the RF band of the energy receiver shown in Fig. 1.1, while in the case of integrated receiver, the power splitter is inserted at point 'B' in the baseband.

First, we consider the case of separated information and energy receiver. As shown in Fig. 2.2, a power splitter is inserted at point 'A', such that the received signal $y(t)$ by the antenna is split into two signal streams with power levels specified by $\rho(t)$ in the RF band, which are then separately fed to the conventional energy receiver (cf. Fig. 1.1) and information receiver (cf. Fig. 1.3) for harvesting energy and decoding information, respectively. The achievable R-E region for this type of receivers with DPS will be studied in Section 2.4.

Next, we consider the integrated information and energy receiver, as motivated by the following key observation. Since the transmitted power in a wireless power transfer system can be varied over time provided that the average power delivered to the receiver is above a certain required target, we can encode information in the energy signal by varying its power levels over time, thus achieving continuous information transfer without degrading the power transfer efficiency. To emphasize this dual use of signal power in both WPT as well as WIT, the modulation scheme is called *energy modulation*. A constellation example, namely, *pulse energy modulation* (PEM), is provided later in Section 2.7. Note that to decode the energy modulated

information at the receiver, we need to detect the power variation in the received signal within a certain accuracy, by applying techniques such as *energy detection* [18]. Recall that in Section 2.2.3, for the energy receiver in Fig. 1.1, the received RF signal $y(t)$ is converted to a DC signal $i_{\mathrm{DC}}(t)$ given in (2.12) by a rectifier. Note that this RF to DC conversion is analogous to the RF band to baseband conversion in conventional wireless information receivers in Fig. 1.3. Thus, $i_{\mathrm{DC}}(t)$ can be treated as a baseband signal for information decoding (via energy detection).

Based on the above observation, we propose the integrated information and energy receiver as shown in Fig. 2.3, by inserting a power splitter at point 'B' of the conventional energy receiver. With DPS, $i_{\mathrm{DC}}(t)$ is split into two portions specified by $\rho(t)$ for energy harvesting and information decoding, respectively. Note that unlike the traditional information receiver in Fig. 1.3, the information receiver in the integrated receiver does not implement any RF band to baseband conversion, since this operation has been *integrated* to the energy receiver (via the rectifier). The achievable R-E region for this type of receivers will be studied in Section 2.5.

2.4 Performance Analysis for Separated Receiver

In this section, we study the achievable R-E region for the separated information and energy receiver shown in Fig. 2.2. With DPS, the average SNR at the information receiver for the k-th transmitted symbol, $k = 1, \ldots, N$, is denoted by $\tau(\rho_k)$, and given by

$$\tau(\rho_k) = \frac{(1-\rho_k)hP}{(1-\rho_k)\sigma_{\mathrm{A}}^2 + \sigma_{\mathrm{cov}}^2}. \tag{2.18}$$

From (2.18), we obtain the achievable R-E region for the DPS scheme in the case of separated receiver as

$$\mathcal{C}_{\mathrm{R-E}}^{\mathrm{DPS}}(P) \triangleq \bigcup_{\boldsymbol{\rho}} \Bigg\{ (R,Q) : Q \leq \frac{1}{N}\sum_{k=1}^{N} \rho_k \zeta h P, \\ R \leq \frac{1}{N}\sum_{k=1}^{N} \log_2\left(1 + \frac{(1-\rho_k)hP}{(1-\rho_k)\sigma_{\mathrm{A}}^2 + \sigma_{\mathrm{cov}}^2}\right) \Bigg\}. \tag{2.19}$$

Next, we address the two special cases of DPS, i.e., the TS scheme and the PS scheme. Substituting (2.15) into (2.19), the achievable R-E region for the TS scheme is given by

$$\mathcal{C}_{\mathrm{R-E}}^{\mathrm{TS}}(P) \triangleq \bigcup_{\alpha} \left\{ (R,Q) : Q \leq \alpha\zeta hP,\, R \leq (1-\alpha)\log_2\left(1 + \frac{hP}{\sigma_{\mathrm{A}}^2 + \sigma_{\mathrm{cov}}^2}\right) \right\}. \tag{2.20}$$

Let $\hat{R}_{\max} = \log_2\left(1 + hP/(\sigma_{\mathrm{A}}^2 + \sigma_{\mathrm{cov}}^2)\right)$ given in (2.4) and $\hat{Q}_{\max} = \zeta hP$ given in (2.13). It is noted that the boundary of $\mathcal{C}_{\mathrm{R-E}}^{\mathrm{TS}}(P)$ is simply a straight line connecting the two points $(\hat{R}_{\max}, 0)$ and $(0, \hat{Q}_{\max})$ as α sweeps from 0 to 1.

Substituting (2.16) into (2.19), the achievable R-E region for the PS scheme is given by

$$\mathcal{C}_{\mathrm{R-E}}^{\mathrm{PS}}(P) \triangleq \bigcup_{\rho} \left\{ (R,Q) : Q \leq \rho\zeta hP,\, R \leq \log_2\left(1 + \frac{(1-\rho)hP}{(1-\rho)\sigma_{\mathrm{A}}^2 + \sigma_{\mathrm{cov}}^2}\right) \right\}. \tag{2.21}$$

Proposition 2.4.1. *For the separated information and energy receiver, the PS scheme is the optimal DPS scheme, i.e.,* $\mathcal{C}_{\mathrm{R-E}}^{\mathrm{DPS}}(P) = \mathcal{C}_{\mathrm{R-E}}^{\mathrm{PS}}(P), P \geq 0$.

Proof. Please refer to Appendix A. □

From Proposition 2.4.1, it suffices for us to consider the PS scheme for the optimal R-E trade-off in the case of separated receivers. In particular, if $\sigma_{\mathrm{A}}^2 \ll \sigma_{\mathrm{cov}}^2$, i.e., the processing noise is dominant over the antenna noise, from (2.18) the SNR at the information receiver $\tau(\rho) \to (1-\rho)hP/\sigma_{\mathrm{cov}}^2$. In this case, it can be shown that $\mathcal{C}_{\mathrm{R-E}}^{\mathrm{TS}}(P) \subseteq \mathcal{C}_{\mathrm{R-E}}^{\mathrm{PS}}(P)$. In the other extreme case with $\sigma_{\mathrm{A}}^2 \gg \sigma_{\mathrm{cov}}^2$, from (2.18) we have

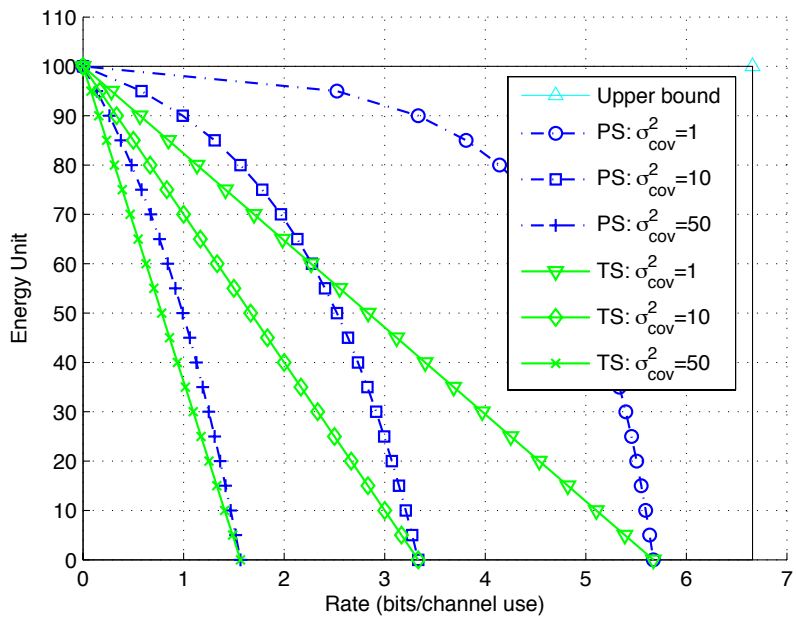

Figure 2.4: Rate-energy trade-off for TS vs. PS based separated receiver with $h = 1, P = 100, \zeta = 1$ and $\sigma_{\mathrm{A}}^2 = 1$.

$\tau(\rho) \to hP/\sigma_{\mathrm{A}}^2$, which is independent of ρ. Thus, the optimal rate-energy trade-off is achieved when infinitesimally small power is split to the information receiver, i.e., $\rho \to 1$. In this case, it can be shown that when $\zeta = 1$, $\mathcal{C}_{\mathrm{R-E}}^{\mathrm{PS}}(P) \to \mathcal{C}_{\mathrm{R-E}}^{\mathrm{UB}}(P)$, which is the R-E trade-off outer bound given in (2.14).

Fig. 2.4 shows the achievable R-E regions under different noise power setups for the separated information and energy receiver (SepRx). It is assumed that $h = 1$, $P = 100$, $\zeta = 1$, and the antenna noise power is set to be $\sigma_{\mathrm{A}}^2 = 1$. With normalization, for convenience we denote the information rate and harvested energy in terms of bits/channel use and energy unit, respectively. In Fig. 2.4, it is observed that for SepRx, the PS scheme always achieves larger R-E pairs than the TS scheme for different values of the processing (RF band to baseband conversion) noise power σ_{cov}^2. Moreover, as σ_{cov}^2 increases, the gap between $\mathcal{C}_{\mathrm{R-E}}^{\mathrm{TS}}(P)$ and $\mathcal{C}_{\mathrm{R-E}}^{\mathrm{PS}}(P)$ shrinks, while as σ_{cov}^2 decreases, the achievable R-E region with PS enlarges and will eventually approach to the R-E region upper bound given in (2.14) when $\sigma_{\mathrm{cov}}^2 \to 0$.

2.5 Performance Analysis for Integrated Receiver

In this section, we study the rate-energy performance for the integrated information and energy receiver shown in Fig. 2.3. In the integrated receiver, due to the RF to baseband conversion by the rectifier, we shall see that the equivalent baseband channel is nonlinear, as opposed to that of the separated receiver where the channel is linear.

From (2.12), for convenience we re-express $i_{\mathrm{DC}}(t)$ as follows:

$$i_{\mathrm{DC}}(t) = \left|\sqrt{hP}A(t)e^{j(\theta+\phi(t))} + \tilde{n}_{\mathrm{A}}(t)\right|^2 + n_{\mathrm{rec}}(t). \tag{2.22}$$

Since planar rotation does not change the statistics of $\tilde{n}_{\mathrm{A}}(t)$, (2.22) can be equivalently written as

$$i_{\mathrm{DC}}(t) = \left|\sqrt{hP}A(t) + \tilde{n}_{\mathrm{A}}(t)\right|^2 + n_{\mathrm{rec}}(t). \tag{2.23}$$

As shown in Fig. 2.3, after the noiseless power splitter and ADC, the output $\hat{y}[k], k = 1, \ldots, N$, is given by

$$\hat{y}[k] = (1-\rho_k)\left(\left|\sqrt{hP}A[k] + \tilde{n}_{\mathrm{A}}[k]\right|^2 + n_{\mathrm{rec}}[k]\right). \tag{2.24}$$

In the above it is worth noting that the average SNR at any k is independent of ρ_k provided that $\rho_k < 1$. Thus, to minimize the power split for information decoding (or maximize the power split for energy harvesting), we should let $\rho_k \to 1, \forall k$, i.e., splitting infinitesimally small power to the information receiver all the time. Thereby, DPS becomes an equivalent PS with $\rho \to 1$ in the case of integrated receiver.

With $\rho_k \to 1, \forall k$ in (2.24), the equivalent discrete-time memoryless channel for

the information decoder is modeled as

$$Y = \left|\sqrt{hPX} + Z_2\right|^2 + Z_1 \tag{2.25}$$

where X denotes the signal power, which is the nonnegative channel input; Y denotes the channel output; $Z_2 \sim \mathcal{CN}(0, \sigma_{\mathrm{A}}^2)$ denotes the antenna noise; and $Z_1 \sim \mathcal{N}(0, \sigma_{\mathrm{rec}}^2)$ denotes the rectifier noise. It is worth noting that for the channel (2.25) information is encoded in the power (amplitude) of the transmitted signal $x(t)$, rather than the phase of $x(t)$. The channel in (2.25) is nonlinear and thus it is challenging to determine its capacity C_{NL} and corresponding optimal input distribution subject to $X \geq 0$ and $\mathbb{E}[X] \leq 1$, where X is real. Similar to the case of separated receiver, we consider the following two special noise power setups:

- Case 1 (Negligible Antenna Noise) with $\sigma_{\mathrm{A}}^2 \to 0$: In practice, this case may be applicable when the antenna noise power is much smaller than the rectifier noise power, thus the antenna noise can be omitted. With $\sigma_{\mathrm{A}}^2 \to 0$, we have $Z_2 \to 0$. Thus, the channel in (2.25) becomes

$$Y = hPX + Z_1 \tag{2.26}$$

  where $X \geq 0$ and real-valued, which is known as the *optical intensity channel*. It is shown in [19] that the optimal input distribution to this channel is discrete. According to [20], the capacity C_1 for the channel (2.26) is upper-bounded by

$$\begin{aligned} C_1^{\mathrm{ub}} &= \log_2\left(\beta e^{-\frac{\delta^2}{2\sigma_{\mathrm{rec}}^2}} + \sqrt{2\pi}\sigma_{\mathrm{rec}}\mathcal{Q}\left(\frac{\delta}{\sigma_{\mathrm{rec}}}\right)\right) \\ &+ \left(\frac{1}{2}\mathcal{Q}\left(\frac{\delta}{\sigma_{\mathrm{rec}}}\right) + \frac{1}{\beta}\left(\delta + hP + \frac{\sigma_{\mathrm{rec}} e^{-\frac{\delta^2}{2\sigma_{\mathrm{rec}}^2}}}{\sqrt{2\pi}}\right)\right)\log_2 e \\ &+ \left(\frac{\delta e^{-\frac{\delta^2}{2\sigma_{\mathrm{rec}}^2}}}{2\sqrt{2\pi}\sigma_{\mathrm{rec}}} + \frac{\delta^2}{2\sigma_{\mathrm{rec}}^2}\left(1 - \mathcal{Q}\left(\frac{\delta + hP}{\sigma_{\mathrm{rec}}}\right)\right)\right)\log_2 e - \frac{1}{2}\log_2 2\pi e\sigma_{\mathrm{rec}}^2 \end{aligned} \tag{2.27}$$

  where $\mathcal{Q}(\cdot) = \frac{1}{\sqrt{2\pi}}\int_x^\infty e^{-\frac{t^2}{2}}dt$ denotes the $\mathcal{Q}$-function, and $\beta > 0$, $\delta \geq 0$ are

free parameters. The details of choice for β and δ are provided in [20], and thus are omitted for brevity. Moreover, the asymptotic capacity at high power ($P \to \infty$) is given by [20]

$$C_1^{\infty} = \log_2 \frac{hP}{\sigma_{\text{rec}}} + \frac{1}{2} \log_2 \frac{e}{2\pi}. \tag{2.28}$$

- Case 2 (Negligible Rectifier Noise) with $\sigma_{\text{rec}} \to 0$: This case is applicable when the antenna noise power is much greater than the rectifier noise power; thus, the rectifier noise can be omitted. With $\sigma_{\text{rec}} \to 0$, we have $Z_1 \to 0$. The channel in (2.25) is then simplified as

$$Y = \left| \sqrt{hPX} + Z_2 \right|^2 \tag{2.29}$$

which is equivalent to the *noncoherent AWGN channel*. It is shown in [21] that the optimal input distribution to this channel is discrete and possesses an infinite number of mass points. The capacity C_2 for the channel (2.29) is upper-bounded by [21]

$$C_2^{\text{ub}} = \frac{1}{2} \log_2 \left(1 + \frac{hP}{\sigma_{\text{A}}^2} \right) + \frac{1}{2} \left(\log_2 \frac{2\pi}{e} - C_E \log_2 e \right) \tag{2.30}$$

where C_E is Euler's constant. Moreover, the asymptotic capacity at high power ($P \to \infty$) is given by [21, 22]

$$C_2^{\infty} = \frac{1}{2} \log_2 \left(1 + \frac{hP}{2\sigma_{\text{A}}^2} \right) \tag{2.31}$$

which is achieved by choosing X to be central chi-square distributed with one degree of freedom[4].

In general, the capacity C_{NL} of the channel given in (2.25) can be upper-bounded

[4]In this case, the input amplitude is distributed as the positive normal distribution, with probability density function $f_{\text{A}}(a) = \sqrt{\frac{2}{\pi}} e^{-\frac{a^2}{2}}$.

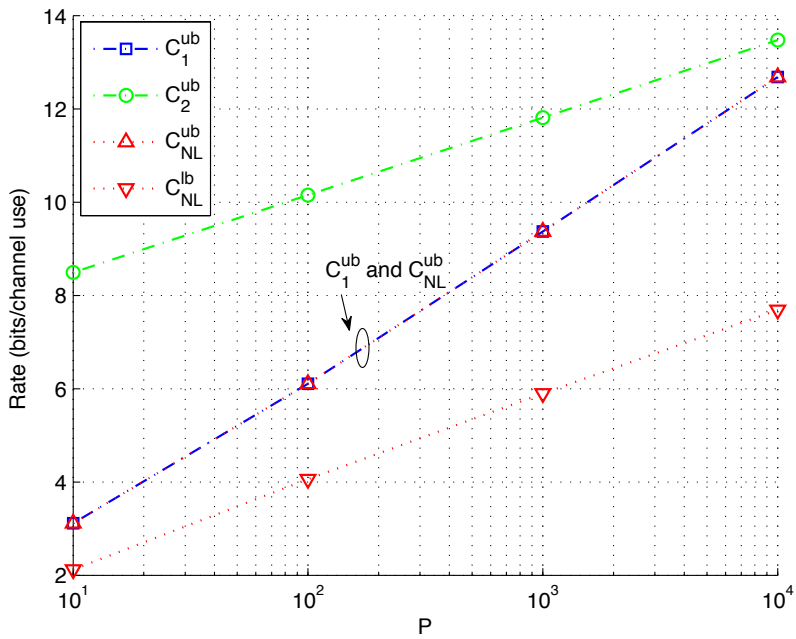

Figure 2.5: Capacity bounds for the channels (2.25), (2.26) and (2.29) with $h = 1, \sigma_{\mathrm{A}}^2 = 10^{-4}$ and $\sigma_{\mathrm{rec}} = 1$.

by

$$C_{\mathrm{NL}}^{\mathrm{ub}} = \min\{C_1^{\mathrm{ub}}, C_2^{\mathrm{ub}}\} \tag{2.32}$$

and a capacity lower bound $C_{\mathrm{NL}}^{\mathrm{lb}}$ for the channel (2.25) is given by the mutual information obtained from any input distribution satisfying the constraint $X \geq 0$ and $\mathbb{E}[X] \leq 1$. It is worth noting that at high power ($P \to \infty$) from (2.28) and (2.31), C_1^{∞} grows like $\log_2 P$; while C_2^{∞} grows like $\frac{1}{2}\log_2 P$. Thus the channel (2.29) provides a tighter upper bound for the asymptotic capacity of the channel (2.25) than the channel (2.26) at high SNR.

Fig. 2.5 shows the capacity bounds for the above three channels (2.25), (2.26) and (2.29). It is assumed that $h = 1, \sigma_{\mathrm{A}}^2 = 10^{-4}$ and $\sigma_{\mathrm{rec}} = 1$. The capacity lower bound $C_{\mathrm{NL}}^{\mathrm{lb}}$ for the channel given in (2.25) is computed by assuming the input (power) distribution is a central chi-square distribution with one degree of freedom. We shall use this lower bound as the achievable rate for the integrated receiver in the

subsequent numerical results. It is observed that in this case with dominant rectifier noise, the capacity upper bound C_1^{ub} in (2.27) is tighter than C_2^{ub} in (2.30). It is also observed that the gap between the capacity upper and lower bounds, namely $C_{\text{NL}}^{\text{ub}}$ and $C_{\text{NL}}^{\text{lb}}$, is still notably large under this setup, which can be further reduced by optimizing the input distribution.

To summarize, the achievable R-E region for the case of integrated receivers by PS with $\rho \to 1$ is given by

$$\mathcal{C}_{\text{R-E}}^{\text{PS}}(P) \triangleq \{(R, Q) : R \leq C_{\text{NL}}(P), Q \leq \zeta h P\} \tag{2.33}$$

where $C_{\text{NL}}(P)$ denotes the capacity of the nonlinear channel given in (2.25) subject to $X \geq 0$ and $\mathbb{E}[X] \leq 1$.

<u>Remark</u> 2.5.1. We have characterized the rate-energy performance for the integrated receiver assuming an ideal ADC with zero quantization noise. Now we extend our results to the case of nonzero quantization noise $n_{\text{ADC}}(t)$. It is assumed that $n_{\text{ADC}}(t) \sim \mathcal{N}(0, \sigma_{\text{ADC}}^2)$ for the integrated receiver [23, 24]. With nonzero ADC noise, (2.24) is modified as

$$\hat{y}[k] = (1 - \rho_k) \left(\left| \sqrt{hP} A[k] + \tilde{n}_{\text{A}}[k] \right|^2 + n_{\text{rec}}[k] \right) + n_{\text{ADC}}[k]. \tag{2.34}$$

Thus, for given k the equivalent channel in (2.25) still holds, where $Z_1 \sim \mathcal{N}\left(0, \sigma_{\text{rec}}^2 + \frac{\sigma_{\text{ADC}}^2}{(1-\rho_k)^2}\right)$ denotes the equivalent processing noise. It is worth noting that the equivalent processing noise power is a function of the power splitting ratio ρ_k; thus, the capacity in channel (2.25) is also a function of ρ_k. The achievable R-E region for the integrated receiver by DPS is thus given by

$$\mathcal{C}_{\text{R-E}}^{\text{DPS}}(P) \triangleq \bigcup_{\boldsymbol{\rho}} \left\{ (R, Q) : R \leq \frac{1}{N} \sum_{k=1}^{N} C_{\text{NL}}(P, \rho_k), Q \leq \frac{1}{N} \sum_{k=1}^{N} \rho_k \zeta h P \right\}. \tag{2.35}$$

For the separated receiver, the results in Section 2.4 can be easily extended to the case with nonzero ADC noise by adding the ADC noise power to the total processing

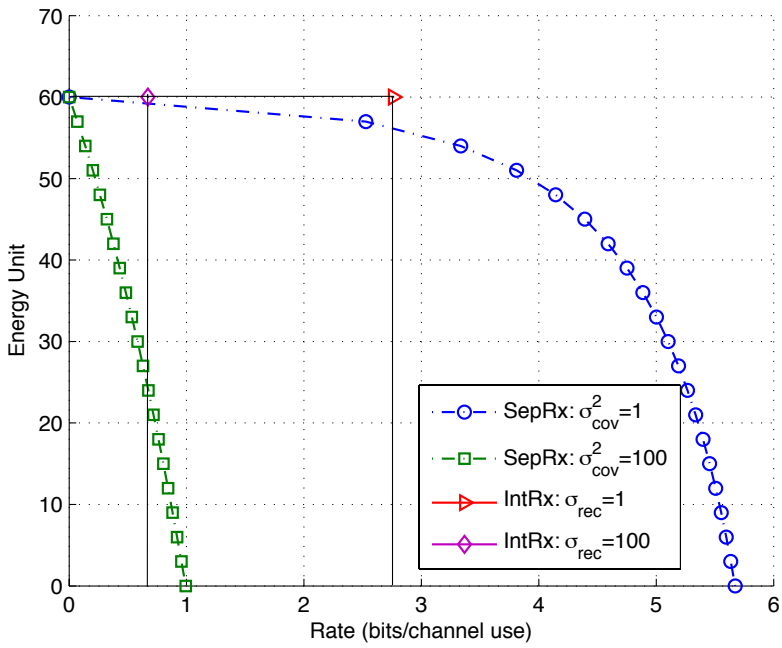

Figure 2.6: Rate-energy trade-off for separated receiver (SepRx) vs. integrated receiver (IntRx) with $h = 1, P = 100, \zeta = 0.6$, $\sigma_{\mathrm{A}}^2 = 1$ and $\sigma_{\mathrm{ADC}}^2 = 0$.

noise power.

Figs. 2.6 and 2.7 show the achievable R-E regions under different noise power setups for both cases of SepRx and IntRx. For both figures, it is assumed that $h = 1, P = 100, \zeta = 0.6$, and $\sigma_{\mathrm{A}}^2 = 1$. In Fig. 2.6, it is assumed that $\sigma_{\mathrm{ADC}}^2 = 0$. In Fig. 2.7, it is assumed that $\sigma_{\mathrm{ADC}}^2 = 1$, and $\rho_k = \rho, \forall k$ in (2.35) with $0 \leq \rho \leq 1$. Note that in practice, the degradation of ADC noise is usually modeled by a so-called signal-to-quantization-noise ratio (SQNR), approximately given by $6K$ dB, where K is the number of quantization bits. Here, by assuming $P = 100$ and $\sigma_{\mathrm{ADC}}^2 = 1$, the SQNR equals to 20dB, which implies $K \approx 3.3$bits. It follows that the number of quantization levels is approximately 10. In Figs. 2.6 and 2.7, the achievable rates for IntRx are computed as the capacity lower bound for the channel given in (2.25) assuming the input to be central chi-square distributed with one degree of freedom.

As shown in Fig. 2.6, the achievable R-E regions for IntRx with zero ADC noise are marked by boxes as given in (2.33). In addition, when the processing noise

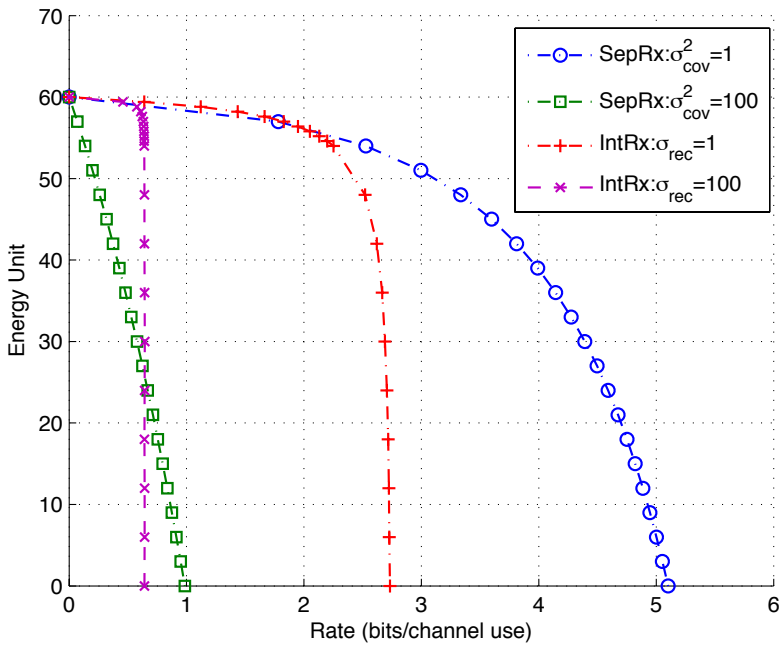

Figure 2.7: Rate-energy trade-off for separated receiver (SepRx) vs. integrated receiver (IntRx) with $h = 1, P = 100, \zeta = 0.6$ and $\sigma_{\mathrm{A}}^2 = \sigma_{\mathrm{ADC}}^2 = 1$.

power (σ_{cov}^2 for SepRx and σ_{rec} for IntRx) equals to the antenna noise power, i.e., $\sigma_{\mathrm{A}}^2 = \sigma_{\mathrm{cov}}^2 = \sigma_{\mathrm{rec}} = 1$, the achievable rate for IntRx is notably lower than that for SepRx, due to the use of noncoherent (energy) modulation by IntRx as compared to the use of coherent modulation by SepRx. However, when the processing noise power is much greater than the antenna noise power (as in most practical systems), the achievable R-E region of IntRx becomes superior compared to that of SepRx with the same processing noise power, i.e., $\sigma_{\mathrm{cov}}^2 = \sigma_{\mathrm{rec}} = 100$. This is due to the fact that for IntRx, the processing (rectifier) noise incurs prior to the power splitter and thus only infinitesimally small power is required to be split by the power splitter to implement the energy detection for information decoding (cf. (2.25)), while for SepRx, more power needs to be split to the information decoder to compensate for the processing (RF band to baseband conversion) noise that incurs after the power splitter. Moreover, in Fig. 2.6 it is observed that IntRx is more suitable than SepRx when more wireless power is desired.

In Fig. 2.7, it is observed that the achievable R-E regions for IntRx with nonzero ADC noise are no longer boxes. Comparing Fig. 2.7 with Fig. 2.6, it is observed that the achievable rate by IntRx with nonzero ADC noise is less than that by IntRx with zero ADC noise, especially when more harvested energy is desired.

2.6 Performance Analysis with Receiver Circuit Power Consumption

In Sections 2.4 and 2.5, the harvested energy is characterized as the energy harvested by the energy receiver without consideration of power consumption by the receiver circuits. For energy receiver, there is no energy consumption since both the Schottky diode and LPF are passive devices[5]. However, for information receiver, some amount of power will be consumed to supply the information decoding circuits. In particular, for the separated receiver shown in Fig. 2.2, the circuit power consumed by information decoding, denoted by P_{S}, is given by $P_{\mathrm{S}} = P_{\mathrm{m}} + P_{\mathrm{ADC}}$, where P_{m} and P_{ADC} denote the power consumed by the RF band mixer and the ADC, respectively. For the integrated receiver shown in Fig. 2.3, however, the circuit power consumed by information decoding, denoted by P_{I}, is only given by $P_{\mathrm{I}} = P_{\mathrm{ADC}}$.[6] Note that in general P_{S} will be much greater than P_{I}, since the RF band mixer consumes comparable amount of power as compared to the ADC. Thus the *net energy* stored in the battery will be the harvested energy subtracted by that consumed by information decoding circuits. In this section, we study the rate-energy trade-off for both separated and integrated receivers with receiver circuit power consumption taken into account.

[5]In practice, some RF energy harvesting systems have additional control circuits which consume power, however, this power consumption has been included in the conversion efficiency ζ.

[6]Here P_{S} and P_{I} are defined according to the two architectures in Fig. 2.2 and Fig. 2.3, respectively. In practice, the information decoding circuits may contain additional components, such as a low noise amplifier in the separated receiver. In general, the power consumed by the additional components can be added to P_{S} or P_{I}.

2.6.1 Separated Receiver

For the separated receiver shown in Fig. 2.2, by modifying (2.19) to account for the circuit power P_{S}, the achievable R-E region for the DPS scheme is given by

$$\mathcal{C}_{\mathrm{R-E}}^{\mathrm{DPS}'}(P) \triangleq \bigcup_{\boldsymbol{\rho}} \Bigg\{ (R,Q) : 0 \leq Q \leq \frac{1}{N} \left(\sum_{k=1}^{N} \rho_k \zeta h P - \sum_{k=\alpha N+1}^{N} P_{\mathrm{S}} \right), \\ R \leq \frac{1}{N} \sum_{k=\alpha N+1}^{N} \log_2 \left(1 + \frac{(1-\rho_k) h P}{(1-\rho_k)\sigma_{\mathrm{A}}^2 + \sigma_{\mathrm{cov}}^2} \right) \Bigg\}. \tag{2.36}$$

Next, we address one special case of DPS, i.e., the OPS scheme. Substituting (2.17) into (2.36), the achievable R-E region for the OPS scheme is given by

$$\mathcal{C}_{\mathrm{R-E}}^{\mathrm{OPS}'}(P) \triangleq \bigcup_{\alpha,\rho} \Bigg\{ (R,Q) : 0 \leq Q \leq \alpha \zeta h P + (1-\alpha)\rho \zeta h P \\ -(1-\alpha) P_{\mathrm{S}}, R \leq (1-\alpha) \log_2 \left(1 + \frac{(1-\rho) h P}{(1-\rho)\sigma_{\mathrm{A}}^2 + \sigma_{\mathrm{cov}}^2} \right) \Bigg\}. \tag{2.37}$$

Proposition 2.6.1. *For the separated information and energy receiver with $P_{\mathrm{S}} > 0$, the OPS scheme is the optimal DPS scheme, i.e., $\mathcal{C}_{\mathrm{R-E}}^{\mathrm{DPS}'}(P) = \mathcal{C}_{\mathrm{R-E}}^{\mathrm{OPS}'}(P), P \geq 0$.*

Proof. Please refer to Appendix B. □

From Proposition 2.6.1, it suffices to consider the OPS scheme for the optimal R-E trade-off in the case of separated receivers. Unlike the case of $P_{\mathrm{S}} = 0$, where the boundary of $\mathcal{C}_{\mathrm{R-E}}^{\mathrm{DPS}} = \mathcal{C}_{\mathrm{R-E}}^{\mathrm{PS}}$ is achieved as ρ sweeps from 0 to 1, the optimal power splitting pairs (α^*, ρ^*) that achieve the boundary of $\mathcal{C}_{\mathrm{R-E}}^{\mathrm{DPS}'} = \mathcal{C}_{\mathrm{R-E}}^{\mathrm{OPS}'}$ has to be determined. We thus consider the following optimization problem:

$$\begin{aligned} (\mathrm{P0}): \ \ & \max_{\alpha,\rho} \ \ R = (1-\alpha) \log_2 \left(1 + \frac{(1-\rho) h P}{(1-\rho)\sigma_{\mathrm{A}}^2 + \sigma_{\mathrm{cov}}^2} \right) \\ & \mathtt{s.t.} \ \ \alpha \zeta h P + (1-\alpha)\rho \zeta h P - (1-\alpha) P_{\mathrm{S}} \geq Q, \\ & \qquad 0 \leq \alpha \leq 1, \ 0 \leq \rho \leq 1, \end{aligned}$$

Problem (P0) is feasible if and only if $Q \leq \zeta h P$. It is easy to verify that

$(R, Q) = (0, \zeta hP)$ is achieved by $\alpha = 1$. Next, we consider Problem (P0) for given $Q \in [0, \zeta hP)$ and $0 \leq \alpha < 1$. The optimal solution of (P0) is obtained with the first constraint strictly equal, otherwise we can always decrease α or ρ to obtain a larger rate R. Thus the boundary points (R, Q) satisfy the following two equations,

$$Q = \alpha\zeta hP + (1-\alpha)\rho\zeta hP - (1-\alpha)P_{\mathrm{S}}, \tag{2.38}$$

$$R = (1-\alpha)\log_2\left(1 + \frac{(1-\rho)hP}{(1-\rho)\sigma_{\mathrm{A}}^2 + \sigma_{\mathrm{cov}}^2}\right). \tag{2.39}$$

From (2.38), we have

$$\rho = \frac{Q - \alpha\zeta hP + (1-\alpha)P_{\mathrm{S}}}{(1-\alpha)\zeta hP}. \tag{2.40}$$

From (2.40), we have $\alpha \in \left[\max\{\frac{Q+P_{\mathrm{S}}-\zeta hP}{P_{\mathrm{S}}}, 0\}, \frac{Q+P_{\mathrm{S}}}{\zeta hP+P_{\mathrm{S}}}\right]$ such that $0 \leq \rho \leq 1$. Substituting (2.40) to (2.39), we have

$$R = (1-\alpha)\log_2\left(1 + \frac{\frac{\zeta hP-Q-(1-\alpha)P_{\mathrm{S}}}{\zeta}}{\frac{\zeta hP-Q-(1-\alpha)P_{\mathrm{S}}}{\zeta hP}\sigma_{\mathrm{A}}^2 + \sigma_{\mathrm{cov}}^2(1-\alpha)}\right). \tag{2.41}$$

From (2.41), R is a function of α with fixed Q. For convenience, we rewrite (2.41) as follows:

$$R(s) = s\log_2\left(1 + \frac{cs+d}{as+b}\right) \tag{2.42}$$

where $s = 1-\alpha$, $a = \sigma_{\mathrm{cov}}^2 - \frac{\sigma_{\mathrm{A}}^2 P_{\mathrm{S}}}{\zeta hP}$, $b = \sigma_{\mathrm{A}}^2\left(1 - \frac{Q}{\zeta hP}\right) > 0$, $c = -\frac{P_{\mathrm{S}}}{\zeta} < 0$ and $d = hP\left(1 - \frac{Q}{\zeta hP}\right) > 0$. It is worth noting that $s \in \left[\frac{\zeta hP-Q}{\zeta hP+P_{\mathrm{S}}}, \min\{\frac{\zeta hP-Q}{P_{\mathrm{S}}}, 1\}\right]$, or equivalently, $s \in \left[\frac{d}{hP-c}, \min\{-\frac{d}{c}, 1\}\right]$, since $\alpha \in \left[\max\{\frac{Q+P_{\mathrm{S}}-\zeta hP}{P_{\mathrm{S}}}, 0\}, \frac{Q+P_{\mathrm{S}}}{\zeta hP+P_{\mathrm{S}}}\right]$. The following lemma describes the behavior of $R(s)$ in terms of s, which is important for determining the boundary points (R, Q).

Lemma 2.6.1. *With $Q \in [0, \zeta hP)$, $R(s)$ is concave in $s \in [\frac{d}{hP-c}, \min\{-\frac{d}{c}, 1\}]$.*

Proof. Please refer to Appendix C. □

By Lemma 2.6.1, the optimal $s^* \in [\frac{d}{hP-c}, \min\{-\frac{d}{c}, 1\}]$ that maximizes $R(s)$ can be efficiently obtained by searching over $s \in [\frac{d}{hP-c}, \min\{-\frac{d}{c}, 1\}]$ using the bisection

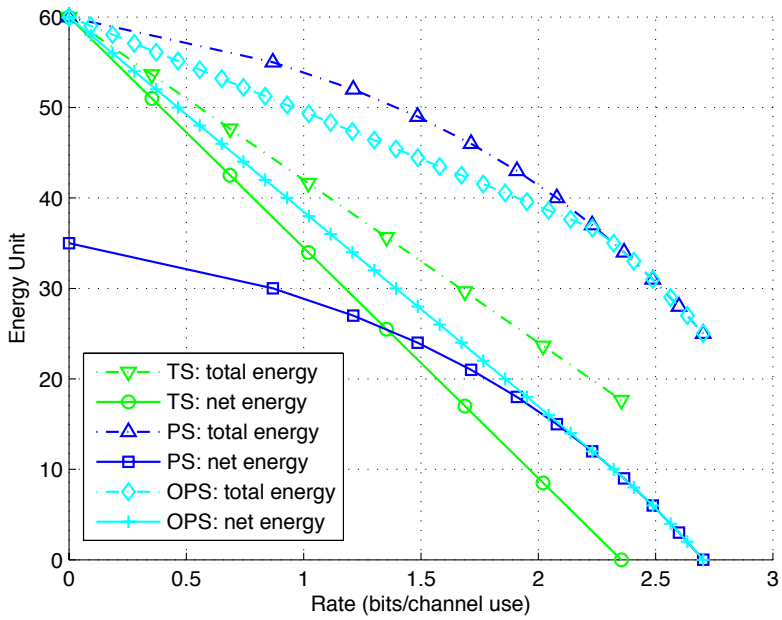

Figure 2.8: Rate-energy trade-off for the separated receiver with receiver circuit power consumption. It is assumed that $h = 1, P = 100, \zeta = 0.6, \sigma_{\mathrm{A}}^2 = 1, \sigma_{\mathrm{cov}}^2 = 10$ and $P_{\mathrm{S}} = 25$.

method. The optimal α^* is thus given by $\alpha^* = 1 - s^*$. The optimal ρ^* is given by (2.40) with $\alpha = \alpha^*$. The corresponding R is given by (2.39) with $\alpha = \alpha^*$ and $\rho = \rho^*$. To summarize, each boundary point (R, Q) of $\mathcal{C}_{\mathrm{R-E}}^{\mathrm{OPS}'}$ is achieved by a unique power splitting pair (α^*, ρ^*).

Fig. 2.8 shows the achievable R-E regions (labeled as "net energy") for SepRx with receiver circuit power consumption. The total harvested energy (labeled as "total energy"), including both the net energy stored in the battery and the energy consumed by information decoding, is also shown in Fig. 2.8 as a reference. For SepRx with $P_{\mathrm{S}} = 25$, it is observed that $\mathcal{C}_{\mathrm{R-E}}^{\mathrm{TS}'} \subseteq \mathcal{C}_{\mathrm{R-E}}^{\mathrm{OPS}'}$ and $\mathcal{C}_{\mathrm{R-E}}^{\mathrm{PS}'} \subseteq \mathcal{C}_{\mathrm{R-E}}^{\mathrm{OPS}'}$. Moreover, PS achieves the RE-region boundary only at low harvested energy region, where $\mathcal{C}_{\mathrm{R-E}}^{\mathrm{PS}'}$ and $\mathcal{C}_{\mathrm{R-E}}^{\mathrm{OPS}'}$ partially coincide. However, the performance of PS becomes worse (even worse than TS) when more harvested energy is desired, since it is unwise and energy-inefficient to keep information receiver always on during the whole transmission time.

2.6.2 Integrated Receiver

For the integrated receiver, the achievable R-E region for the DPS scheme taking into account circuit power P_{I} is given by

$$\mathcal{C}_{\mathrm{R-E}}^{\mathrm{DPS}'}(P) \triangleq \bigcup_{\boldsymbol{\rho}} \left\{ (R,Q) : 0 \leq Q \leq \frac{1}{N} \left(\sum_{k=1}^{N} \rho_k \zeta h P - \sum_{k=\alpha N+1}^{N} P_{\mathrm{I}} \right), \right.$$
$$\left. R \leq \frac{1}{N} \sum_{k=\alpha N+1}^{N} C_{\mathrm{NL}} \right\}. \tag{2.43}$$

Since R is independent of ρ_k, we should set $\rho_k \to 1$ for all $k = \alpha N + 1, \ldots, N$. Thus, the OPS scheme with $\rho \to 1$ is the optimal DPS scheme for the integrated receiver with $P_{\mathrm{I}} > 0$. Then (2.43) can be simplified as

$$\mathcal{C}_{\mathrm{R-E}}^{\mathrm{OPS}'}(P) \triangleq \bigcup_{\alpha} \left\{ (R,Q) : 0 \leq Q \leq \zeta h P - (1-\alpha) P_{\mathrm{I}},\, R \leq (1-\alpha) C_{\mathrm{NL}} \right\}. \tag{2.44}$$

Note that when $P_{\mathrm{I}} < \zeta h P$, the boundary of $\mathcal{C}_{\mathrm{R-E}}^{\mathrm{OPS}'}(P)$ is determined by two lines as α sweeps from 0 to 1, with one vertical line connecting the two points $(C_{\mathrm{NL}}, 0)$ and $(C_{\mathrm{NL}}, \zeta h P - P_{\mathrm{I}})$, and another line connecting the two points $(C_{\mathrm{NL}}, \zeta h P - P_{\mathrm{I}})$ and $(0, \zeta h P)$. While $P_{\mathrm{I}} \geq \zeta h P$, the boundary of $\mathcal{C}_{\mathrm{R-E}}^{\mathrm{OPS}'}(P)$ is simply a straight line connecting the two points $(\zeta h P C_{\mathrm{NL}}/P_{\mathrm{I}}, 0)$ and $(0, \zeta h P)$ as α sweeps from $1 - \zeta h P/P_{\mathrm{I}}$ to 1.

Fig. 2.9 shows the achievable R-E regions for both cases of SepRx and IntRx with receiver circuit power consumption. We consider two setups for the receiver circuit power consumption, i.e., low circuit power with $P_{\mathrm{S}} = 25, P_{\mathrm{I}} = 10$, and high circuit power with $P_{\mathrm{S}} = 200, P_{\mathrm{I}} = 80$. For the low circuit power with $P_{\mathrm{S}} = 25, P_{\mathrm{I}} = 10$, IntRx is superior over SepRx when more harvested energy is desired, while SepRx is superior when less harvested energy (no greater than 37 energy units) is required. For the high circuit power with $P_{\mathrm{S}} = 200, P_{\mathrm{I}} = 80$, IntRx is always superior over SepRx, since for SepRx much more transmission time needs to be allocated for harvesting energy to compensate the power consumed by information decoding.

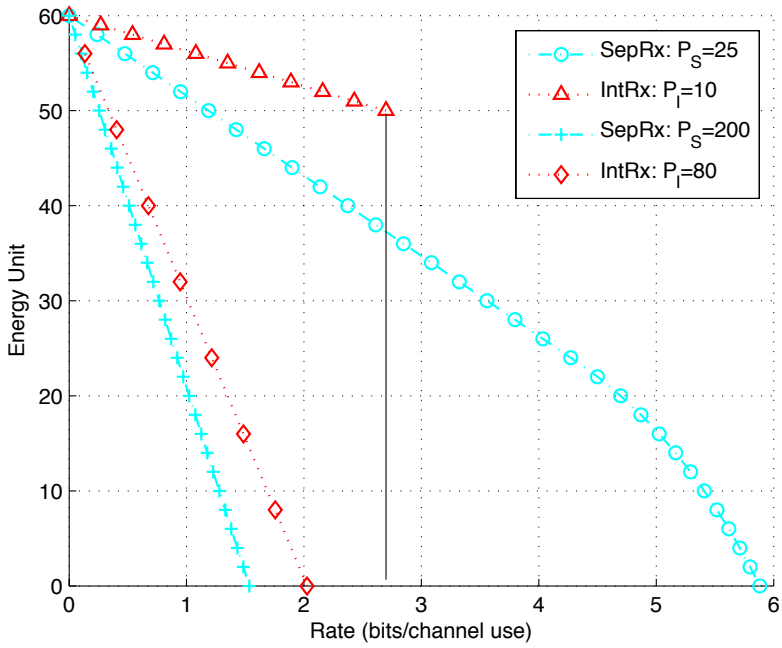

Figure 2.9: Rate-energy trade-off for separated receiver (SepRx) vs. integrated receiver (IntRx) with receiver circuit power consumption. It is assumed that $h = 1, P = 100, \zeta = 0.6, \sigma_{\mathrm{A}}^2 = 0.01, \sigma_{\mathrm{cov}}^2 = 1$ and $\sigma_{\mathrm{rec}} = 10$.

2.7 Practical Modulation

In this section, we study the performances for the two types of receivers under a realistic system setup that employs practical modulation. Let the signal set (constellation) be denoted by $\mathcal{X}$. The size of $\mathcal{X}$ is denoted by M with $M = 2^l$, and $l \geq 1$ being an integer. It is assumed that the maximum rate that the practical modulation can support is $l \leq 10$ bits/channel use. The i-th constellation point in $\mathcal{X}$ is denoted by $x_i, i = 1, \ldots, M$, with equal probability $p_X(x_i) = 1/M$ for simplicity. For the separated receiver, we assume that coherent M-ary quadrature amplitude modulation (QAM) is utilized for transmission. The symbol error rate (SER), denoted by $P_{\mathrm{s}}^{\mathrm{QAM}}$, is approximated by [8]

$$P_{\mathrm{s}}^{\mathrm{QAM}} \approx \frac{4(\sqrt{M}-1)}{\sqrt{M}} \mathcal{Q}\left(\sqrt{\frac{3\tau_s}{M-1}}\right) \tag{2.45}$$

where τ_{s} denotes the average SNR per symbol at the information receiver[7]. The approximation is tight at high SNR, and is taken to be exact for simplicity in the sequel. For the integrated receiver, as mentioned earlier in Section 2.5, information is encoded by the energy (power) of the transmitted signal. Similar to the pulse amplitude modulation, we assume the PEM, with equispaced *positive* constellation points given by

$$x_i = \frac{2(i-1)}{M-1}, \; i = 1, \ldots, M. \tag{2.46}$$

A closed-form expression for the symbol error rate $P_{\mathrm{s}}^{\mathrm{PEM}}$ appears intractable, due to the coupled antenna and rectifier noise for the channel (2.25). For most practical systems, the rectifier noise power will be much greater than the antenna noise power, while the antenna noise is approximately at the thermal noise level. This justifies the assumption that $\sigma_{\mathrm{A}}^2 \ll \sigma_{\mathrm{rec}}$ and we thus approximate the channel (2.25) with (2.26). For simplicity, the decision boundary is chosen as the perpendicular bisector

[7]Binary phase shift keying is used when $l = 1$. For simplicity, we use (2.45) to approximate the SER of binary phase shift keying at high SNR.

of each pair of adjacent two points, and the symbol error rate can be derived to be

$$P_{\mathrm{s}}^{\mathrm{PEM}} = \frac{2(M-1)}{M}\mathcal{Q}\left(\frac{\tau_s'}{M-1}\right) \tag{2.47}$$

where $\tau_s' = hP/\sigma_{\mathrm{rec}}$ is defined as the average SNR per symbol at the information receiver.

For both separated and integrated receivers, we assume the transmitter can adapt the transmission rate such that the symbol error rate is less than a target value $P_{\mathrm{s}}^{\mathrm{tgt}}$, i.e., $P_{\mathrm{s}}^{\mathrm{QAM}} \leq P_{\mathrm{s}}^{\mathrm{tgt}}$ and $P_{\mathrm{s}}^{\mathrm{PEM}} \leq P_{\mathrm{s}}^{\mathrm{tgt}}$ for the separated and integrated receivers, respectively. Moreover, we assume that there is a minimum net harvested energy requirement Q_{req} at the receiver side, i.e., $Q \geq Q_{\mathrm{req}}$, where $0 \leq Q_{\mathrm{req}} \leq \zeta hP$. With the SER constraint and minimum harvested energy constraint, our objective is to achieve the maximum rate. For the separated receiver with OPS scheme, the maximum achievable rate can be obtained by

$$\begin{aligned}
(\mathrm{P1}):\ & \underset{\alpha,\rho,M}{\texttt{max.}}\ R = (1-\alpha)\log_2 M \\
& \texttt{s.t.}\ \frac{4(\sqrt{M}-1)}{\sqrt{M}}\mathcal{Q}\left(\sqrt{\frac{3}{M-1}\cdot\frac{(1-\rho)hP}{(1-\rho)\sigma_{\mathrm{A}}^2+\sigma_{\mathrm{cov}}^2}}\right) \leq P_{\mathrm{s}}^{\mathrm{tgt}}, && (2.48)\\
& \alpha\zeta hP + (1-\alpha)\rho\zeta hP - (1-\alpha)P_{\mathrm{S}} \geq Q_{\mathrm{req}}, && (2.49)\\
& 0 \leq \alpha \leq 1,\ 0 \leq \rho \leq 1, \\
& M = 2^l,\ l \in \{1,2,\ldots,10\}
\end{aligned}$$

Here, the optimization variables are the power splitting pair (α, ρ) and the modulation size M.

For the integrated receiver with OPS scheme, the maximum achievable rate can

be obtained by

$$
\begin{aligned}
(\text{P2}): \quad & \underset{\alpha, M}{\texttt{max.}} \quad R = (1-\alpha)\log_2 M \\
& \texttt{s.t.} \quad \frac{2(M-1)}{M}\mathcal{Q}\left(\frac{1}{M-1}\cdot\frac{hP}{\sigma_{\text{rec}}}\right) \leq P_{\text{s}}^{\text{tgt}}, \\
& \qquad \zeta hP - (1-\alpha)P_{\text{I}} \geq Q_{\text{req}}, \\
& \qquad 0 \leq \alpha \leq 1, \\
& \qquad M = 2^l,\ l \in \{1, 2, \ldots, 10\}
\end{aligned}
\tag{2.50}
$$

Note that here the optimization variables only include α and M, since the OPS scheme with $\rho \to 1$ is optimal for the integrated receiver (c.f. Section 2.6).

We denote the maximum rate for (P1) and (P2) as R_1^* and R_2^*, respectively. Similarly, the optimal variables for (P1) and (P2) are denoted with corresponding superscripts and subscripts, e.g., α_1^*, ρ_1^*, etc. With $0 \leq Q_{\text{req}} \leq \zeta hP$ and reasonable SNR (such that the SER constraints can be satisfied by some M), the optimal solution for (P1) is obtained by an exhaustive search for ρ_1^*: for each fixed $\rho_1 \in [0, 1)$, we have $R_1^* = (1-\alpha_1^*)\log_2 M_1^*$, where $\alpha_1^* = \left(\frac{Q_{\text{req}}-\rho_1\zeta hP+P_{\text{S}}}{(1-\rho_1)\zeta hP+P_{\text{S}}}\right)^+$, $(x)^+ \triangleq \max(0, x)$, and M_1^* attains the maximum value under the SER constraint (2.48); the optimal ρ_1^* is then obtained to maximize R_1^*. The optimal solution for (P2) is given by $R_2^* = (1-\alpha_2^*)\log_2 M_2^*$, where $\alpha_2^* = \left(\frac{Q_{\text{req}}-\zeta hP+P_{\text{I}}}{P_{\text{I}}}\right)^+$ and M_2^* is maximized under the SER constraint (2.50). For both (P1) and (P2), the achievable rate R is determined by both the modulation size M and the time percentage α that the information decoder operates in the off mode. Moreover, as the received signal power hP decreases, M decreases to satisfy the modulation constraint and α increases to satisfy the harvested energy constraint, both of which result in a decrease of the achievable rate.

Typically for practical systems we have $P_{\text{S}} > P_{\text{I}} > 0$, since the RF band mixer in the separated receiver will consume additional circuit power. Henceforth, we assume $P_{\text{S}} > P_{\text{I}} > 0$.

Proposition 2.7.1. *For separated and integrated receivers with* $0 \leq Q_{\text{req}} \leq \zeta hP$ *and* $P_{\text{S}} \geq P_{\text{I}} > 0$*, we have* $\alpha_1^* \geq \alpha_2^*$*. Moreover, if* $M_1^* \leq M_2^*$*, then the maximum achievable rate by the separated receiver will be no greater than that by the integrated receiver, i.e.,* $R_1^* \leq R_2^*$*.*

Proof. Please refer to Appendix D. □

Most practical systems of interest typically operate at the high SNR regime for the information receiver, due to the high-power operating requirement for the energy receiver. Thus, for sufficiently small transmission distance, it is expected that both receivers can support the maximum modulation size under the SER constraint, i.e., $M_1^* = M_2^* = 2^{10}$. Thus, by Proposition 2.7.1, the integrated receiver outperforms the separated receiver for sufficiently small transmission distance.

Fig. 2.10 shows an example of the maximum achievable rate for a practical point-to-point wireless system with separated or integrated receiver. The corresponding modulation size M and time percentage α are shown in Fig. 2.11. The transmitter power is assumed to be $P = 1$W or 30dBm. The distance from the transmitter to the receiver is assumed to be d meters with $d \geq 1$. Assuming the path-loss exponent is three, the signal power attenuation at transmission distance d (in meter) is approximately $(-31.5 - 30\log_{10} d)$dB at a carrier frequency assumed as $f_{\text{c}} = 900$MHz. The bandwidth of the transmitted signal is assumed to be 10MHz. For information receiver, the antenna noise temperature is assumed to be 290K, which corresponds to $\sigma_{\text{A}}^2 = -104$dBm over the bandwidth of 10MHz. As in most practical wireless communication systems, it is assumed that the processing noise power is much greater than the antenna noise power, in which case the antenna noise can be omitted. In particular, it is assumed that $\sigma_{\text{cov}}^2 = -70$dBm for the separated receiver [25] and $\sigma_{\text{rec}} = -50$dBm for the integrated receiver. The circuit power consumed by information decoding is assumed to be $P_{\text{S}} = 0.5$mW for the separated receiver, and $P_{\text{I}} = 0.2$mW for the integrated receiver. For energy receiver, the energy conversion efficiency is assumed to be $\zeta = 0.6$. The minimum harvested energy requirement Q_{req} is set to be zero, which is the minimum requirement for a

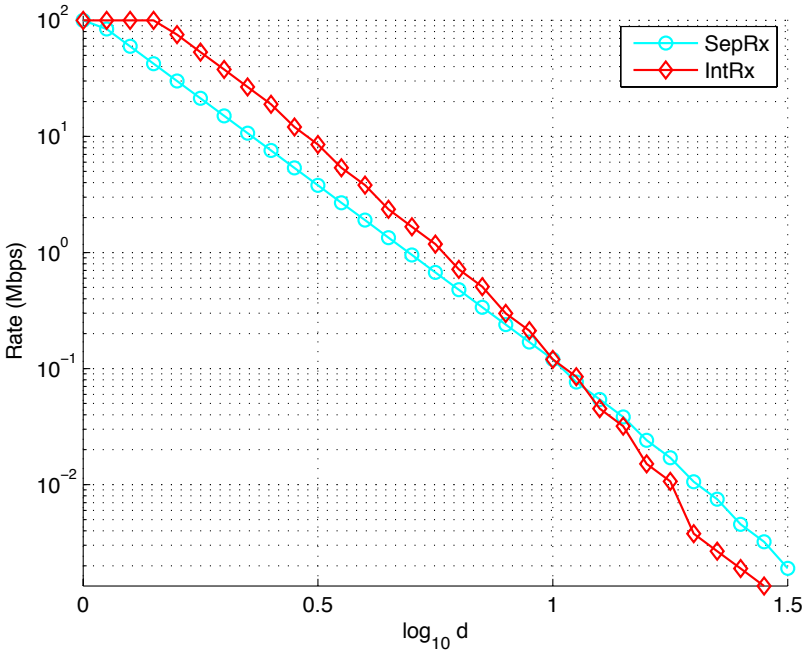

Figure 2.10: Maximum achievable rate for separated receiver (SepRx) and integrated receiver (IntRx) over different transmission distance.

zero-net-energy system that does not need external power source, i.e., the receiver is "self-sustainable". The symbol error rate target is assumed to be $P_{\mathrm{s}}^{\mathrm{tgt}} = 10^{-5}$.

In Fig. 2.10, it is observed that when $0 \leq \log_{10} d \leq 1$, IntRx achieves more rate than SepRx. By Proposition 2.7.1, IntRx outperforms SepRx over the range $0 \leq \log_{10} d \leq 0.4$ with $M_1^* = M_2^* = 2^{10}$; however, Proposition 2.7.1 provides only a sufficient condition, numerical results show that IntRx outperforms SepRx over longer distances up to $\log_{10} d \leq 1$. This is due to the fact that although SepRx supports higher-order constellations (larger M) than IntRx when $0.4 < \log_{10} d \leq 1$, the information receiver of SepRx needs to operate in the off mode for more time (larger α) to compensate the power consumed by information decoding (c.f. Fig. 2.11). It turns out that over this range, the average rate over the whole transmission time of SepRx is less than that achieved by IntRx. As $\log_{10} d$ increases, the rate gap between SepRx and IntRx shrinks and converges when $\log_{10} d$ is around 1. When $1.1 \leq \log_{10} d \leq 1.5$, SepRx achieves more rate than IntRx, since α for both receivers

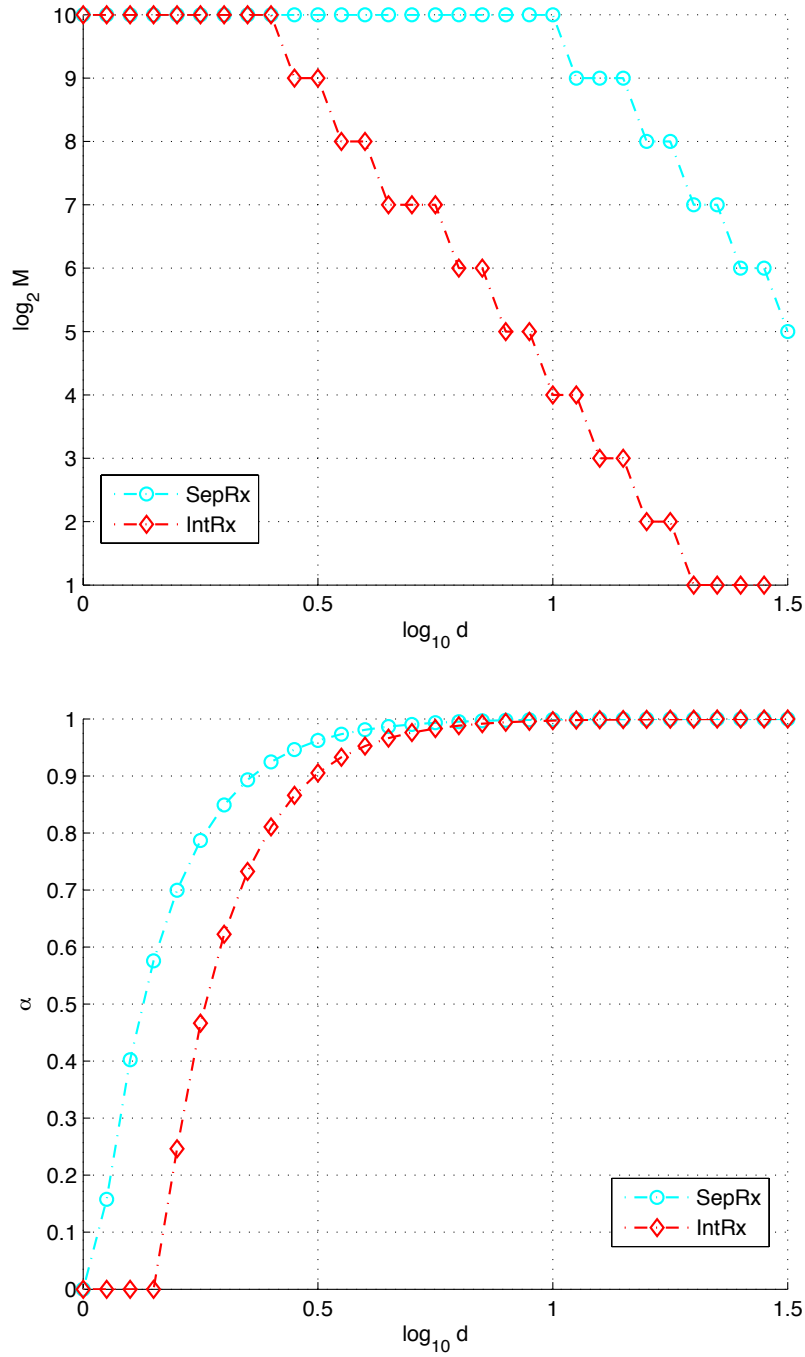

Figure 2.11: Optimal modulation size (M) and information receiver off-time percentage (α) for separated receiver (SepRx) and integrated receiver (IntRx).

approaches to 1 (c.f. Fig. 2.11), while the achievable rates are dominated by the modulation size (M, c.f. Fig. 2.11). Note that when $\log_{10} d = 1.5$, no modulation can support IntRx due to the extremely low received SNR; however, SepRx can still achieve some positive rate. In addition, Fig. 2.11 shows that in general IntRx exploits lower complexity (smaller M) in generating signal constellation.

2.8 Chapter Summary

In this chapter we investigated practical receiver designs for SWIPT. Based on DPS, we proposed a novel practical receiver architecture, namely, the integrated information and energy receiver, in which part of the information decoding implementation, i.e., the RF to baseband conversion, is integrated to the energy receiver via the rectifier. We characterized the rate-energy performance taking circuit power consumption into account for both conventional separated receiver and the proposed integrated receiver. Numerical results showed that when the circuit power consumptions are small (compared with the received signal power), the separated receiver is superior at low harvested energy region; whereas the integrated receiver performs better at high harvested energy region. When the circuit power consumptions are large, the integrated receiver is superior. Moreover, the performance for the two types of receivers was studied under a realistic system setup that employs practical modulation. With symbol error rate constraint and minimum harvested energy constraint, the maximum achievable rates by the two types of receivers were compared. It was shown that for a system with zero-net-energy consumption, the integrated receiver achieves more rate than separated receiver at short transmission distances.

Chapter 3

SWIPT in Multiuser OFDM System

3.1 Introduction

In Chapter 2, we studied the single-user narrowband SWIPT system. In this Chapter, we extend our study to SWIPT in the multiuser OFDM system. For ease of implementation, we assume that separated receivers with TS or PS schemes are employed. We propose two schemes to coordinate the energy and information transmissions to multiple users, namely, TDMA with TS receivers and OFDMA with PS receivers. For both schemes, we address the problem of maximizing the weighted sum-rate over all users by jointly optimizing the power allocation over time and frequency, and TS or PS ratio, subject to the minimum harvested energy constraint for each receiver as well as the peak and/or average power constraint at the transmitter. For the first scheme where we employ TDMA with TS receivers, by an appropriate variable transformation the problem is reformulated as a convex problem, for which the optimal power allocation and TS ratios are obtained by the Lagrange duality method. For the second scheme where we employ OFDMA with PS receivers, we propose an efficient algorithm to iteratively optimize the power and SC allocation, and the PS ratios. The rate-energy trade-off of the two proposed schemes are compared both numerically by simulations and analytically for the special case of single-user system setup. Our results provide key insights to the joint transmitter and receiver strategies design for SWIPT system in practice.

The rest of this chapter is organized as follows. Section 3.2 presents the

literature review. Section 3.3 presents the system model and problem formulation. Section 3.4 studies the special case of a single-user OFDM-based SWIPT system. Section 3.5 derives the resource allocation solutions for the two proposed schemes in the multiuser OFDM-based SWIPT system. Finally, Section 3.6 summarizes the conclusion.

3.2 Literature Review

SWIPT that exploits flat-fading channel variations is studied in [26, 27], where the receiver performs dynamic time switching [26] or DPS [27] to coordinate between EH and ID. Interestingly in [26], interference is utilized as a source for EH, in contrast to the traditional view of taking interference as an undesired factor that jeopardizes the wireless channel capacity. SWIPT in interference channels is considered in [28] with PS receivers, in [29, 30] with TS receivers. SWIPT in relay channels is studied in [31–35], where energy-constrained relays harvests energy from the received signal from the source nodes and uses that harvested energy to forward the source information to the destination nodes, with either TS or PS employed at the relays. SWIPT for secure communications is studied in [36–38].

SWIPT over a single-user OFDM channel has been studied in [7] assuming ideal receiver. It is shown in [7] that a trade-off exists between the achievable rate and the transferred power by power allocation in the frequency bands: for sufficiently small transferred power, the optimal power allocation is given by the WF allocation to maximize the information transmission rate, whereas as the transferred power increases, more power needs to be allocated to the channels with larger channel gain and finally the optimal power allocation approaches that with all power allocated to the channel with largest channel gain. Power control for SWIPT in a multiuser multi-antenna OFDM system is considered in [39], where the information decoder and energy harvester are attached to two separate antennas. In [39], each user only harvests the energy carried by the subcarriers for the SCs that are allocated to that user for ID, which is inefficient in energy utilization, since the energy carried

by the subcarriers allocated to other users for ID can be potentially harvested. Moreover, [39] focuses on power control by assuming a predefined SC allocation. [40] considers SWIPT in a multiuser single-antenna OFDM system with PS receivers. In [40], it is assumed that the splitting ratio can be different for different SCs. However, in practical circuits, (analog) power splitting is performed before (digital) OFDM demodulation. Thus, for an OFDM-based SWIPT system, *all* subcarriers would have to be power split with the same power ratio at each receiver even though only a subset of the subcarriers contain information for the receiver. In contrast, for the case of a single-carrier system, a receiver simply harvests energy from all signals that do not contain information for this receiver.

3.3 System Model and Problem Formulation

We consider an OFDM system with one transmitter and K users. The transmitter and all users are each equipped with one antenna. The total bandwidth of the system is equally divided into N SCs. The SC set is denoted by $\mathcal{N} = \{1, \ldots, N\}$. The power allocated to SC n is denoted by $p_n, n = 1, \ldots, N$. Assume that the total transmission power is at most P. The maximum power allocated to each SC is denoted by P_{peak}, i.e., $0 \leq p_n \leq P_{\text{peak}}, \forall n \in \mathcal{N}$, where $P_{\text{peak}} \geq P/N$. The channel power gain of SC n as seen by the user k is denoted by $h_{k,n}, k = 1, \ldots, K, n = 1, \ldots, N$. We consider a slow-fading environment, where all the channels are assumed to be constant within the transmission scheduling period of our interest. For simplicity, we assume the total transmission time to be one. Moreover, it is assumed that the channel gains on all the SCs for all the users are known at the transmitter. At the receiver side, each user performs EH in addition to ID. It is assumed that the minimum harvested energy during the unit transmission time is $\overline{E}_k > 0$ for user $k, k = 1, \ldots, K$.

3.3.1 Time Switching

We first consider the case of TDMA-based information transmission with TS applied at each receiver. It is worth noting that for a single-user SWIPT system with TS applied at the receiver, the transmission time needs to be divided into two time slots to coordinate the EH and ID processes at the receiver. Thus, in the SWIPT system with K users, we consider $K+1$ time slots without loss of generality, where the additional time slot, which we called the *power* slot, may be allocated for all users to perform EH only. In contrast, in conventional TDMA systems without EH, the power slot is not required. We assume that slot $k, k = 1, \ldots, K$ is assigned to user k for transmitting information, while slot $K+1$ is the power slot. With total time duration of $K+1$ slots to be at most one, the (normalized) time duration for slot $k, k = 1, \ldots, K+1$ is variable and denoted by the TS ratio α_k, with $0 \leq \alpha_k \leq 1$ and $\sum_{k=1}^{K+1} \alpha_k \leq 1$. In addition, the power p_n allocated to SC n at slot k is specified as $p_{k,n}$, where $0 \leq p_{k,n} \leq P_{\text{peak}}, k = 1, \ldots, K+1, n = 1, \ldots, N$. The average transmit power constraint is thus given by

$$\sum_{k=1}^{K+1} \alpha_k \sum_{n=1}^{N} p_{k,n} \leq P. \tag{3.1}$$

Consider user $k, k = 1, \ldots, K$. At the receiver side, user k decodes its intended information at slot k when its information is sent and harvests energy during all the other slots $i \neq k$. The receiver noise at each user is assumed to be independent over SCs and is modelled as a CSCG random variable with zero mean and variance σ^2 at all SCs. Moreover, the gap for the achievable rate from the channel capacity due to a practical modulation and coding scheme (MCS) is denoted by $\Gamma \geq 1$. The achievable rate in bps/Hz for the information receiver of user k is thus given by

$$R_k = \frac{\alpha_k}{N} \sum_{n=1}^{N} \log_2 \left(1 + \frac{h_{k,n} p_{k,n}}{\Gamma \sigma^2}\right). \tag{3.2}$$

Assuming that the conversion efficiency of the energy harvesting process at each

receiver is denoted by $0 < \zeta < 1$, the harvested energy in joule at the energy receiver of user k is thus given by

$$E_k = \zeta \sum_{i \neq k}^{K+1} \alpha_i \sum_{n=1}^{N} h_{k,n} p_{i,n}. \tag{3.3}$$

An example of the energy utilization at receivers for the TS case in a two-user OFDM-based SWIPT system is illustrated in Fig. 3.1. As shown in Fig. 3.1(a) for user 1, the received energy on all SCs during slot 1 is utilized for ID; while the received energy on all SCs during slot 2 and slot 3 is utilized for EH. In Fig. 3.1(b) for user 2, the received energy on all SCs during slot 2 is utilized for ID; while the received energy on all SCs during slot 1 and slot 3 is utilized for EH.

Our objective is to maximize the weighted sum-rate of all users by varying the transmission power in the time and frequency domains jointly with TS ratios, subject to EH constraints and the transmission power constraints. Thus, the following optimization problem is formulated.

$$\begin{aligned}
(\mathrm{P-TS}): \quad & \max_{\{p_{k,n}\},\{\alpha_k\}} \quad \frac{1}{N} \sum_{k=1}^{K} \sum_{n=1}^{N} w_k \alpha_k \log_2 \left(1 + \frac{h_{k,n} p_{k,n}}{\Gamma \sigma^2}\right) \\
& \texttt{s.t.} \quad \zeta \sum_{i \neq k}^{K+1} \alpha_i \sum_{n=1}^{N} h_{k,n} p_{i,n} \geq \overline{E}_k, \quad k = 1, \ldots, K, \\
& \qquad \sum_{k=1}^{K+1} \alpha_k \sum_{n=1}^{N} p_{k,n} \leq P, \\
& \qquad 0 \leq p_{k,n} \leq P_{\text{peak}}, k = 1, \ldots, K+1, \forall n, \\
& \qquad \sum_{k=1}^{K+1} \alpha_k \leq 1, \quad 0 \leq \alpha_k \leq 1, k = 1, \ldots, K+1,
\end{aligned}$$

where $w_k \geq 0$ denotes the non-negative rate weight assigned to user k.

Problem (P-TS) is feasible when all the constraints in Problem (P-TS) can be satisfied by some $\{\{p_{k,n}\}, \{\alpha_k\}\}$. From (3.3), the harvested energy at all users is maximized when $\alpha_{K+1} = 1$, while $\alpha_k = 0, p_{k,n} = 0$ for $k = 1, \ldots, K, n = 1, \ldots, N$, i.e., all users harvest energy during the entire transmission time. Therefore, Problem

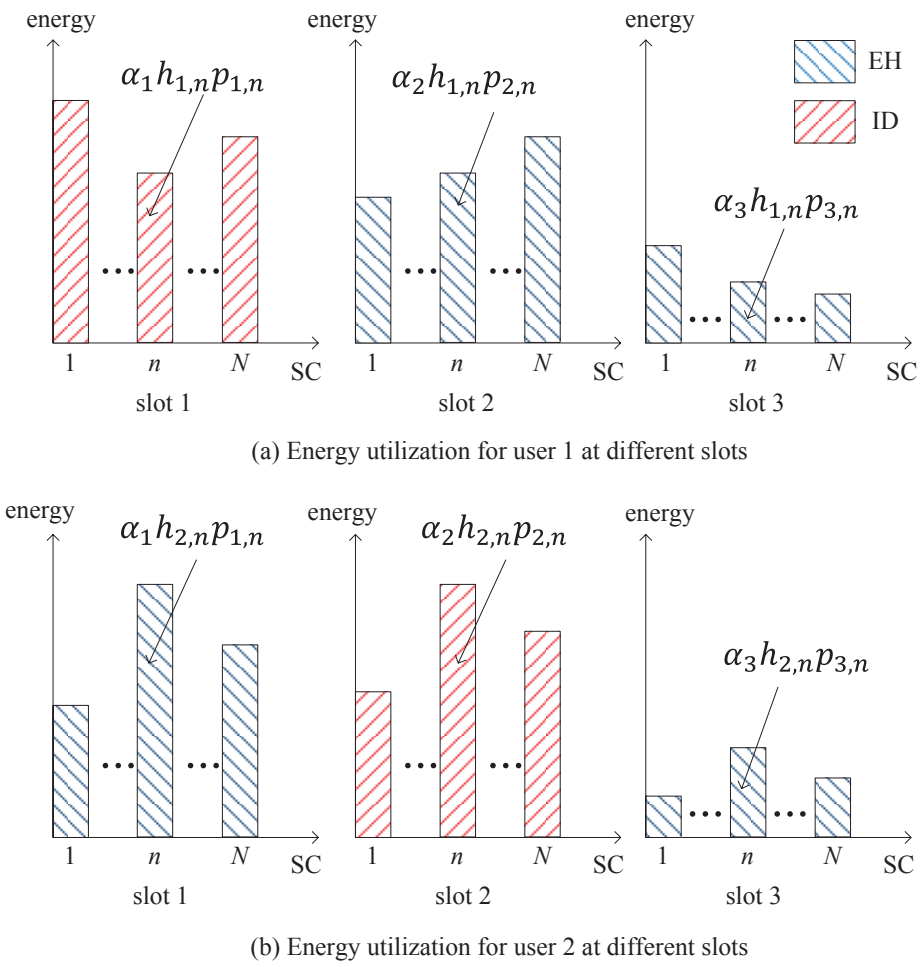

Figure 3.1: Energy utilization at receivers for a two-user OFDM-based SWIPT system: TDMA-based information transmission with TS applied at each receiver.

(P-TS) is feasible if and only if the following linear programming (LP) is feasible.

$$\begin{aligned} \underset{\{p_{K+1,n}\}}{\texttt{max.}} \quad & 0 \\ \texttt{s.t.} \quad & \zeta \sum_{n=1}^{N} h_{k,n} p_{K+1,n} \geq \overline{E}_k, \quad k = 1, \ldots, K, \\ & \sum_{n=1}^{N} p_{K+1,n} \leq P, \\ & 0 \leq p_{K+1,n} \leq P_{\text{peak}}, \quad n = 1, \ldots, N. \end{aligned} \tag{3.4}$$

It is easy to check the feasibility for the above LP. We thus assume Problem (P-TS) is feasible subsequently.

Problem (P-TS) is non-convex in its current form. We will solve this problem in Section 3.5.1.

3.3.2 Power Splitting

Next, we consider the case of OFDMA-based information transmission with PS applied at each receiver. As is standard in OFDMA transmissions, each SC is allocated to at most one user in each slot, i.e., no SC sharing is allowed. We define a SC allocation function $\Pi(n) \in \{1, \ldots, K\}$, i.e., the SC n is allocated to user $\Pi(n)$. The total transmission power constraint is given by

$$\sum_{n=1}^{N} p_n \leq P. \tag{3.5}$$

At the receiver, the received signal at user k is processed by a power splitter, where a ratio ρ_k of power is split to its energy receiver and the remaining ratio $1 - \rho_k$ is split to its information receiver, with $0 \leq \rho_k \leq 1, \forall k$. The achievable rate in bps/Hz at SC n assigned to user $\Pi(n)$ is thus

$$R_n = \log_2 \left(1 + \frac{(1 - \rho_{\Pi(n)}) h_{\Pi(n),n} p_n}{\Gamma \sigma^2} \right), \quad n = 1, \ldots, N. \tag{3.6}$$

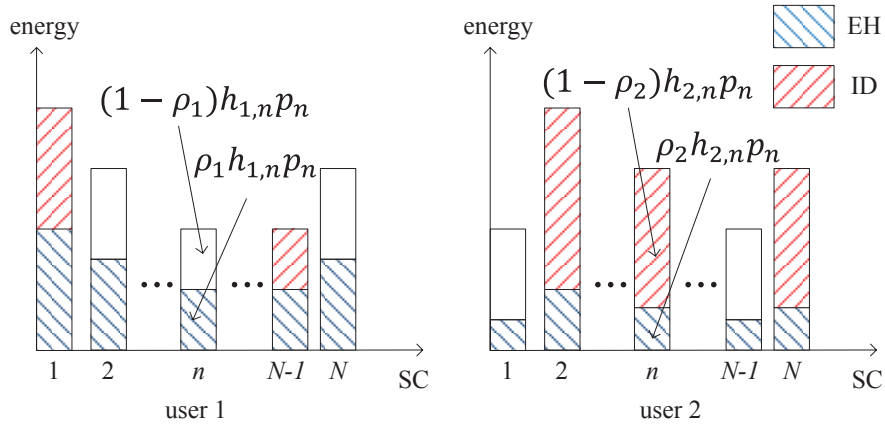

Figure 3.2: Energy utilization at receivers for a two-user OFDM-based SWIPT system: OFDMA-based information transmission with PS applied at each receiver.

With energy conversion efficiency ζ, the harvested energy in joule at the energy receiver of user k is thus given by

$$E_k = \rho_k \zeta \sum_{n=1}^{N} h_{k,n} p_n, \quad k = 1, \ldots, K. \tag{3.7}$$

An example of the energy utilization at receivers for the PS case in a two-user OFDM-based SWIPT system is illustrated in Fig. 3.2. As shown in Fig. 3.2, the received signals at all SCs share the same splitting ratio ρ_k at each user $k, k = 1, 2$. It is worth noting that only ρ_1 of the power at each of the SCs allocated to user 2 for ID is harvested by user 1, the remaining $1 - \rho_1$ of power at those SCs is neither utilized for EH nor ID at user 1, similarly as for user 2 with PS ratio ρ_2.

With the objective of maximizing the weighted sum-rate of all users by varying the transmission power in the frequency domain, the SC allocation, jointly with the PS ratios at receivers, subject to a given set of EH constraints and the transmission

power constraints, the following optimization problem is formulated.

$$
\begin{aligned}
(\mathrm{P}-\mathrm{PS}): \quad & \underset{\{p_n\},\{\Pi(n)\},\{\rho_k\}}{\mathtt{max.}} \quad \frac{1}{N}\sum_{n=1}^{N} w_{\Pi(n)} \log_2\left(1+\frac{(1-\rho_{\Pi(n)})h_{\Pi(n),n}p_n}{\Gamma\sigma^2}\right) \\
& \mathtt{s.t.} \quad \rho_k \zeta \sum_{n=1}^{N} h_{k,n}p_n \geq \overline{E}_k, \quad \forall k \\
& \qquad \sum_{n=1}^{N} p_n \leq P, \quad 0 \leq p_n \leq P_{\text{peak}}, \forall n \\
& \qquad 0 \leq \rho_k \leq 1, \quad \forall k.
\end{aligned}
$$

From (3.7), the harvested energy at all users is maximized when $\rho_k = 1, k = 1, \ldots, K$, i.e., all power is split to the energy receiver at each user. Therefore, Problem (P-PS) is feasible if and only if Problem (P-PS) with $\rho_k = 1, k = 1, \ldots, K$ is feasible. It is worth noting that Problem (P-PS) and Problem (P-TS) are subject to the same feasibility conditions as given by Problem (3.4).

It can be verified that Problem (P-PS) is non-convex in its current form. We will solve this problem in Section 3.5.2.

3.3.3 Performance Upper Bound

An upper bound for the optimization problems (P-TS) and (P-PS) can be obtained by assuming that each receiver is able to decode the information in its received signal and at the same time harvest the received energy without any implementation loss [7]. We thus consider the following optimization problem.

$$
\begin{aligned}
(\mathrm{P}-\mathrm{UB}): \quad & \underset{\{p_n\},\{\Pi(n)\}}{\mathtt{max.}} \quad \frac{1}{N}\sum_{n=1}^{N} w_{\Pi(n)} \log_2\left(1+\frac{h_{\Pi(n),n}p_n}{\Gamma\sigma^2}\right) \\
& \mathtt{s.t.} \quad \zeta \sum_{n=1}^{N} h_{k,n}p_n \geq \overline{E}_k, \quad \forall k \\
& \qquad \sum_{n=1}^{N} p_n \leq P, \quad 0 \leq p_n \leq P_{\text{peak}}, \forall n.
\end{aligned}
$$

Note that Problem (P-UB), as well as Problem (P-TS) and Problem (P-PS) are subject to the same feasibility conditions as given by Problem (3.4). Also note that any infeasible Problem (P-UB) can be modified to become a feasible one by increasing the transmission power P or by decreasing the minimum required harvested energy $\overline{E}_k$ at some user k. In the sequel, we assume that all the three problems are feasible, thus optimal solutions exist.

The solution for Problem (P-UB) is obtained in Section 3.5.2 (see Remark 3.5.2).

3.4 Resource Allocation in Single-User System

To obtain tractable analytical results, in this section, we consider the special case that $K = 1$, i.e., a single user OFDM-based SWIPT system. For brevity, $h_{1,n}$, $\overline{E}_1$, and ρ_1 are replaced with h_n, $\overline{E}$, and ρ, respectively. Without loss of generality, we assume that $h_1 \geq h_2 \geq \ldots \geq h_N$ and $w_1 = 1$. With $K = 1$, Problem (P-TS) and Problem (P-PS) are then simplified respectively as follows

$$\begin{aligned}
\underset{\{p_{1,n}\},\{p_{2,n}\},\alpha_1,\alpha_2}{\texttt{max.}} \quad & \frac{\alpha_1}{N}\sum_{n=1}^{N}\log_2\left(1+\frac{h_n p_{1,n}}{\Gamma\sigma^2}\right) \\
\texttt{s.t.} \quad & \zeta\alpha_2\sum_{n=1}^{N} h_n p_{2,n} \geq \overline{E}, \\
& \alpha_1\sum_{n=1}^{N} p_{1,n} + \alpha_2\sum_{n=1}^{N} p_{2,n} \leq P, \\
& 0 \leq p_{i,n} \leq P_{\text{peak}}, \quad \forall n, i = 1, 2, \\
& \alpha_1 + \alpha_2 \leq 1, \quad 0 \leq \alpha_i \leq 1, i = 1, 2.
\end{aligned} \tag{3.8}$$

$$\begin{aligned}
\max_{\{p_n\},\rho} \quad & \frac{1}{N}\sum_{n=1}^{N}\log_2\left(1+\frac{(1-\rho)h_n p_n}{\Gamma\sigma^2}\right) \\
\text{s.t.} \quad & \rho\zeta\sum_{n=1}^{N} h_n p_n \geq \overline{E}, \\
& \sum_{n=1}^{N} p_n \leq P, \\
& 0 \leq p_n \leq P_{\text{peak}}, \quad \forall n, \\
& 0 \leq \rho \leq 1.
\end{aligned} \tag{3.9}$$

To obtain useful insight, we first look at the two extreme cases, i.e., $P_{\text{peak}} \to \infty$ and $P_{\text{peak}} = P/N$. We shall see that the peak power constraint plays an important role in the performance comparison between the TS and PS schemes. Note that $P_{\text{peak}} \to \infty$ implies the case of no peak power constraint on each SC; and $P_{\text{peak}} = P/N$ implies the case of only peak power constraint on each SC, since the total power constraint is always satisfied and thus becomes redundant. Given P and P_{peak}, the maximum rates achieved by the TS scheme and the PS scheme are denoted by $R_{\text{TS}}(P, P_{\text{peak}})$ and $R_{\text{PS}}(P, P_{\text{peak}})$, respectively. For the case of $P_{\text{peak}} \to \infty$, we have the following proposition for the TS scheme. We recall that $\alpha_2 = 1 - \alpha_1$ is the TS ratio for the power slot.

Proposition 3.4.1. *Assuming $\overline{E} > 0$, in the case of a single-user OFDM-based SWIPT system with $P_{\text{peak}} \to \infty$, the maximum rate by the TS scheme, i.e., $R_{\text{TS}}(P, \infty)$, is achieved by $\alpha_1 \to 1$ and $\alpha_2 \to 0$.*

Proof. Clearly, we have $\alpha_2 > 0$; otherwise, no energy is harvested, which violates the EH constraint $\overline{E} > 0$. Thus, $\alpha_1 < 1$. To maximize the objective function subject to the EH constraint, it can be easily shown that the optimal α_2 and $p_{2,n}$ should satisfy $\zeta\alpha_2 h_1 p_{2,1} = \overline{E}$ and $p_{2,n} = 0, n = 2, \ldots, N$. It follows that the minimum transmission energy consumed to achieve the harvested energy $\overline{E}$ is given by $\overline{E}/(\zeta h_1)$, i.e., $\alpha_2 \sum_{n=1}^{N} p_{2,n} \geq \overline{E}/(\zeta h_1)$. Thus, in Problem (3.8), the achievable rate $R_{\text{TS}}(P, \infty)$ is given by maximizing $\frac{\alpha_1}{N}\sum_{n=1}^{N}\log_2\left(1+\frac{h_n p_{1,n}}{\Gamma\sigma^2}\right)$ subject

to $\alpha_1 \sum_{n=1}^{N} p_{1,n} \leq P - \overline{E}/(\zeta h_1)$ and $0 \leq \alpha_1 < 1$. Let $q_{1,n} = \alpha_1 p_{1,n}, \forall n$, the above problem is then equivalent to maximizing $\frac{\alpha_1}{N} \sum_{n=1}^{N} \log_2 \left(1 + \frac{h_n q_{1,n}}{\Gamma \sigma^2 \alpha_1}\right)$ subject to $\sum_{n=1}^{N} q_{1,n} \leq P - \overline{E}/(\zeta h_1)$ and $0 \leq \alpha_1 < 1$. For given $\{q_{1,n}\}$, the objective function is an increasing function of α_1; thus, $R_{\text{TS}}(P, \infty)$ is maximized when $\alpha_1 \to 1$. It follows that $\alpha_2 \to 0$, which completes the proof. □

Remark 3.4.1. By Proposition 3.4.1, to achieve $R_{\text{TS}}(P, \infty)$ with $\overline{E} > 0$, the portion of transmission time α_2 allocated to EH in each transmission block should asymptotically go to zero. For example, let m denote the number of transmitted symbols in each block, by allocating $O(\log m)$ symbols for EH in each block and the remaining symbols for ID results in $\alpha = \log m/m \to 0$ as $m \to \infty$, which satisfies the optimality condition provided in Proposition 3.4.1. It is worth noting that $R_{\text{TS}}(P, \infty)$ is achieved under the assumption that the transmitter and receiver are able to operate in the regime of infinite power in the EH time slot due to $\alpha_2 \to 0$. For a finite P_{peak}, a nonzero time ratio should be scheduled to the power slot to collect sufficient energy to satisfy the EH constraint.

Moreover, we have the following proposition showing that the PS scheme performs no better than the TS scheme for the case of $P_{\text{peak}} \to \infty$.

Proposition 3.4.2. *In the case of a single-user OFDM-based SWIPT system with $P_{\text{peak}} \to \infty$, the maximum rate achieved by the PS scheme is no larger than that achieved by the TS scheme, i.e., $R_{\text{PS}}(P, \infty) \leq R_{\text{TS}}(P, \infty)$.*

Proof. For the PS scheme, from the EH constraint $\rho\zeta \sum_{n=1}^{N} h_n p_n \geq \overline{E}$, it follows that $\rho \geq \overline{E}/(\zeta h_1 P)$ must hold. Thus, $R_{\text{PS}}(P, \infty)$ is upper bounded by maximizing $\frac{1}{N} \sum_{n=1}^{N} \log_2 \left(1 + \frac{(1-\rho) h_n p_n}{\Gamma \sigma^2}\right)$ subject to $\rho \geq \overline{E}/(\zeta h_1 P)$ and $\sum_{n=1}^{N} p_n \leq P$. Let $p'_n = (1 - \rho) p_n, \forall n$, the above problem is then equivalent to maximizing $\frac{1}{N} \sum_{n=1}^{N} \log_2 \left(1 + \frac{h_n p'_n}{\Gamma \sigma^2}\right)$ subject to $\rho \geq \overline{E}/(\zeta h_1 P)$ and $\sum_{n=1}^{N} p'_n \leq (1 - \rho) P$. Since $\rho \geq \overline{E}/(\zeta h_1 P)$, it follows that $(1 - \rho) P \leq P - \overline{E}/(\zeta h_1)$. Note that according to Proposition 3.4.1,

$R_{\text{TS}}(P,\infty)$ is obtained (with $\alpha_1 \to 1$) by maximizing $\frac{1}{N}\sum_{n=1}^{N}\log_2\left(1+\frac{h_n p_{1,n}}{\Gamma\sigma^2}\right)$ subject to $\sum_{n=1}^{N} p_{1,n} \leq P - \overline{E}/(\zeta h_1)$. Therefore, we have $R_{\text{PS}}(P,\infty) \leq R_{\text{TS}}(P,\infty)$. □

For the other extreme case when $P_{\text{peak}} = P/N$, we have the following proposition.

Proposition 3.4.3. *In the case of a single-user OFDM-based SWIPT system with $P_{\text{peak}} = P/N$, the maximum rate achieved by the TS scheme is no larger than that achieved by the PS scheme, i.e., $R_{\text{TS}}(P,P/N) \leq R_{\text{PS}}(P,P/N)$.*

Proof. With $P_{\text{peak}} = P/N$, the total power constraint is redundant for both TS and PS. Thus, the optimal power allocation for TS is given by $p_{1,n}^* = p_{2,n}^* = P_{\text{peak}}, \forall n$. It follows that $\alpha_2 \geq \frac{\overline{E}}{\zeta P_{\text{peak}}\sum_{n=1}^{N} h_n}$. Then we have the optimal $\alpha_1^* = 1 - \frac{\overline{E}}{\zeta P_{\text{peak}}\sum_{n=1}^{N} h_n}$. $R_{\text{TS}}(P,P/N)$ is thus given by $\frac{\alpha_1^*}{N}\sum_{n=1}^{N}\log_2\left(1+\frac{h_n P_{\text{peak}}}{\Gamma\sigma^2}\right)$. On the other hand, the optimal power allocation for PS is given by $p_n^* = P_{\text{peak}}, \forall n$. It follows that $\rho^* = \frac{\overline{E}}{\zeta P_{\text{peak}}\sum_{n=1}^{N} h_n} = 1-\alpha_1^*$. $R_{\text{PS}}(P,P/N)$ is thus given by $\frac{1}{N}\sum_{n=1}^{N}\log_2\left(1+\frac{\alpha_1^* h_n P_{\text{peak}}}{\Gamma\sigma^2}\right)$. Due to the concavity of the logarithm function, we have $R_{\text{TS}}(P,P/N) \leq R_{\text{PS}}(P,P/N)$, which completes the proof. □

In fact, from the proof of Proposition 3.4.3, we have $R_{\text{TS}}(P,P/N) \leq R_{\text{PS}}(P,P/N)$ provided that equal power allocation (not necessarily equals to P_{peak}) over all SCs are employed for both TS and PS schemes. Note that for a single-user OFDM-based SWIPT system with $P/N < P_{\text{peak}} < \infty$, the performance comparison between the TS scheme and the PS scheme remains unknown analytically. From Proposition 3.4.2 and Proposition 3.4.3, neither the TS scheme nor the PS scheme is always better. It suggests that for a single-user OFDM-based SWIPT system with sufficiently small peak power, the PS scheme may be better; with sufficiently large peak power, the TS scheme may be better.

For the special case that $N = 1$, i.e., a single-carrier point-to-point SWIPT system, the following proposition shows that: for $P_{\text{peak}} \to \infty$, the TS and PS schemes

achieve the same rate; for a finite peak power $P/N \leq P_{\text{peak}} < \infty$, the TS scheme performs no better than the PS scheme.

Proposition 3.4.4. *In the case of a single-carrier point-to-point SWIPT system with $N = 1$, we have $R_{\text{TS}}(P, P_{\text{peak}}) \leq R_{\text{PS}}(P, P_{\text{peak}})$, with equality if $P_{\text{peak}} \to \infty$.*

Proof. Since $N = 1$, we remove the SC index n in the subscripts of h_n, $p_{1,n}$, $p_{2,n}$ and p_n. For the PS scheme, to satisfy the EH constraint, we have $\rho \geq \overline{E}/(\zeta h P)$; thus, with $\rho = \overline{E}/(\zeta h P)$, the maximum rate by the PS scheme is given by $R_{\text{PS}}(P, P_{\text{peak}}) = \log_2\left(1 + \frac{hP - \overline{E}/\zeta}{\Gamma\sigma^2}\right)$. For the TS scheme, we have $\alpha_2 p_2 \geq \overline{E}/(\zeta h)$ to satisfy the EH constraint. It follows that $\alpha_1 p_1 \leq P - \overline{E}/(\zeta h)$. Therefore, $R_{\text{TS}}(P, P_{\text{peak}}) \leq \alpha_1 \log_2\left(1 + \frac{hP - \overline{E}/\zeta}{\alpha_1 \Gamma\sigma^2}\right) \leq R_{\text{PS}}(P, P_{\text{peak}})$, and the equality holds if $\alpha_1 \to 1$. By Proposition 3.4.1, $R_{\text{TS}}(P, \infty)$ is achieved by $\alpha_1 \to 1$; thus, the above equality holds if $P_{\text{peak}} \to \infty$, which completes the proof. □

Figs. 3.3 and 3.4 show the achievable rates by different schemes versus different minimum required harvested energy $\overline{E}$. For Fig. 3.3, the total bandwidth is assumed to be 10MHz, which is equally divided as $N = 64$ SCs. The six-tap exponentially distributed power profile is used to generate the frequency-selective fading channel. For Fig. 3.4 with $N = 1$, i.e., a single-carrier point-to-point SWIPT system, the bandwidth is assumed to be 1MHz. For both figures, the transmit power is assumed to be 1W or 30dBm. The distance from the transmitter to the receiver is 1m, which results in -31.5dB path-loss for all the channels at a carrier frequency 900MHz with path-loss exponent equal to 3. For the energy receivers, it is assumed that $\zeta = 0.2$. For the information receivers, the noise spectral density is assumed to be -112dBm/Hz. The MCS gap is assumed to be $\Gamma = 9$dB.

In both Fig. 3.3 and Fig. 3.4, it is observed that for both TS and PS schemes, the achievable rate decreases as the minimum required harvested energy $\overline{E}$ increases, since the available energy for information decoding decreases as $\overline{E}$ increases. In Fig. 3.3 with $N = 64$, it is observed that there is a significant gap between the achievable rate by TS with $P_{\text{peak}} = 4P/N$ and that by TS with $P_{\text{peak}} \to \infty$; moreover, the gap increases as $\overline{E}$ increases. This is because that with $P_{\text{peak}} \to \infty$, all transmission

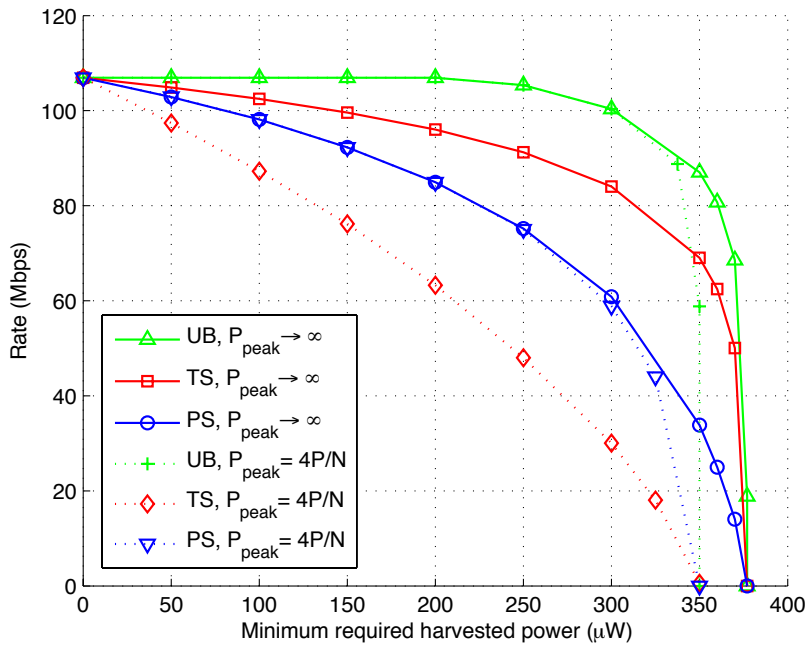

Figure 3.3: Achievable rate versus minimum required harvested energy in a single-user OFDM-based SWIPT system, where $N = 64$.

time can be utilized for information decoding by letting $\alpha_1 \to 1$ (c.f. Proposition 3.4.1); whereas for a finite $P_{\text{peak}} = 4P/N$, a nonzero transmission time needs to be scheduled for energy harvesting. For the PS scheme, this performance gap due to finite peak power constraint is only observed when $\overline{E}$ is sufficiently large. Comparing the TS and PS schemes in Fig. 3.3, it is observed that TS outperforms PS when $P_{\text{peak}} \to \infty$; however, for sufficiently small P_{peak}, e.g., $P_{\text{peak}} = 4P/N$, PS outperforms TS. In Fig. 3.4 with $N = 1$, it is observed that when $P_{\text{peak}} \to \infty$, the achievable rate by the TS scheme is the same as that by the PS scheme; when $P_{\text{peak}} = 4P$, the achievable rate by the TS scheme is no larger than that by the PS scheme, which is in accordance with Proposition 3.4.4.

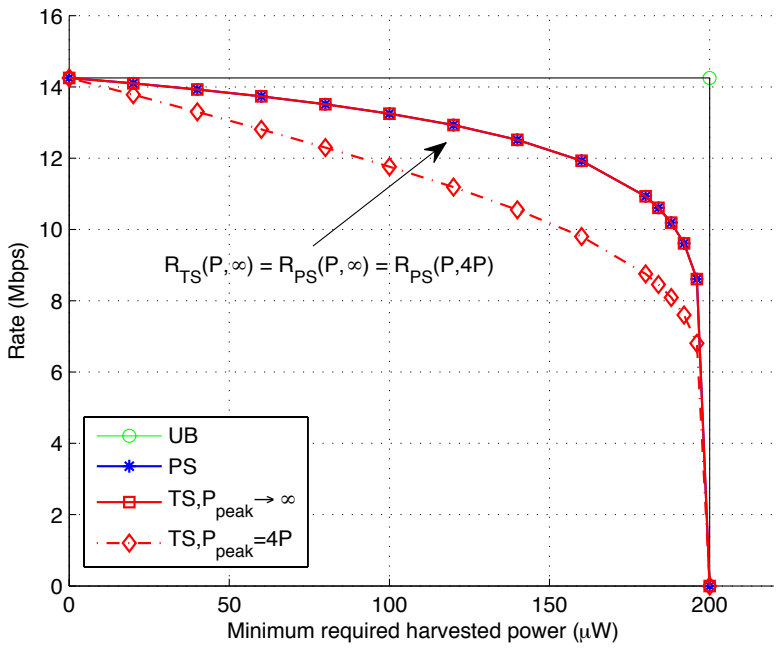

Figure 3.4: Achievable rate versus minimum required harvested energy in a single-carrier point-to-point SWIPT system, i.e., $N = 1$.

3.5 Resource Allocation in Multiuser System

In this section, we consider the general case of an OFDM-based SWIPT system with multiple users. We derive the optimal transmission strategies for the two schemes proposed in Section 3.3, and compare their performances.

3.5.1 Time Switching

We first reformulate Problem (P-TS) by introducing a set of new non-negative variables: $q_{k,n} = \alpha_k p_{k,n}, k = 1, \ldots, K+1, n = 1, \ldots, N$. Moreover, we define $\alpha_k \log_2\left(1 + \frac{h_{k,n} q_{k,n}}{\Gamma \sigma^2 \alpha_k}\right) = 0$ at $\alpha_k = 0$ to keep continuity at $\alpha_k = 0$. (P-TS) is thus

equivalent to the following problem:[1]

$$\begin{aligned}
\max_{\{q_{k,n}\},\{\alpha_k\}} \quad & \frac{1}{N}\sum_{k=1}^{K}\sum_{n=1}^{N} w_k\alpha_k \log_2\left(1+\frac{h_{k,n}q_{k,n}}{\Gamma\sigma^2\alpha_k}\right) \\
\text{s.t.} \quad & \zeta\sum_{i\neq k}^{K+1}\sum_{n=1}^{N} h_{k,n}q_{i,n} \geq \overline{E}_k, \quad k=1,\ldots,K, \\
& \sum_{k=1}^{K+1}\sum_{n=1}^{N} q_{k,n} \leq P, \\
& 0 \leq q_{k,n} \leq \alpha_k P_{\text{peak}}, k=1,\ldots,K+1, \forall n, \\
& \sum_{k=1}^{K+1} \alpha_k \leq 1,\ 0 \leq \alpha_k \leq 1, k=1,\ldots,K+1. \qquad (3.10)
\end{aligned}$$

After finding the optimal $\{q^*_{k,n}\}$ and $\{\alpha^*_k\}$ for Problem (3.10), the optimal power allocation $\{p^*_{k,n}\}$ for Problem (P-TS) is given by $p^*_{k,n} = q^*_{k,n}/\alpha^*_k, k=1,\ldots,K+1, n=1,\ldots,N$ provided that $\alpha^*_k > 0$. From the constraint $0 \leq q_{k,n} \leq \alpha_k P_{\text{peak}}, k=1,\ldots,K+1, n=1,\ldots,N$, we have $q_{k,n}=0$ if $\alpha_k=0$ and $P_{\text{peak}}<\infty$. Thus, if $\alpha^*_k=0, k=1,\ldots,K+1$ and $P_{\text{peak}}<\infty$, the allocated power will be $p^*_{k,n}=0, n=1\ldots,N$, since no information/power transmission is scheduled at slot k. For the extreme case of $P_{\text{peak}}\to\infty$, if $q^*_{k,n}=0, \alpha^*_k=0, k=1,\ldots,K+1, n=1,\ldots,N$, then the allocated power will be $p^*_{k,n}=0$; if $q^*_{k,n}>0$ and $\alpha^*_k=0$, then we have $p^*_{k,n}\to\infty$.

Lemma 3.5.1. *Function $f(q_{k,n},\alpha_k)$ is jointly concave in $\alpha_k \geq 0$ and $q_{k,n} \geq 0$, where*

$$f(q_{k,n},\alpha_k) = \begin{cases} \alpha_k \log_2\left(1+\frac{h_{k,n}q_{k,n}}{\Gamma\sigma^2\alpha_k}\right), & \alpha_k > 0, \\ 0, & \alpha_k = 0. \end{cases} \qquad (3.11)$$

Proof. Please refer to Appendix E. □

From Lemma 3.5.1, as a non-negative weighted sum of $f(q_{k,n},\alpha_k)$, the new objective function of Problem (3.10) is jointly concave in $\{\alpha_k\}$ and $\{q_{k,n}\}$. Since the

[1]Similar to the single-user system (c.f. Remark 3.4.1), for the case of $P_{\text{peak}}\to\infty$, we allow $\alpha_k\to 0$ while $q_{k,n}>0$ by letting $p_{k,n}\to\infty$.

constraints are now all affine, Problem (3.10) is convex, and thus can be optimally solved by applying the Lagrange duality method, as will be shown next.

The Lagrangian of Problem (3.10) is given by

$$\mathcal{L}\left(\{q_{k,n}\},\{\alpha_k\},\{\lambda_i\},\mu,\nu\right)=\frac{1}{N}\sum_{k=1}^{K}\sum_{n=1}^{N}w_k\alpha_k\log_2\left(1+\frac{h_{k,n}q_{k,n}}{\Gamma\sigma^2\alpha_k}\right)$$
$$+\sum_{i=1}^{K}\lambda_i\left(\zeta\sum_{k\neq i}^{K+1}\sum_{n=1}^{N}h_{i,n}q_{k,n}-\overline{E}_i\right)+\mu\left(P-\sum_{k=1}^{K+1}\sum_{n=1}^{N}q_{k,n}\right)+\nu\left(1-\sum_{k=1}^{K+1}\alpha_k\right) \tag{3.12}$$

where $\lambda_i, i=1,\ldots,K$, μ, and ν are the non-negative dual variables associated with the corresponding constraints in (3.10). The dual function $g\left(\{\lambda_i\},\mu,\nu\right)$ is then defined as the optimal value of the following problem.

$$\begin{aligned}\max_{\{q_{k,n}\},\{\alpha_k\}}\quad & \mathcal{L}\left(\{q_{k,n}\},\{\alpha_k\},\{\lambda_i\},\mu,\nu\right)\\ \text{s.t.}\quad & 0\leq q_{k,n}\leq\alpha_k P_{\text{peak}},\ k=1,\ldots,K+1,\forall n,\\ & 0\leq\alpha_k\leq 1,\quad k=1,\ldots,K+1.\end{aligned} \tag{3.13}$$

The dual problem is thus defined as $\min_{\{\lambda_i\},\mu,\nu} g\left(\{\lambda_i\},\mu,\nu\right)$.

First, we consider the maximization problem in (3.13) for obtaining $g\left(\{\lambda_i\},\mu,\nu\right)$ with a given set of $\{\lambda_i\}$, μ, and ν. We define $\mathcal{L}_k, k=1,\ldots,K$ as

$$\begin{aligned}\mathcal{L}_k :=&\frac{w_k\alpha_k}{N}\sum_{n=1}^{N}\log_2\left(1+\frac{h_{k,n}q_{k,n}}{\Gamma\sigma^2\alpha_k}\right)+\zeta\sum_{i\neq k}^{K}\lambda_i\sum_{n=1}^{N}h_{i,n}q_{k,n}\\ &-\mu\sum_{n=1}^{N}q_{k,n}-\nu\alpha_k,\quad 1\leq k\leq K\end{aligned} \tag{3.14}$$

We define $\mathcal{L}_k, k=K+1$ as

$$\mathcal{L}_k:=\zeta\sum_{i=1}^{K}\lambda_i\sum_{n=1}^{N}h_{i,n}q_{k,n}-\mu\sum_{n=1}^{N}q_{k,n}-\nu\alpha_k,\quad k=K+1. \tag{3.15}$$

Then for the Lagrangian in (3.12), we have

$$\mathcal{L} = \sum_{k=1}^{K+1} \mathcal{L}_k - \sum_{i=1}^{K} \lambda_i \overline{E}_i + \mu P + \nu. \tag{3.16}$$

Thus, for each given k, the maximization problem in (3.13) can be decomposed as

$$\begin{aligned} \underset{\{q_{k,n}\},\alpha_k}{\texttt{max.}} \quad & \mathcal{L}_k \\ \texttt{s.t.} \quad & 0 \le q_{k,n} \le \alpha_k P_{\text{peak}}, \ n = 1, \ldots, N \\ & 0 \le \alpha_k \le 1. \end{aligned} \tag{3.17}$$

We first study the solution for Problem (3.17) with given $k = 1, \ldots, K$. From (3.14) and (3.15), we have

$$\frac{\partial \mathcal{L}_k}{\partial q_{k,n}} = \frac{w_k \alpha_k h_{k,n}}{N(\Gamma \sigma^2 \alpha_k + h_{k,n} q_{k,n}) \ln 2} + \zeta \sum_{i \neq k}^{K} \lambda_i h_{i,n} - \mu, \forall n. \tag{3.18}$$

Given $\alpha_k, k = 1, \ldots, K$, the $q_{k,n}, n = 1, \ldots, N$ that maximizes $\mathcal{L}_k$ can be obtained by setting $\frac{\partial \mathcal{L}_k}{\partial q_{k,n}} = 0$ to give

$$q_{k,n} = \alpha_k \min \left(\left(\frac{w_k}{N \left(\mu - \zeta \sum\limits_{i \neq k}^{K} \lambda_i h_{i,n} \right) \ln 2} - \frac{\Gamma \sigma^2}{h_{k,n}} \right)^+, P_{\text{peak}} \right). \tag{3.19}$$

For given $\{q_{k,n}\}$, it appears that there is no closed-form expression for the optimal α_k that maximizes $\mathcal{L}_k$. However, since $\mathcal{L}_k$ is a concave function of α_k with given $\{q_{k,n}\}$, α_k can be found numerically by a simple bisection search over $0 \le \alpha_k \le 1$. To summarize, for given $k = 1, \ldots, K$, Problem (3.17) can be solved by iteratively optimizing between $\{q_{k,n}\}$ and α_k with one of them fixed at one time, which is known to as block-coordinate descent method [41].

Next, we study the solution for Problem (3.17) for $k = K+1$, i.e., for the power

slot, which is a LP. Define the set $\mathcal{N}_1 = \left\{ n \in \mathcal{N} : \zeta \sum_{i=1}^{K} \lambda_i h_{i,n} - \mu > 0 \right\}$. From (3.14) and (3.15), to maximize $\mathcal{L}_{K+1}$ we have

$$q_{K+1,n} = \begin{cases} \alpha_{K+1} P_{\text{peak}}, & n \in \mathcal{N}_1, \\ 0, & n \in \mathcal{N} \backslash \mathcal{N}_1 \end{cases} \tag{3.20}$$

and

$$\alpha_{K+1} = \begin{cases} 1, & \text{if } \sum_{n \in \mathcal{N}_1} \left(\zeta \sum_{i=1}^{K} \lambda_i h_{i,n} - \mu \right) P_{\text{peak}} - \nu > 0, \\ 0, & \text{otherwise.} \end{cases} \tag{3.21}$$

After obtaining $g(\{\lambda_i\}, \mu, \nu)$ with given $\{\lambda_i\}$, μ, and ν, the minimization of $g(\{\lambda_i\}, \mu, \nu)$ over $\{\lambda_i\}$, μ, and ν can be efficiently solved by the ellipsoid method [42]. A subgradient of this problem required for the ellipsoid method is provided by the following proposition.

Proposition 3.5.1. *For Problem (3.10) with a dual function $g(\{\lambda_i\}, \mu, \nu)$, the following choice of $\boldsymbol{d}$ is a subgradient for $g(\{\lambda_i\}, \mu, \nu)$:*

$$d_i = \begin{cases} \zeta \sum_{k \neq i}^{K+1} \sum_{n=1}^{N} h_{i,n} \dot{q}_{k,n} - \overline{E}_i, & i = 1, \ldots, K, \\ P - \sum_{k=1}^{K+1} \sum_{n=1}^{N} \dot{q}_{k,n}, & i = K+1, \\ 1 - \sum_{k=1}^{K+1} \dot{\alpha}_k, & i = K+2. \end{cases} \tag{3.22}$$

where $\{\dot{q}_{k,n}\}$ and $\{\dot{\alpha}_k\}$ is the solution of the maximization problem (3.13) with given $\{\lambda_i\}, \mu$ and ν.

Proof. Please refer to Appendix F. □

Note that the optimal $q^*_{k,n}, k = 1 \ldots, K, n = 1, \ldots, N$ and $\alpha^*_k, k = 1, \ldots, K$ are obtained at optimal $\{\lambda^*_i\}$, μ^*, and ν^*. Given $\{q_{k,n}\}$, the objective function in Problem (3.10) is an increasing function of $\alpha_k, k = 1, \ldots, K$. Thus, the optimal

α_k^*'s, $k = 1, \ldots, K+1$ satisfy $\sum_{k=1}^{K+1} \alpha_k^* = 1$; otherwise, the objective can be improved by increasing some of the α_k's, $k = 1, \ldots, K$. Then, the optimal α_{K+1} is given by $\alpha_{K+1}^* = 1 - \sum_{k=1}^{K} \alpha_k^*$. With $\alpha_k = \alpha_k^*, k = 1, \ldots, K+1$, $q_{k,n} = q_{k,n}^*, k = 1, \ldots, K, n = 1, \ldots, N$, Problem (3.10) becomes a LP with variables $\{q_{K+1,n}\}$. The optimal values of $\{q_{K+1,n}\}$ are obtained by solving this LP.

To summarize, one algorithm to solve (P-TS) is given in Table 3.1. For the algorithm given in Table 3.1, the computation time is dominated by the ellipsoid method in steps I)-III) and the LP in step V). In particular, the time complexity of steps 1)-3) is of order K^2N, step 4) is of order N, step 5) is of order K^2N, and step 6) is of order K^2. Thus, the time complexity of steps 1)-6) is of order K^2N, i.e., $\mathcal{O}(K^2N)$. Note that step II) iterates $\mathcal{O}(K^2)$ to converge [42], thus the time complexity of steps I)-III) is $\mathcal{O}(K^4N)$. The time complexity of the LP in step V) is $\mathcal{O}(KN^2 + N^3)$ [43]. Therefore, the time complexity of the algorithm in Table 3.1 is $\mathcal{O}(K^4N + KN^2 + N^3)$.

Similar with the single-user case, we have the following proposition.

Proposition 3.5.2. *In the case of a multiuser OFDM-based SWIPT system with $K \geq 2$ and $P_{\text{peak}} \to \infty$, the maximum rate by the TS scheme, i.e., $R_{\text{TS}}(P, \infty)$, is achieved by $\alpha_{K+1} = 0$ or $\alpha_{K+1} \to 0$.*

Proof. In the equivalent Problem (3.10) with $P_{\text{peak}} \to \infty$, the EH constraints and the total power constraint are independent of $\alpha_k, k = 1, \ldots, K+1$. The objective in Problem (3.10) is an increasing function of $\alpha_k, k = 1, \ldots, K$ for given $\{q_{k,n}\}$. Thus, the maximum achievable rate is obtained by minimizing the time allocated to the power slot, i.e., $\alpha_{K+1} = 0$ (when $q_{K+1,n}^* = 0, \forall n$) or $\alpha_{K+1} \to 0$ (when $q_{K+1,n}^* > 0$ for some n). □

It is worth noting that for the multiuser system with $K \geq 2$ and $P_{\text{peak}} \to \infty$, it is possible that the maximum rate by the TS scheme is achieved by $\alpha_{K+1} = 0$, in which case no additional power slot is scheduled and all users simply harvest energy at the slot scheduled for other users to transmit information. In contrast, for the

Table 3.1: Algorithm for solving Problem (P-TS).

I) Initialize $\{\lambda_i > 0\}$, $\mu > 0$ and $\nu > 0$.

II) **repeat**

1) Initialize $\alpha_k = 1/K, k = 1, \ldots, K$.
2) **repeat**
   a) For $k = 1, \ldots, K$, compute $\{q_{k,n}\}$ by (3.19).
   b) For $k = 1, \ldots, K$, obtain α_k that maximizes $\mathcal{L}_k$ with given $\{q_{k,n}\}$ by bisection search.
3) **until** improvement of $\mathcal{L}_k, k = 1, \ldots, K$ converges to a prescribed accuracy.
4) Compute $\{q_{K+1,n}\}$ and α_{K+1} by (3.20) and (3.21).
5) Compute the subgradient of $g(\{\lambda_i\}, \mu, \nu)$ by (3.22).
6) Update $\{\lambda_i\}$, μ and ν according to the ellipsoid method.

III) **until** $\{\lambda_i\}$, μ and ν converge to a prescribed accuracy.

IV) Set $q^*_{k,n} = q_{k,n}, k = 1, \ldots, K, n = 1, \ldots, N$, $\alpha^*_k = \alpha_k, k = 1, \ldots, K$ and $\alpha^*_{K+1} = 1 - \sum_{k=1}^{K} \alpha^*_k$.

V) Obtain $q^*_{K+1,n}, n = 1, \ldots, N$ by solving Problem (3.10) with $\alpha_k = \alpha^*_k, k = 1, \ldots, K+1$, $q_{k,n} = q^*_{k,n}, k = 1, \ldots, K, n = 1, \ldots, N$.

VI) For $k = 1, \ldots, K+1$ and $n = 1, \ldots, N$, if $\alpha^*_k > 0$, set $p^*_{k,n} = q^*_{k,n}/\alpha^*_k$; if $\alpha^*_k = 0$ and $q^*_{k,n} = 0$, set $p^*_{k,n} = 0$; if $\alpha^*_k = 0$ and $q^*_{k,n} > 0$, set $p^*_{k,n} \to \infty$.

single-user $K = 1$ case, the power slot is always needed if $\overline{E} > 0$.

Remark 3.5.1. In Problem (3.10), when $K \geq 2$ and $\overline{E}_k = 0, k = 1, \ldots, K$, the system becomes a conventional TDMA system without EH constraints. Assume that the harvesting energy at each user by the optimal transmission strategy for this system is given by $E_k^{\text{th}}, k = 1, \ldots, K$. Then for a system with $0 \leq \overline{E}_k \leq E_k^{\text{th}}, k = 1, \ldots, K$, the same rate as that by the conventional TDMA system can be achieved.

3.5.2 Power Splitting

Since Problem (P-PS) is non-convex, the optimal solution may be computationally difficult to obtain. Instead, we propose a suboptimal algorithm to this problem by iteratively optimizing $\{p_n\}$ and $\{\Pi(n)\}$ with fixed $\{\rho_k\}$, and optimizing $\{\rho_k\}$ with fixed $\{p_n\}$ and $\{\Pi(n)\}$.

Note that (P-PS) with given $\{p_n\}$ and $\{\Pi(n)\}$ is a convex problem, of which the objective function is a nonincreasing function of $\rho_k, \forall k$. Thus, the optimal power splitting ratio solution for (P-PS) with a given set of feasible $\{p_n\}$ and $\{\Pi(n)\}$ is obtained as

$$\rho_k = \frac{\overline{E}_k}{\zeta \sum\limits_{n=1}^{N} h_{k,n} p_n}, \quad k = 1, \ldots, K. \tag{3.23}$$

Next, consider (P-PS) with a given set of feasible ρ_k's, i.e.,

$$\begin{aligned} \max_{\{p_n\},\{\Pi(n)\}} \quad & \frac{1}{N} \sum_{n=1}^{N} w_{\Pi(n)} \log_2 \left(1 + \frac{h_{\Pi(n),n}^{\text{ID}} p_n}{\Gamma \sigma^2} \right) \\ \text{s.t.} \quad & \zeta \sum_{n=1}^{N} h_{k,n}^{\text{EH}} p_n \geq \overline{E}_k, \quad k = 1, \ldots, K, \\ & \sum_{n=1}^{N} p_n \leq P, \quad 0 \leq p_n \leq P_{\text{peak}}, n = 1, \ldots, N \end{aligned} \tag{3.24}$$

where $h_{k,n}^{\text{ID}} \triangleq (1 - \rho_k) h_{k,n}, \forall k, n$ and $h_{k,n}^{\text{EH}} \triangleq \rho_k h_{k,n}, \forall k, n$ can be viewed as the equivalent channel power gains for the information and energy receivers, respectively.

The problem in (3.24) is non-convex, due to the integer SC allocation $\Pi(n)$. However, it has been shown that the duality gap of a similar problem to (3.24) without the harvested energy constrains converges to zero as the number of SCs, N, increases to infinity [44, 45]. Thus, we solve Problem (3.24) by applying the Lagrange duality method assuming that it has a zero duality gap.[2]

The Lagrangian of Problem (3.24) is given by

$$\begin{aligned}\mathcal{L}\left(\{p_n\},\{\Pi(n)\},\{\lambda_k\},\mu\right) &= \frac{1}{N}\sum_{n=1}^{N} w_{\Pi(n)}\log_2\left(1+\frac{h^{\mathrm{ID}}_{\Pi(n),n}p_n}{\Gamma\sigma^2}\right)\\ &+\sum_{k=1}^{K}\lambda_k\left(\zeta\sum_{n=1}^{N}h^{\mathrm{EH}}_{k,n}p_n-\overline{E}_k\right)+\mu\left(P-\sum_{n=1}^{N}p_n\right)\end{aligned} \tag{3.25}$$

where λ_k's and μ are the non-negative dual variables associated with the corresponding constraints in (3.24). The dual function is then defined as

$$g\left(\{\lambda_k\},\mu\right)=\max_{\{p_n\},\{\Pi(n)\}}\mathcal{L}\left(\{p_n\},\{\Pi(n)\},\{\lambda_k\},\mu\right). \tag{3.26}$$

The dual problem is thus given by $\min_{\{\lambda_k\},\mu} g\left(\{\lambda_k\},\mu\right)$.

Consider the maximization problem in (3.26) for obtaining $g\left(\{\lambda_k\},\mu\right)$ with a given set of $\{\lambda_k\}$ and μ. For each given SC n, the maximization problem in (3.26) can be decomposed as

$$\begin{aligned}\max_{p_n,\Pi(n)}\quad & \mathcal{L}_n := \frac{w_{\Pi(n)}}{N}\log_2\left(1+\frac{h^{\mathrm{ID}}_{\Pi(n),n}p_n}{\Gamma\sigma^2}\right)+\zeta\sum_{k=1}^{K}\lambda_k h^{\mathrm{EH}}_{k,n}p_n-\mu p_n\\ \text{s.t.}\quad & 0\le p_n\le P_{\mathrm{peak}}.\end{aligned} \tag{3.27}$$

Note that for the Lagrangian in (3.25), we have

$$\mathcal{L}=\sum_{n=1}^{N}\mathcal{L}_n-\sum_{k=1}^{K}\lambda_k\overline{E}_k+\mu P. \tag{3.28}$$

[2]In our simulation setup considered in Section 3.5.3 with $N = 64$, the duality gap of Problem (3.24) is observed to be negligibly small and thus can be ignored.

From (3.27), we have

$$\frac{\partial \mathcal{L}_n}{\partial p_n} = \frac{w_{\Pi(n)} h^{\mathrm{ID}}_{\Pi(n),n}}{N(\Gamma\sigma^2 + h^{\mathrm{ID}}_{\Pi(n),n} p_n)\ln 2} + \zeta \sum_{k=1}^{K} \lambda_k h^{\mathrm{EH}}_{k,n} - \mu. \tag{3.29}$$

Thus, for any given SC allocation $\Pi(n)$, the optimal power allocation for Problem (3.27) is obtained as

$$p^*_n(\Pi) = \min\left(\left(\frac{w_{\Pi(n)}}{N\left(\mu - \zeta \sum\limits_{k=1}^{K} \lambda_k h^{\mathrm{EH}}_{k,n}\right)\ln 2} - \frac{\Gamma\sigma^2}{h^{\mathrm{ID}}_{\Pi(n),n}}\right)^+, P_{\mathrm{peak}}\right). \tag{3.30}$$

Thus, for each given n, the optimal SC allocation $\Pi^*(n)$ to maximize $\mathcal{L}_n$ can be obtained as

$$\Pi^*(n) = \arg\max_{\Pi(n)} \left(\frac{w_{\Pi(n)}}{N}\left(\log_2\left(\frac{w_{\Pi(n)} v}{N\ln 2}\right)\right)^+ - \left(\frac{w_{\Pi(n)}}{N\ln 2} - \frac{1}{v}\right)^+\right). \tag{3.31}$$

where

$$v = \frac{h^{\mathrm{ID}}_{\Pi(n),n}}{\Gamma\sigma^2\left(\mu - \zeta \sum\limits_{k=1}^{K} \lambda_k h^{\mathrm{EH}}_{k,n}\right)} \tag{3.32}$$

Note that (3.31) can be solved by exhaustive search over the user set $\{1, \ldots, K\}$.

After obtaining $g(\{\lambda_k\}, \mu)$ with given $\{\lambda_k\}$ and μ, the minimization of $g(\{\lambda_k\}, \mu)$ over $\{\lambda_k\}$ and μ can be efficiently solved by the ellipsoid method [42]. A subgradient of this problem required for the ellipsoid method is provided by the following proposition.

Proposition 3.5.3. *For Problem (3.24) with a dual function $g(\{\lambda_k\}, \mu)$, the following choice of $\boldsymbol{d}$ is a subgradient for $g(\{\lambda_k\}, \mu)$:*

$$d_k = \begin{cases} \zeta \sum\limits_{n=1}^{N} h^{\mathrm{EH}}_{k,n} \dot{p}_n - \overline{E}_k, & k = 1, \ldots, K, \\ P - \sum\limits_{n=1}^{N} \dot{p}_n, & k = K+1. \end{cases} \tag{3.33}$$

where $\{\dot{p}_n\}$ is the solution of the maximization problem (3.26) with given $\{\lambda_k\}$ and μ.

Proof. The proof is similar as the proof of Proposition 3.5.1, and thus is omitted. □

Remark 3.5.2. The optimal solution for (P-UB) can be obtained by setting $h_{k,n}^{\mathrm{EH}} = h_{k,n}^{\mathrm{ID}} = h_{k,n}, \forall k, n$ in Problem (3.24). Hence, the above developed solution is also applicable for Problem (P-UB).

For (P-PS) with given $\{\rho_k\}$, the optimal $\{p_n\}$ and $\{\Pi(n)\}$ are obtained by (3.30) and (3.31), respectively. Define the corresponding optimal value of Problem (3.24) as $R(\boldsymbol{\rho})$, where $\boldsymbol{\rho} = [\rho_1, \ldots, \rho_K]^T$. Then $R(\boldsymbol{\rho})$ can be increased by optimizing ρ_k's by (3.23). The above procedure can be iterated until $R(\boldsymbol{\rho})$ cannot be further improved. Note that Problem (3.24) is guaranteed to be feasible at each iteration, provided that the initial ρ_k's are feasible, since at each iteration we simply decrease ρ_k's to make all the harvested energy constraints tight. Thus, with given initial $\{\rho_k\}$, the iterative algorithm is guaranteed to converge to a local optimum of (P-PS) when all the harvested energy constraints in (3.24) are tight.

Note that the above local optimal solution depends on the choice of initial $\{\rho_k\}$. To obtain a robust performance, we randomly generate M feasible $\{\rho_k\}$ as the initialization steps, where M is a sufficiently large number.[3] For each initialization step, the iterative algorithm is applied to obtain a local optimal solution for (P-PS). The final solution is selected as the one that achieves the maximum weighted sum-rate from all the solutions.

To summarize, the above iterative algorithm to solve (P-PS) is given in Table 3.2. For the algorithm given in Table 3.2, the computation time is dominated by the ellipsoid method in steps A)-C). In particular, in step B), the time complexity of step a) is of order KN, step b) is of order KN, and step c) is of order K^2. Thus, the time complexity of steps a)-c) is of order $K^2 + KN$, i.e., $\mathcal{O}(K^2 + KN)$. Note that

[3]In general, as the number of users increases, the number of initialization steps needs to be increased to guarantee the robustness and optimality of the algorithm. However, large number of initialization steps increases the computation complexity, which may not be suitable for real-time applications.

step B) iterates $\mathcal{O}(K^2)$ to converge [42], thus the time complexity of the ellipsoid method is $\mathcal{O}(K^4 + K^3N)$. Considering further the number of initialization steps M, the time complexity of the algorithm in Table 3.2 is $\mathcal{O}(K^4M + K^3NM)$.

Table 3.2: Iterative algorithm for solving Problem (P-PS).

I) Randomly generate M feasible $\{\rho_k\}$ as different initialization steps.

II) For each initialization step:

1) Initialize $\{\rho_k\}$.
2) **repeat**
   A) Compute $\{h_{k,n}^{\mathrm{EH}}\}$ and $\{h_{k,n}^{\mathrm{ID}}\}$. Initialize $\{\lambda_k > 0\}$ and $\mu > 0$.
   B) **repeat**
      a) Compute $\{p_n\}$ and $\{\Pi(n)\}$ by (3.30) and (3.31) with given $\{\lambda_k\}$ and μ.
      b) Compute the subgradient of $g(\{\lambda_k\}, \mu)$ by (3.33).
      c) Update $\{\lambda_k\}$ and μ according to the ellipsoid method.
   C) **until** $\{\lambda_k\}$ and μ converge to a prescribed accuracy.
   D) Update $\{\rho_k\}$ by (3.23) with fixed $\{p_n\}$ and $\{\Pi(n)\}$.
3) **until** $\left|\zeta \sum_{n=1}^{N} h_{k,n}^{\mathrm{EH}} p_n - \overline{E}_k\right| < \delta, \forall k$, where $\delta > 0$ controls the algorithm accuracy.

III) Select the one that achieves the maximum weighted sum-rate from the M solutions.

3.5.3 Performance Comparison

We provide simulation results under a practical system setup. For each user, we use the same parameters as the single-user case with $N = 64$ in Section 3.4. The channels for different users are generated independently. In addition, it is assumed that $w_k = 1, \forall k$, i.e., sum-rate maximization is considered. The minimum harvested energy is assumed to be the same for all users, i.e., $\overline{E}_k = \overline{E}, \forall k$. The number of initialization steps M is set to be 100.

Figs. 3.5 and 3.6 show the achievable rates versus the minimum required

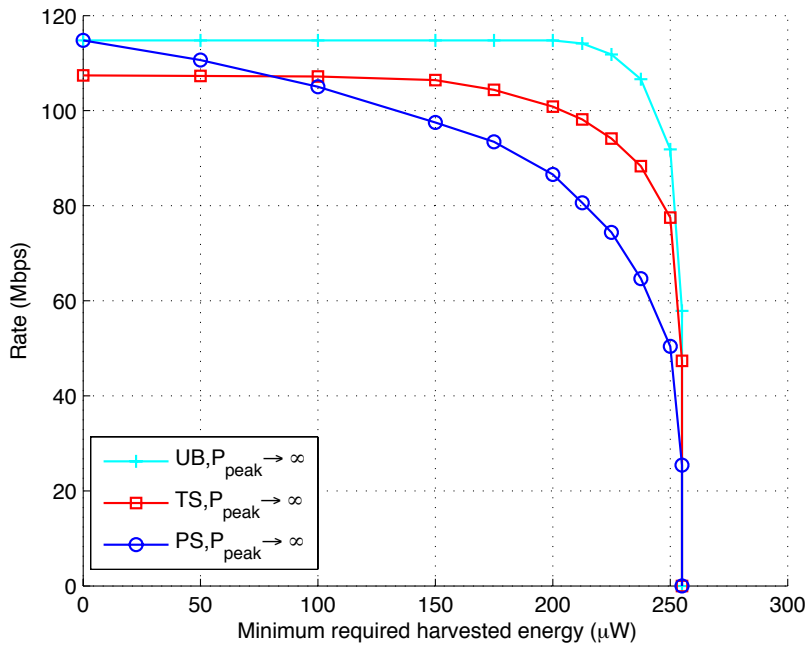

Figure 3.5: Achievable rates versus minimum required harvested energy in a multiuser OFDM-based SWIPT system, where $K = 4$, $N = 64$, and $P_{\text{peak}} \to \infty$.

harvested energy by different schemes with $K = 4$. We assume $P_{\text{peak}} \to \infty$ in Fig. 3.5, and $P_{\text{peak}} = 4P/N$ in Fig. 3.6. Fig. 3.7 shows the time ratio of the EH slot versus minimum required harvested energy for the TS scheme in Fig. 3.6. In Fig. 3.5 with $P_{\text{peak}} \to \infty$, it is observed that when $\overline{E} > 0$, the achievable rates by both TS and PS are less than the upper bound. For the TS scheme, the maximum rate is achieved when $\overline{E}$ is less than 150μW (c.f. Remark 3.5.1); when $\overline{E}$ is larger than 150μW, the achievable rate decreases as $\overline{E}$ increases. For the PS scheme, the achievable rate decreases as $\overline{E}$ increases, since for larger $\overline{E}$ more power needs to be split for EH at each receiver. Comparing the TS and PS schemes, it is observed that for sufficiently small $\overline{E}$ ($0 \leq \overline{E} \leq 80\mu$W), the achievable rate by PS is larger than that by TS. This is because that when the required harvested energy is sufficiently small, only a small portion of power needs to be split for energy harvesting, and the PS scheme may take the advantage of the frequency diversity by SC allocation. For sufficiently large $\overline{E}$ ($80 < \overline{E} \leq 255\mu$W), it is observed that the achievable rate by

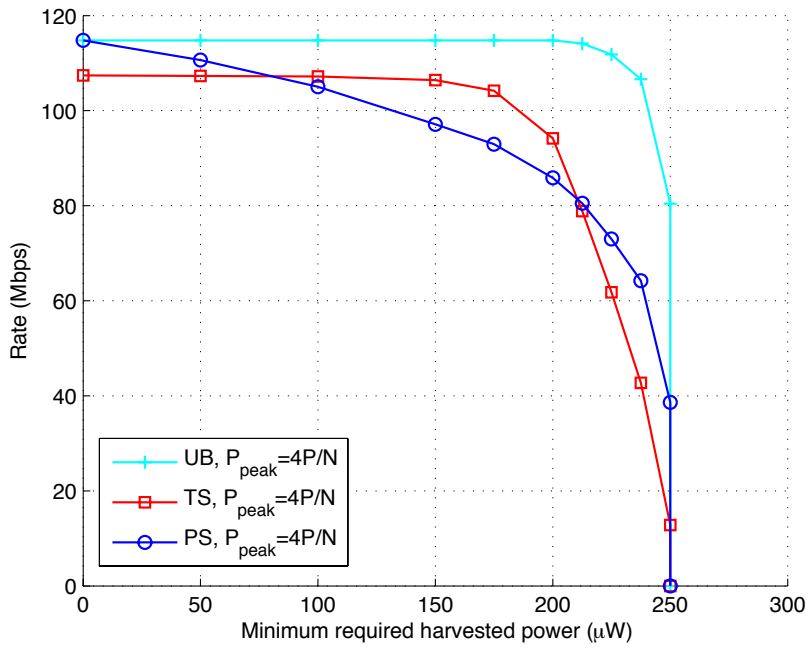

Figure 3.6: Achievable rates versus minimum required harvested energy in a multiuser OFDM-based SWIPT system, where $K = 4$, $N = 64$, and $P_{\text{peak}} = 4P/N$.

TS is larger than that by PS. In Fig. 3.6 with $P_{\text{peak}} = 4P/N$, it is observed that when $\overline{E}$ is sufficiently large, the TS scheme becomes worse than the PS scheme. This is because that for a finite peak power constraint on each SC, as $\overline{E}$ becomes sufficiently large, the TS scheme needs to schedule a nonzero EH slot to ensure all users harvest sufficient energy (see Fig. 3.7), the total information transmission time $1 - \alpha_{K+1}$ then decreases and results in a degradation of achievable rate. However, for $80 < \overline{E} \leq 208\mu$W, in which case the system achieves large achievable rate (larger than 70% of UB) while each user harvests a reasonable value of energy (about 32% to 84% of the maximum possible value), the TS scheme still outperforms the PS scheme.

Fig. 3.8 shows the achievable rates versus the number of users by different schemes under fixed minimum required harvested energy $\overline{E}_k = \overline{E} = 150\mu$W and $P_{\text{peak}} = 4P/N$. In Fig. 3.8, it is observed that for both TS and PS schemes, the achievable rate increases as the number of users increases, and the rate tends to be

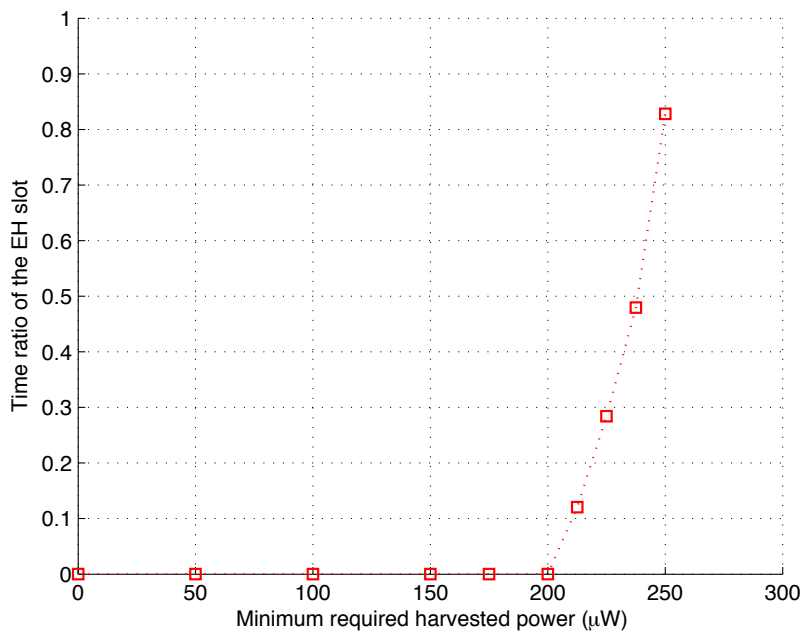

Figure 3.7: Time ratio of the EH slot versus minimum required harvested energy for the TS scheme in Fig. 3.6.

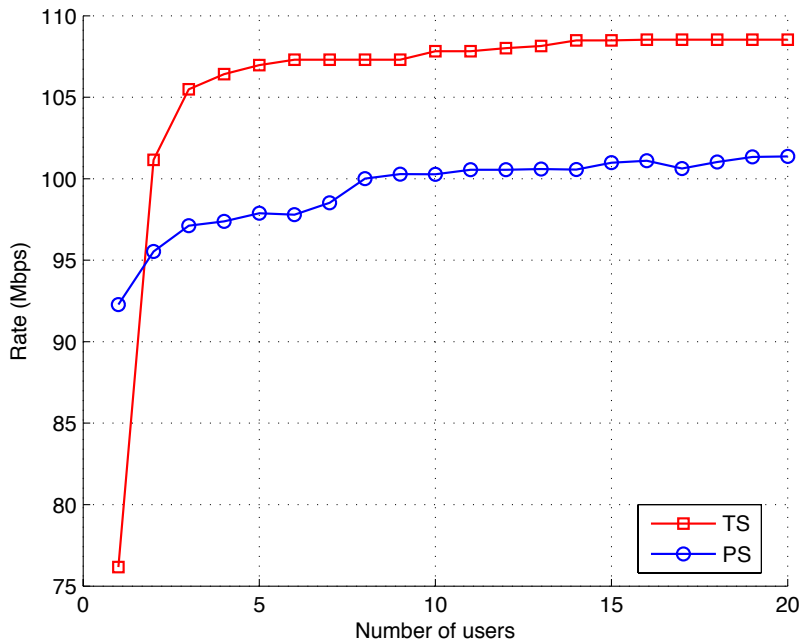

Figure 3.8: Achievable rates versus number of users, where $P_{\text{peak}} = 4P/N$ and $\overline{E}_k = \overline{E} = 150\mu\text{W}$.

saturated due to the bandwidth and the transmission power of the system is fixed. In particular, for the TS scheme, the achievable rate with $K = 2$ is much larger (about 32.8%) than that with $K = 1$. This is because that for the case $K = 2$, one of the user decodes information when the other user is harvesting energy; however, for the single user case $K = 1$, the transmission time when the user is harvesting energy is not utilized for information transmission. It is also observed in Fig. 3.8 that for a general multiuser system with large $K \geq 2$, the TS scheme outperforms the PS scheme. This is intuitively due to the fact that as the number of users increases, the portion of energy discarded at the information receiver at each user after power splitting also becomes larger (c.f. Fig. 3.2), hence using PS becomes inefficient for large K.

3.6 Chapter Summary

In this chapter, we studied the resource allocation optimization for a multiuser OFDM-based SWIPT system. Two schemes were investigated, namely, TDMA-based information transmission with TS receiver, and OFDMA-based information transmission with PS receiver. For both cases, the weighted sum-rate was maximized subject to a given set of harvested energy constraints as well as the peak and/or total transmission power constraint. Our study suggests that, for the TS scheme, the system can achieve the same rate as the conventional TDMA system, and at the same time each user is still able to harvest a reasonable value of energy. In general, the TS scheme outperforms the PS scheme for a moderate EH requirement at users. When the harvested energy required at users is sufficiently large, however, a nonzero EH slot may be needed. This in turn degrades the rate of the TS scheme significantly; as a result, the PS scheme may outperform the TS scheme for strong EH requirement at users. From the view of implementation, the TS scheme is easier to implement at the receiver side by simply switching between the two operations of EH and ID.

Chapter 4

WPC in OFDM System

4.1 Introduction

In Chapter 3, we investigated the resource allocation problem for SWIPT in OFDM system, where the OFDM users harvest energy in addition to receiving information from the same RF signals sent by the HAP. In this chapter, we shift our focus to the resource allocation problem for WPC in OFDM system, where the OFDM users harvest energy from the EAP to power their information transmission to the DAP.

We consider the WPC system shown in Fig. 1.5 with one OFDM user, where the energy and information transmissions are scheduled over finite number of time slots. The channels of both WPT and WIT links may vary over different slots and SCs. To avoid interference to WIT, WPT and WIT are scheduled over orthogonal SCs at any slot. We maximize the achievable rate by jointly optimizing the SC allocation over time, and also the power allocation over time and SCs, for both WPT and WIT links. The problem is investigated under two assumptions on the availability of CSI for the WPT and WIT links, namely, full CSI and causal CSI. Given full CSI, we propose an offline algorithm to solve the problem by exploiting the specific structure of the optimal power allocation. Given causal CSI, we propose a low-complexity online algorithm. Our numerical results demonstrate the superiority of WPC over the communication system powered by opportunistic EH. Moreover, our results provide useful insights to the joint energy and information transmissions

design for WPC system in practice.

The rest of this chapter is organized as follows. Section 4.2 presents the literature review. Section 4.3 introduces the system model. Section 4.4 presents the problem formulation. Section 4.5 considers offline algorithm given full CSI. Section 4.6 proposes online algorithm given causal CSI. Section 4.7 provides numerical examples. Finally, Section 4.8 summarizes the conclusion.

4.2 Literature Review

4.2.1 Protocol Design and Resource Allocation for WPC

The pioneering works [10, 11] on WPC inspire investigations for WPC under various setups. The work [10] is extended to a full-duplex HAP setup in [46, 47], where the DL energy transmission and UL information receiving is performed simultaneously at the HAP for performance enhancement. One key challenge for such full-duplex HAP system is that part of the energy transmission signal by the HAP causes self-interference to its own information receiving at the same time. In [46, 47], this problem is tackled by applying successive interference cancellation at the HAP. In [48], the authors extend the work in [10] by considering separated EAP/DAP, where the EAP is equipped with multiple antennas. As an extension of [11], [49] studies the case of imperfect CSI by considering practical channel estimation. Cooperative communication for WPC is studied in [50, 51]. In [50], near users help to relay the information from far users to the HAP to overcome the doubly near-far problem. In [51], the source and relay harvest energy from the HAP in DL to supply the UL cooperative information transmission by a so-called "harvest-then-cooperate" protocol. Furthermore, [52] investigates the limiting distribution of the stored energy, the average error rate, and outage probability at the user when on-off transmission policy is adopted at the user assuming no CSI for both WPT/WIT links. The capacity of large-size WPC network with geographically distributed users is studied in [53] and [54] for the separated EAP/DAP case, and

in [55] for the co-located EAP/DAP case, based on the tool of stochastic geometry.

4.2.2 Wireless Communication Powered by Opportunistic Energy Harvesting

Instead of using dedicated wireless power as EH source for transmitters, another line of research focuses on wireless communications powered by opportunistic EH, where the energy sources for EH are typically provided by the environment, such as solar energy, wind energy, thermal energy, and piezoelectric energy, etc. For such systems, the amount of harvested energy greatly depends on the conditions of the environment. The works [56,57] study the information transmission scheduling over finite time slots in fading channels, where the throughput is maximized by power allocation over time. In contrast to a conventional transmitter with fixed power source, where the data transmission is adapted to the communication channels, the EH transmitter adapts its transmission both to the communication channels and to the dynamics of energy arrivals. It is shown in [56, 57] that when the battery at a transmitter has infinite storage, the optimal transmission power over slots follows a staircase water-filling (SWF) structure, where the water-levels (WLs) are nondecreasing over slots. This is in contrast with the case of total energy constraint at the transmitter, in which the optimal transmission power is given by conventional WF, where all slots share the same WL. The works [56,57] are extended to a two-hop relay network in [58–61], where both source and relay nodes employ EH to power their information transmission.

4.3 System Model

We consider an OFDM-based WPC system, where one user harvests energy from an EAP to power its information transmission to a DAP (see Fig. 4.1 for separated EAP/DAP). The EAP and DAP are each equipped with one antenna, while the user is equipped with two antennas, for energy harvesting

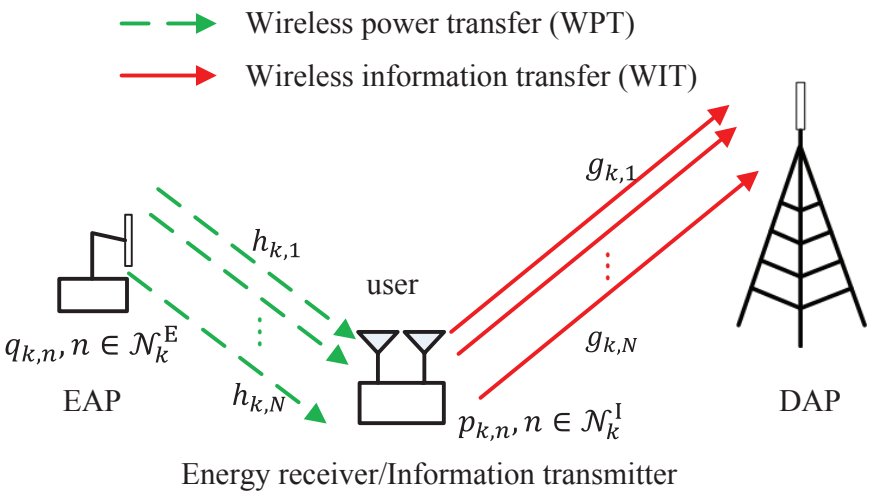

Figure 4.1: A WPC system with one user.

and information transmission, respectively. The EAP and DAP are connected to stable power supplies, whereas the user has no embedded energy sources. Consider energy/information transmission in one block, which is equally divided into K time slots, with each slot being of duration T. Let $T = 1$ for convenience. The slots are indexed in increasing order by $k \in \mathcal{K} \triangleq \{1, \ldots, K\}$. The total bandwidth of the system is equally divided into N orthogonal SCs. The SC set is denoted by $\mathcal{N} = \{1, \ldots, N\}$. The channel power gain from the EAP to the user, i.e., the WPT link, during slot k at SC n is denoted by $h_{k,n} > 0, k \in \mathcal{K}, n \in \mathcal{N}$. The channel power gain from the user to the DAP, i.e., the WIT link, during slot k at SC n is denoted by $g_{k,n} > 0, k \in \mathcal{K}, n \in \mathcal{N}$. It is assumed that $h_{k,n}$'s and $g_{k,n}$'s are constant within one slot and SC, but vary over slots and SCs. In practice, for the co-located EAP/DAP case, $h_{k,n}$ and $g_{k,n}$ are correlated; while for the separated EAP/DAP case, $h_{k,n}$ and $g_{k,n}$ are independent. Our model is applicable for both scenarios.

Before the energy/information transmission during each slot k, the CSI of the WPT and WIT links, i.e., $h_{k,n}, g_{k,n}, n \in \mathcal{N}$, is estimated. It is assumed that the channel estimation is sufficiently accurate such that the performance degradation due to the estimation error is negligible. Based on the CSI, energy/information transmission for the WPT/WIT links is jointly scheduled. To avoid interference at

the DAP from the transmission signals by the EAP, WPT and WIT are scheduled over orthogonal SCs[1]. For notational simplicity, we define a dummy SC $n = 0$, where $h_{k,0} = g_{k,0} = 0$ for $k \in \mathcal{K}$, since there may be no SCs allocated for WPT in slot k. The extended SC set is denoted by $\mathcal{N}' = \{0\} \cup \mathcal{N}$. For each slot $k \in \mathcal{K}$, the SC set $\mathcal{N}'$ is partitioned into two complementary disjoint subsets for WPT and WIT, denoted by $\mathcal{N}_k^{\mathrm{E}}$ and $\mathcal{N}_k^{\mathrm{I}}$, respectively, where $\mathcal{N}_k^{\mathrm{E}} \subseteq \mathcal{N}', \mathcal{N}_k^{\mathrm{I}} \subseteq \mathcal{N}'$, and $\mathcal{N}_k^{\mathrm{I}} = \mathcal{N}' \backslash \mathcal{N}_k^{\mathrm{E}}$. The transmission power by the EAP during slot k on SC n is denoted by $q_{k,n} \geq 0, k \in \mathcal{K}, n \in \mathcal{N}_k^{\mathrm{E}}$. The average transmission power at the EAP[2] over K slots in each block is denoted by Q, i.e.,

$$\frac{1}{K} \sum_{k=1}^{K} \sum_{n \in \mathcal{N}_k^{\mathrm{E}}} q_{k,n} \leq Q. \tag{4.1}$$

The user harvests energy from the EAP by an energy receiver, and the energy is then stored in an energy buffer to power the information transmitter. Assume the stored energy in the energy buffer at time instant k^-, i.e., the time instant just before slot k, is denoted by B_k. The initial energy at the buffer, i.e., B_1, is known. The transmission power by the information transmitter during slot k at SC n is denoted by $p_{k,n} \geq 0, k \in \mathcal{K}, n \in \mathcal{N}_k^{\mathrm{I}}$. Assume the harvested energy during slot k is ready for transmission at the end of slot k, the transmission power constraint at the user is thus given by

$$\sum_{n \in \mathcal{N}_k^{\mathrm{I}}} p_{k,n} \leq B_k, k \in \mathcal{K}. \tag{4.2}$$

We assume the storage of the energy buffer is sufficiently large compared to the harvested energy from the EAP, hence, no energy overflow at the energy buffer. We further assume except data transmission, other circuits at the user consume

[1]In practice, strict orthogonality of SCs imposes high requirements for hardware design. Energy leakage from one SC to adjacent SC may result in performance degradation, which is severe especially for the co-located EAP/DAP case as transmission power for the WPT link is in general much larger than that for the WIT link. For more detailed discussions, please refer to [62].

[2]In practice, the transmission power at each slot and SC may also be constrained by a peak power. In this chapter, we assume the peak power constraint is sufficiently large compared to the transmission power, as WPC in general operates at low power.

negligible energy. This is justified when data transmission consumes much larger power than that by other circuits, which is reasonable for most low-power (e.g., sensor) networks. The stored energy in the energy buffer at time instant $(k+1)^-$ is thus given by

$$B_{k+1} = B_k + \zeta \sum_{n \in \mathcal{N}_k^{\mathrm{E}}} h_{k,n} q_{k,n} - \sum_{n \in \mathcal{N}_k^{\mathrm{I}}} p_{k,n}, \quad k \in \mathcal{K} \tag{4.3}$$

where ζ denotes the energy efficiency at the user, accounting for both conversion and discharging losses. Note that in (4.3), mathematically the effect of ζ can be equivalent to a scaling of the channel power gain $h_{k,n}$'s. Hence, in the sequel we let $\zeta = 1$ for simplicity. Combine (4.2) and (4.3), leading to the energy causality constraint

$$\sum_{k=1}^{i} \sum_{n \in \mathcal{N}_k^{\mathrm{I}}} p_{k,n} \leq \sum_{k=1}^{i-1} \sum_{n \in \mathcal{N}_k^{\mathrm{E}}} h_{k,n} q_{k,n} + B_1, \ i \in \mathcal{K}. \tag{4.4}$$

At the DAP, the receiver noise is modeled as a CSCG random variable with zero mean and variance σ^2. Due to frequency orthogonal transmission of energy and information, the energy signal from EAP will not interfere with the information reception at DAP. Moreover, the gap for the achievable rate from the channel capacity due to a practical MCS is denoted by $\Gamma \geq 1$. The average achievable rate at the DAP in bps/Hz is thus

$$R = \frac{1}{KN} \sum_{k=1}^{K} \sum_{n \in \mathcal{N}_k^{\mathrm{I}}} \log_2 \left(1 + \frac{g_{k,n} p_{k,n}}{\Gamma \sigma^2}\right). \tag{4.5}$$

4.4 Problem Formulation

Our objective is to maximize the average rate at the DAP by jointly optimizing the SC allocation over time and the power allocation over SCs and time for both

WPT and WIT links. This leads to the following optimization problem.

$$\max_{\{\mathcal{N}_k^{\mathrm{E}}\},\{q_{k,n}\},\{p_{k,n}\}} \quad \frac{1}{KN}\sum_{k=1}^{K}\sum_{n\in\mathcal{N}_k^{\mathrm{I}}}\log_2\left(1+\frac{g_{k,n}p_{k,n}}{\Gamma\sigma^2}\right)$$

$$\text{s.t.} \quad \frac{1}{K}\sum_{k=1}^{K}\sum_{n\in\mathcal{N}_k^{\mathrm{E}}} q_{k,n} \le Q, \tag{4.6a}$$

$$\sum_{k=1}^{i}\sum_{n\in\mathcal{N}_k^{\mathrm{I}}} p_{k,n} \le \sum_{k=1}^{i-1}\sum_{n\in\mathcal{N}_k^{\mathrm{E}}} h_{k,n}q_{k,n} + B_1, \quad i\in\mathcal{K}. \tag{4.6b}$$

The SCs for WIT are not explicit optimization variables because by definition a SC is used either for WIT or WPT only. The case where a SC n is neither used for WPT nor WIT is covered by assigning it to be used for WPT with $q_{k,n}=0$ or WIT with $p_{k,n}=0$. Since the energy harvested during the last slot K is not available for any information transmission, without loss of optimality there should be no energy transmission at the last slot, i.e., $\mathcal{N}_K^{\mathrm{E}}=\{0\}, \mathcal{N}_K^{\mathrm{I}}=\mathcal{N}$, as assumed henceforth. The optimal solutions are denoted by $\{\mathcal{N}_k^{\mathrm{E}*}, k\in\mathcal{K}\}$, $\{q_{k,n}^*, k\in\mathcal{K}, n\in\mathcal{N}_k^{\mathrm{E}*}\}$, $\{p_{k,n}^*, k\in\mathcal{K}, n\in\mathcal{N}_k^{\mathrm{I}*}\}$, and the maximum average rate by R^*.

Suppose that the SC allocation and power allocation for the WPT are given, such that the constraint (4.6a) is satisfied. Then Problem (4.6) is reduced to the conventional EH transmitter with energy arrivals $\left\{\sum_{n\in\mathcal{N}_k^{\mathrm{E}}} h_{k,n}q_{k,n}, k\in\mathcal{K}\right\}$ [56, 57]. Hence, Problem (4.6) is more general with additional design freedoms available via the SC allocation and power allocation for the WPT link, which will in turn influence the power allocation for the WIT link.

We first solve Problem (4.6) assuming full CSI available in Section 4.5. Based on the results for full CSI, we propose an online algorithm for Problem (4.6) under causal CSI in Section 4.6.

4.5 Offline Algorithm for Joint Power and Sub-Channel Allocation

In this section, we consider Problem (4.6) when full CSI is available, where all the $h_{k,n}$'s and $g_{k,n}$'s are *a priori* known by a central controller at the beginning of each block transmission. Our aim is to study the structural properties of the optimal transmission policy, which will provide important insights. Given SC allocation, by Propositions 4.5.1 and 4.5.2, we show that WPT may occur only on the so-called causally dominating slots. Furthermore, Proposition 4.5.3 shows that the power allocated for WPT matches to the power consumed for WIT during the intervals between the causally dominating slots. The insights will be used for developing heuristic online schemes when only casual CSI is available.

Given SC allocation $\mathcal{N}_k^{\mathrm{E}}, k \in \mathcal{K}$, at slot k, the index of the best SC (i.e., the SC that has the largest channel power gain) for the WPT link among SCs in $\mathcal{N}_k^{\mathrm{E}}$, is denoted by $m(k) \in \mathcal{N}'$. Hence,

$$m(k) = \underset{\{n \in \mathcal{N}_k^{\mathrm{E}}\}}{\arg\max}\ h_{k,n}. \tag{4.7}$$

In the following proposition, we state that with given SC allocation, at each slot k WPT may only occur on the SC $m(k)$.

Proposition 4.5.1. *For Problem* (4.6) *with given SC allocation* $\mathcal{N}_k^{\mathrm{E}}, k \in \mathcal{K}$, *we have* $q_{k,n}^* = 0$ *for* $n \neq m(k)$.

Proof. Please refer to Appendix G. □

The intuition of Proposition 4.5.1 is as follows. Given SC allocation $\mathcal{N}_k^{\mathrm{E}}, k \in \mathcal{K}$, consider energy allocation for the WPT link at any slot k with total energy $\sum_{n \in \mathcal{N}_k^{\mathrm{E}}} q_{k,n}$. Since the harvested energy at the user increases linearly with $q_{k,n}, n \in \mathcal{N}_k^{\mathrm{E}}$, the harvested energy at the user is maximized by allocating all energy to $q_{k,m(k)}$, which has the largest $h_{k,n}$ for $n \in \mathcal{N}_k^{\mathrm{E}}$.

By Proposition 4.5.1, at each slot it is optimal to allocate at most one SC from the set $\mathcal{N}'$ to perform WPT, as the remaining SCs can be utilized for potential WIT. We define a SC allocation function $\Pi(k) \in \mathcal{N}'$ to denote the SC allocated for WPT during slot $k, k \in \mathcal{K}$. Hence, $\mathcal{N}_k^{\mathrm{E}} = \{\Pi(k)\}, \mathcal{N}_k^{\mathrm{I}} = \mathcal{N}' \backslash \{\Pi(k)\}, k \in \mathcal{K}$. Note that $\Pi(k)$ can be assigned to the dummy SC $n = 0$ in case there is no WPT scheduled in slot k. Problem (4.6) is then reformulated by the following problem.

$$\begin{aligned} \max_{\{q_{k,\Pi(k)}\},\{p_{k,n}\},\{\Pi(k)\}} \quad & \frac{1}{KN} \sum_{k=1}^{K} \sum_{n \in \mathcal{N}_k^{\mathrm{I}}} \log_2 \left(1 + \frac{g_{k,n} p_{k,n}}{\Gamma \sigma^2}\right) \\ \text{s.t.} \quad & \frac{1}{K} \sum_{k=1}^{K} q_{k,\Pi(k)} \leq Q, \qquad (4.8\text{a}) \\ & \sum_{k=1}^{i} \sum_{n \in \mathcal{N}_k^{\mathrm{I}}} p_{k,n} \leq \sum_{k=1}^{i-1} h_{k,\Pi(k)} q_{k,\Pi(k)} + B_1, i \in \mathcal{K}. \qquad (4.8\text{b}) \end{aligned}$$

Problem (4.8) is non-convex due to the integer SC allocation function $\Pi(k), k \in \mathcal{K}$. Hence, we solve Problem (4.8) by two stages: we first solve Problem (4.8) with given SC allocation $\Pi(k), k \in \mathcal{K}$, where the joint power allocation for the WPT/WIT links is optimized; next, we propose heuristic schemes for the SC allocation.

4.5.1 Joint Power Allocation

We first consider Problem (4.8) with given $\Pi(k), k \in \mathcal{K}$, where we focus on the joint power allocation design for the WPT/WIT links. Given SC allocation $\Pi(k), k \in \mathcal{K}$, then $\mathcal{N}_k^{\mathrm{E}}, \mathcal{N}_k^{\mathrm{I}}, k \in \mathcal{K}$ are known. For notational simplicity, when the SC allocation $\Pi(k), k \in \mathcal{K}$ is given in Problem (4.8), we drop the subscript $\Pi(k)$ in $q_{k,\Pi(k)}$ and $h_{k,\Pi(k)}$, i.e., $q_k \triangleq q_{k,\Pi(k)}$, $h_k \triangleq h_{k,\Pi(k)}$ for $k \in \mathcal{K}$. We note that $h_k = 0$ when $\Pi(k) = 0, k \in \mathcal{K}$.

First, we investigate the properties for $\{q_k^*\}$ and $\{p_{k,n}^*\}$ for Problem (4.8) with given $\Pi(k), k \in \mathcal{K}$. To this end, given SC allocation $\Pi(k), k \in \mathcal{K}$, we define set $\mathcal{D}$ as

follows

$$\mathcal{D} \triangleq \{1, \text{ if } \Pi(1) \in \mathcal{N}\} \cup \{k \in \{2, \ldots, K-1\} : \Pi(k) \in \mathcal{N}, h_k > h_j, \forall 1 \leq j < k\}. \tag{4.9}$$

We note that for the slots in $\mathcal{D}$, the channel power gain h_k is increasing with the slot index k; hence, the slots in $\mathcal{D}$ are called *causally dominating* slots, with each subsequent slot in $\mathcal{D}$ dominating all previous slots. For convenience, we index the elements in set $\mathcal{D} = \{d_1, d_2, \ldots, d_{|\mathcal{D}|}\}$ such that $d_i < d_j$ for $i < j$. The complementary set of $\mathcal{D}$ is denoted by $\mathcal{D}^c$, i.e., $\mathcal{D}^c = \mathcal{K} \backslash \mathcal{D}$.

We partition the slot set $\mathcal{K}$ for the WIT link into subsets $\mathcal{D}_i \triangleq \{d_{i-1} + 1, \ldots, d_i\}, i = 1, \ldots, |\mathcal{D}| + 1$, referred to as the ith *interval*, where we set $d_0 = 0$ and $d_{|\mathcal{D}|+1} = K$ for notational simplicity. Thus, $\bigcup_i \mathcal{D}_i = \mathcal{K}$ and $\mathcal{D}_i \cap \mathcal{D}_j = \emptyset$ for $i \neq j$. In the following proposition, we show that WPT only occurs in the causally dominating slots in $\mathcal{D}$.

Proposition 4.5.2. *For Problem* (4.8) *with given* $\Pi(k), k \in \mathcal{K}$*, the optimal power allocation satisfies* $q_k^* = 0$ *for* $k \in \mathcal{D}^c$*.*

Proof. Please refer to Appendix H. □

Remark 4.5.1. Proposition 4.5.2 shows that WPT occurs *sparsely* in time, i.e., WPT occurs only when a slot dominating all its previous slots. Intuitively, this is because instead of allocating energy to any slot in $\mathcal{D}^c$, allocating the same amount of energy to an earlier slot in $\mathcal{D}$ which has larger channel power gain at the WPT link will result in a larger feasible region for $\{p_{k,n}\}$.

Further in Proposition 4.5.3, it is shown that if the energy at the user is used up after a particular casually dominating slot, then the energy is used up after later causally dominating slots.

Proposition 4.5.3. *In Problem* (4.8) *with given* $\Pi(k), k \in \mathcal{K}$*, if* $\{q_k^*\}$ *and* $\{p_{k,n}^*\}$

satisfy

$$\sum_{k=1}^{d_j} \sum_{n \in \mathcal{N}_k^{\mathrm{I}}} p_{k,n}^* = \sum_{k=1}^{d_j - 1} h_k q_k^* + B_1 \tag{4.10}$$

where $d_1 \leq d_j \leq d_{|\mathcal{D}|}$*, i.e., constraint* (4.8b) *holds with equality at* $i = d_j$*, then we have*

$$\sum_{k \in \mathcal{D}_{l+1}} \sum_{n \in \mathcal{N}_k^{\mathrm{I}}} p_{k,n}^* = h_{d_l} q_{d_l}^*, \quad l = j, \ldots, |\mathcal{D}|. \tag{4.11}$$

Proof. Please refer to Appendix I. □

Next, we discuss two cases for the initial battery energy B_1, i.e., the special case of $B_1 = 0$ and the general case of $B_1 \geq 0$.

Zero Initial Battery Energy with $B_1 = 0$

We first consider the case $B_1 = 0$. With $B_1 = 0$, from Proposition 4.5.2 and (4.8b), we have

$$\sum_{k=1}^{d_1} \sum_{n \in \mathcal{N}_k^{\mathrm{I}}} p_{k,n} = 0. \tag{4.12}$$

Thus,

$$p_{k,n}^* = 0, \quad k \in \mathcal{D}_1, n \in \mathcal{N}_k^{\mathrm{I}} \tag{4.13}$$

From Proposition 4.5.2, $q_k^* = 0, k \in \mathcal{D}^{\mathrm{c}}$. Henceforth, we consider optimization for $\{p_{k,n}, k = d_1 + 1, \ldots, K, n \in \mathcal{N}_k^{\mathrm{I}}\}$ and $\{q_k, k \in \mathcal{D}\}$.

From (4.12), constraint (4.8b) holds with equality at $i = d_1$, from Proposition 4.5.3 we have

$$\sum_{k \in \mathcal{D}_{l+1}} \sum_{n \in \mathcal{N}_k^{\mathrm{I}}} p_{k,n}^* = h_{d_l} q_{d_l}^*, \quad l = 1, \ldots, |\mathcal{D}|. \tag{4.14}$$

Define the *effective channel power gain* as

$$g'_{k,n} = h_{d_i} g_{k,n}, k \in \mathcal{D}_{i+1}, i = 1, \ldots, |\mathcal{D}|, n \in \mathcal{N}_k^{\mathrm{I}} \tag{4.15}$$

Define $\{p'_{k,n}\}$ as

$$p'_{k,n} = p_{k,n}/h_{d_i}, k \in \mathcal{D}_{i+1}, i = 1, \ldots, |\mathcal{D}|, n \in \mathcal{N}_k^{\mathrm{I}}. \tag{4.16}$$

From (4.13)-(4.16), Problem (4.8) with given $\Pi(k), k \in \mathcal{K}$ and $B_1 = 0$ is equivalent to the following problem.

$$\begin{aligned} \max_{\{q_{d_i}\},\{p'_{k,n}\}} & \frac{1}{KN} \sum_{k=d_1+1}^{K} \sum_{n \in \mathcal{N}_k^{\mathrm{I}}} \log_2 \left(1 + \frac{g'_{k,n} p'_{k,n}}{\Gamma \sigma^2}\right) \\ \text{s.t.} & \sum_{k=d_1+1}^{K} \sum_{n \in \mathcal{N}_k^{\mathrm{I}}} p'_{k,n} = KQ, \qquad (4.17a) \\ & \sum_{k \in \mathcal{D}_{i+1}} \sum_{n \in \mathcal{N}_k^{\mathrm{I}}} p'_{k,n} = q_{d_i}, i = 1, \ldots, |\mathcal{D}|. \qquad (4.17b) \end{aligned}$$

We recognize that the optimization over $\{p'_{k,n}, k = d_1 + 1, \ldots, K, n \in \mathcal{N}_k^{\mathrm{I}}\}$ is then a WF problem over time slots $k \in \{d_1 + 1, \ldots, K\}$ and SCs $n \in \mathcal{N}_k^{\mathrm{I}}$, because $\{q_{d_i}\}$ can be arbitrarily chosen and thus the last constraint becomes redundant. The optimal $\{p'_{k,n}, k = d_1 + 1, \ldots, K, n \in \mathcal{N}_k^{\mathrm{I}}\}$ is then obtained by the so-called WF power allocation over slots/SCs, given by

$$p'_{k,n} = \left(\frac{1}{\lambda KN \ln 2} - \frac{\Gamma \sigma^2}{g'_{k,n}}\right)^+, k = d_1 + 1, \ldots, K \tag{4.18}$$

where $(a)^+ \triangleq \max(0, a)$, and λ satisfies $\sum_{i=d_1+1}^{K} \sum_{n \in \mathcal{N}_k^{\mathrm{I}}} p'_{k,n} = KQ$. The WL is given by $(\lambda KN \ln 2)^{-1}$. From (4.13), (4.16), and (4.18), the optimal $\{p^*_{k,n}, k \in \mathcal{K}, n \in \mathcal{N}_k^{\mathrm{I}}\}$ is given by

$$p^*_{k,n} = \begin{cases} 0, & k \in \mathcal{D}_1, n \in \mathcal{N}_k^{\mathrm{I}} \\ \left(\frac{h_{d_i}}{\lambda KN \ln 2} - \frac{\Gamma \sigma^2}{g_{k,n}}\right)^+, & k \in \mathcal{D}_{i+1}, i = 1, \ldots, |\mathcal{D}|, n \in \mathcal{N}_k^{\mathrm{I}}. \end{cases} \tag{4.19}$$

From (4.17b) and Proposition 4.5.2, the optimal $\{q_k^*, k \in \mathcal{K}\}$ is given by

$$q_j = \begin{cases} \sum\limits_{k \in \mathcal{D}_{i+1}} \sum\limits_{n \in \mathcal{N}_k^{\mathrm{I}}} p'_{k,n}, & j = d_i, i = 1, \ldots, |\mathcal{D}|, \\ 0, & \text{otherwise.} \end{cases} \tag{4.20}$$

Remark 4.5.2. From (4.19), the optimal power allocation for the WIT link is adaptive to channels for both WPT and WIT links. Moreover, the WLs are the same for slots and SCs in the same interval, while the WL for interval $\mathcal{D}_{i+1}$ is increasing over index i. Thus, the power allocation for the WIT link performs SWF over slots.

Arbitrary Initial Battery Energy with $B_1 \geq 0$

Now we consider the case with arbitrary initial battery energy at the user, i.e., $B_1 \geq 0$.

We note that in Problem (4.8) with given $\Pi(k), k \in \mathcal{K}$, $\{q_k^*\}$ and $\{p_{k,n}^*\}$ satisfy constraint (4.8b) with equality at the last slot $K = d_{|\mathcal{D}|+1}$; otherwise, the objective function can be increased by increasing some $p_{K,n}$. Let $d_x, 1 \leq x \leq |\mathcal{D}| + 1$, denote the first slot index in $\mathcal{D} \cup \{K\}$ such that $\{q_k^*\}$ and $\{p_{k,n}^*\}$ satisfy constraint (4.8b) with equality. Hence,

$$\sum_{k=1}^{d_i} \sum_{n \in \mathcal{N}_k^{\mathrm{I}}} p_{k,n}^* < \sum_{k=1}^{i-1} h_{d_k} q_{d_k}^* + B_1, i = 1, \ldots, x-1, \tag{4.21}$$

$$\sum_{k=1}^{d_x} \sum_{n \in \mathcal{N}_k^{\mathrm{I}}} p_{k,n}^* = \sum_{k=1}^{x-1} h_{d_k} q_{d_k}^* + B_1 \tag{4.22}$$

where we define $h_0 \triangleq 1$ and $q_0 \triangleq 0$.

Lemma 4.5.1. *For Problem* (4.8) *with given* $\Pi(k), k \in \mathcal{K}$, $q_{d_k}^* = 0$ *for* $k < x - 1$.

The optimal $\{q_k^*\}$ *and* $\{p_{k,n}^*\}$ *satisfy*

$$\sum_{k=1}^{d_x} \sum_{n \in \mathcal{N}_k^{\mathrm{I}}} p_{k,n}^* = h_{d_{x-1}} q_{d_{x-1}}^* + B_1. \tag{4.23}$$

Proof. Please refer to Appendix J. □

Similar to the case of $B_1 = 0$, we define the *effective channel power gain* as

$$g'_{k,n} = \begin{cases} h_{d_{x-1}} g_{k,n}, & k = 1, \ldots, d_x, n \in \mathcal{N}_k^{\mathrm{I}}, \\ h_{d_i} g_{k,n}, & k \in \mathcal{D}_{i+1}, i = x, \ldots, |\mathcal{D}|, n \in \mathcal{N}_k^{\mathrm{I}}. \end{cases} \tag{4.24}$$

Define $\{p'_{k,n}\}$ as

$$p'_{k,n} = \begin{cases} p_{k,n}/h_{d_{x-1}}, & k = 1, \ldots, d_x, n \in \mathcal{N}_k^{\mathrm{I}}, \\ p_{k,n}/h_{d_i}, & k \in \mathcal{D}_{i+1}, i = x, \ldots, |\mathcal{D}|, n \in \mathcal{N}_k^{\mathrm{I}}. \end{cases} \tag{4.25}$$

In the following lemma, we show that Problem (4.8) with given $\Pi(k), k \in \mathcal{K}$ is equivalent to a problem with optimizing variables $\{p'_{k,n}\}$.

<u>Lemma</u> 4.5.2. *Problem* (4.8) *with given* $\Pi(k), k \in \mathcal{K}$ *is equivalent to the following problem.*

$$\begin{aligned} \max_{\{p'_{k,n}\}} \quad & \frac{1}{KN} \sum_{k=1}^{K} \sum_{n \in \mathcal{N}_k^{\mathrm{I}}} \log_2 \left(1 + \frac{g'_{k,n} p'_{k,n}}{\Gamma \sigma^2}\right) \\ \text{s.t.} \quad & \sum_{k=1}^{K} \sum_{n \in \mathcal{N}_k^{\mathrm{I}}} p'_{k,n} \leq KQ + \frac{B_1}{h_{d_{x-1}}}, && (4.26a) \\ & \sum_{k=1}^{d_{x-1}} \sum_{n \in \mathcal{N}_k^{\mathrm{I}}} p'_{k,n} \leq \frac{B_1}{h_{d_{x-1}}}, && (4.26b) \\ & \sum_{k=1}^{d_x} \sum_{n \in \mathcal{N}_k^{\mathrm{I}}} p'_{k,n} \geq \frac{B_1}{h_{d_{x-1}}}. && (4.26c) \end{aligned}$$

The optimal $\{p^*_{k,n}\}$ *is obtained by (4.25); the optimal* $\{q^*_k\}$ *is obtained by*

$$q_j = \begin{cases} \sum_{k=1}^{d_x} \sum_{n\in\mathcal{N}_k^{\mathrm{I}}} p'_{k,n} - \frac{B_1}{h_{d_{x-1}}}, & j = d_{x-1}, \\ \sum_{k\in\mathcal{D}_{i+1}} \sum_{n\in\mathcal{N}_k^{\mathrm{I}}} p'_{k,n}, & j = d_i, i = x, \ldots, |\mathcal{D}|, \\ 0, & \text{otherwise.} \end{cases} \tag{4.27}$$

Proof. Please refer to Appendix K. □

Problem (4.26) is solved by the following proposition.

Proposition 4.5.4. *For Problem (4.26), the optimal* $\{p'_{k,n}\}$ *is either given by*

$$p'_{k,n} = \left(\frac{1}{\lambda K N \ln 2} - \frac{\Gamma\sigma^2}{g'_{k,n}}\right)^+, k \in \mathcal{K}, n \in \mathcal{N}_k^{\mathrm{I}} \tag{4.28}$$

where λ *satisfies* $\sum_{k=1}^{K} \sum_{n\in\mathcal{N}_k^{\mathrm{I}}} p'_{k,n} = KQ + B_1/h_{d_{x-1}}$*; or given by*

$$p'_{k,n} = \begin{cases} \left(\frac{1}{(\lambda-\mu)KN\ln 2} - \frac{\Gamma\sigma^2}{g'_{k,n}}\right)^+, & k = 1, \ldots, d_x, n \in \mathcal{N}_k^{\mathrm{I}}, \\ \left(\frac{1}{\lambda KN\ln 2} - \frac{\Gamma\sigma^2}{g'_{k,n}}\right)^+, & k = d_x + 1, \ldots, K, n \in \mathcal{N}_k^{\mathrm{I}}. \end{cases} \tag{4.29}$$

where λ *and* μ *satisfy* $\sum_{k=1}^{d_x} \sum_{n\in\mathcal{N}_k^{\mathrm{I}}} p'_{k,n} = B_1/h_{d_{x-1}}$ *and* $\sum_{k=d_x+1}^{K} \sum_{n\in\mathcal{N}_k^{\mathrm{I}}} p'_{k,n} = KQ$.

Proof. Please refer to Appendix L. □

To summarize, Problem (4.8) given $\Pi(k), k \in \mathcal{K}$ can be solved as follows: for each $d_x, 1 \leq x \leq |\mathcal{D}| + 1$, solve Problem (4.26) to obtain $\{q_k\}$, $\{p_{k,n}\}$, and the objective value, denoted by $R(d_x)$. The optimal d_x is then obtained by the d_x which achieves the largest rate $R(d_x)$ and the corresponding power allocation $\{q_k\}$ and $\{p_{k,n}\}$ satisfy the constraints (4.8a) and (4.8b). We propose the algorithm in Table 4.1 to solve Problem (4.8) with given $\Pi(k), k \in \mathcal{K}$.

Table 4.1: Algorithm for solving Problem (4.8) with given $\Pi(k), k \in \mathcal{K}$.

I) **for** each $x = 1, \ldots, |\mathcal{D}| + 1$

1) Set effective channel power gain $\{g'_{k,n}\}$ by (4.24).
2) Obtain $p'_{k,n}, k \in \mathcal{K}, n \in \mathcal{N}_k^{\mathrm{I}}$ by WF algorithm with total power $KQ + B_1/h_{d_{x-1}}$.
3) **if** $\sum_{k=1}^{d_x} \sum_{n \in \mathcal{N}_k^{\mathrm{I}}} p'_{k,n} < B_1/h_{d_{x-1}}$
   a) Obtain $p'_{k,n}, k = 1, \ldots, d_x, n \in \mathcal{N}_k^{\mathrm{I}}$ by WF algorithm with total power $B_1/h_{d_{x-1}}$.
   b) Obtain $p'_{k,n}, k = d_x + 1, \ldots, K, n \in \mathcal{N}_k^{\mathrm{I}}$ by WF algorithm with total power KQ.
4) **end**
5) Obtain $\{p_{k,n}\}$ and $\{q_k\}$ by (4.25) and (4.27), respectively, and obtain the corresponding rate $R(d_x)$.
6) **if** $\{q_k\}$ and $\{p_{k,n}\}$ do not satisfy (4.8a) or (4.8b)
   a) Set $R(d_x)$ as zero.
7) **end**

II) **end**

III) Set $d_x^* = \arg\max_{d_x} R(d_x)$.

IV) The achievable rate for Problem (4.8) with given $\Pi(k), k \in \mathcal{K}$ is given by $R(d_x^*)$. The optimal power allocation $\{q_k^*\}$ and $\{p_{k,n}^*\}$ are obtained by step 5) correspond to the x^*th iteration.

4.5.2 Sub-Channel Allocation

Next, we consider the SC allocation design for Problem (4.8), i.e., the integer function $\Pi(k), k \in \mathcal{K}$. The optimization on the integer function $\Pi(k), k \in \mathcal{K}$ is non-convex. In general, the complexity of exhaustive search over all possible $\Pi(k), k \in \mathcal{K}$ is $\mathcal{O}(N^K)$. Hence, we propose heuristic schemes for the SC allocation, which are easy to implement in practice, namely the dynamic SC scheme and the static SC scheme.

Define a SC allocation function $\tilde{\Pi}(k)$, which allocates the best SC for the WPT link among all SCs $\mathcal{N}'$ at each slot k for WPT, i.e.,

$$\tilde{\Pi}(k) = \arg\max_{n \in \mathcal{N}'} h_{k,n}, \ k \in \mathcal{K}. \tag{4.30}$$

Let $\tilde{\mathcal{D}}$ denote the causally dominating slot set obtained by (4.9) given SC allocation $\tilde{\Pi}(k)$. From Proposition 4.5.2, WPT should occur only at causally dominating slots, hence, we let $\Pi(k) = 0$ for $k \in \tilde{D}^{\mathrm{c}}$ such that potential information transmission can be performed at SCs $\tilde{\Pi}(k), k \in \tilde{D}^{\mathrm{c}}$. In the *dynamic SC scheme*, the SC allocation is then given by

$$\Pi(k) = \begin{cases} \tilde{\Pi}(k), & k \in \tilde{\mathcal{D}}, \\ 0, & \text{otherwise}. \end{cases} \tag{4.31}$$

Remark 4.5.3. In Problem (4.8), a performance upper bound for any SC allocation is obtained by allowing energy and information to transmit simultaneously using the same SC, while employing perfect interference cancellation at the DAP. Mathematically, this is equivalent to letting $\mathcal{N}_k^{\mathrm{E}} = \mathcal{N}_k^{\mathrm{I}} = \mathcal{N}', k \in \mathcal{K}$ in Problem (4.6), which is then solved by the following lemma.

Lemma 4.5.3. *Problem* (4.6) *with* $\mathcal{N}_k^{\mathrm{E}} = \mathcal{N}_k^{\mathrm{I}} = \mathcal{N}', k \in \mathcal{K}$ *achieves same rate as Problem* (4.8) *with* $\Pi(k)$ *given in* (4.31) *and* $\mathcal{N}_k^{\mathrm{I}} = \mathcal{N}', k \in \mathcal{K}$.

Proof. Please refer to Appendix M. □

In the *static SC scheme*, one SC is selected and fixed for WPT throughout the whole transmission block, i.e., $\Pi(k) = n, k \in \mathcal{K}$, where the optimal choice of n is obtained by exhaustive search over the SC set $\mathcal{N}'$ and selecting the one which achieves the largest rate. Therefore, the complexity of exhaustive search over all possible $\Pi(k) = n, k \in \mathcal{K}$ is $\mathcal{O}(N)$.

4.6 Online Algorithm for Sub-Channel Allocation

In this section, we consider online algorithms when causal CSI is available. In general, online algorithms can be designed optimally based on dynamic programming [56]. However, the dynamic programming approach usually involves recursive computation with high computing complexity, which may be complicated for practical implementation. Furthermore, dynamic programming requires knowledge of channel statistics, e.g., the joint probability density function of the channel power gains for the WPT/WIT links, which may be non-stationary or not available. Therefore, we aim to design online algorithm that has low complexity and requires only the past and present channel observations. Motivated by the results for the full CSI case, our online algorithm partitions the transmission block into subsets, and perform WPT on the expected best SC in each subset. In particular, a simple scheme is proposed for the SC selection, which requires channel observations only of the past and present slots for the WPT link.

For the full CSI case (assuming zero initial battery energy), the transmission block is partitioned as intervals according to the channels for the WPT link, and the information transmission during each interval $\mathcal{D}_{i+1}, i = 1, \ldots, |\mathcal{D}|$ is powered by the harvested energy during its prior slot d_i (c.f. Proposition 4.5.3). The required amount of energy for information transmission is harvested at an earlier slot to ensure that there is always sufficient energy for WIT, i.e., no energy outage at the energy buffer. Motivated by this observation, we partition the transmission block $\mathcal{K}$

into subsets, referred to as *windows*, denoted by $\mathcal{W}_i, i = 1, \ldots, W$, where W denotes the number of windows. WPT is performed in each window $\mathcal{W}_i, i = 1, \ldots, W-1$, and the harvested energy during $\mathcal{W}_i$ is utilized to power information transmission during the next window $\mathcal{W}_{i+1}$, which ensures no energy outage for WIT during the block (except the first window). No WPT is performed in the last window. In particular, the first window consists of the first slot, while the remaining $K-1$ slots are partitioned into $W-1$ windows, each window consists of L slots, where L denotes the window size, with $1 \leq L \leq K-1$. For simplicity, we assume $K-1$ is divisible by L; hence, $W = (K-1)/L + 1$. Notice that the partitioned windows for the causal CSI case are fixed, which is independent of the channels for the WPT link.

In each window $\mathcal{W}_i, i = 1, \ldots, W-1$, one SC is selected to perform WPT. We assume the transmission energy at EAP is equally scheduled to the windows $\mathcal{W}_i, i = 1, \ldots, W-1$, hence, the EAP transmit with power $KQ/(W-1)$ at the selected SC in each window. For information transmission at the user, two energy sources are available, i.e., the initial battery energy B_1 and the energy harvested from EAP. Since only causal CSI is available, we assume B_1 is equally scheduled for information transmission over all K slots, hence each slot is scheduled with transmission power B_1/K. The energy harvested during window $\mathcal{W}_i, i = 1, \ldots, W-1$, is utilized for information transmission during the next window $\mathcal{W}_{i+1}$, where each slot is scheduled with equal transmission power. At each slot k, $\{p_{k,n}, n \in \mathcal{N}_k^{\mathrm{I}}\}$ is obtained by the WF power allocation[3] over SCs $n \in \mathcal{N}_k^{\mathrm{I}}$.

Next, we investigate the SC selection in each window $\mathcal{W}_i, i = 1, \ldots, W-1$. As revealed by the full CSI case, WPT is performed on one SC to power its subsequent interval, hence, we aim to select one SC that is expected to have the largest channel power gain for the WPT link among all SCs in each window to perform WPT. It is necessary for a SC to be best among all SCs in a window that it is the best SC

[3]In practice, the user may be imposed on a peak power constraint on its transmission power on each SC n during each slot k, i.e., $p_{k,n} \leq P_{\mathrm{peak}}$. In this case, at each slot k, the power allocation at the user $\{p_{k,n}, n \in \mathcal{N}_k^{\mathrm{I}}\}$ is then obtained by the (revised) WF power allocation with additional peak power constraint $p_{k,n} \leq P_{\mathrm{peak}}$.

at its current slot, hence, the SC is selected from the set $\{\tilde{\Pi}(k), k \in \mathcal{W}_i\}$. For the first window $\mathcal{W}_1 = \{1\}$, the best SC $\tilde{\Pi}(1)$ is selected to perform WPT. Consider other windows $\mathcal{W}_i, i = 2, \ldots, W-1$. Assume the channel power gain at the best SC at the kth slot in the window is denoted by $h_{[k]}$, where $k = 1, \ldots, L$. The SC selection problem is then formulated as a stopping problem described as follows. Given a sequentially occurring random sequence $h_{[1]}, h_{[2]}, \ldots, h_{[L]}$, the permutations of which are equally likely, our objective is to select a slot to stop, the index of which is denoted by s, such that the probability of $h_{[s]} > h_{[j]}, \forall j = 1, \ldots, L, j \neq s$, denoted by P_{r}, is maximized. The challenge is that at any slot $k = 1, \ldots, L$, the decision of whether to stop at current slot (i.e., $s = k$) or stop at latter slots (i.e., $s \neq k$) needs to be made immediately, based on causal information, i.e., $\{h_{[j]}, 1 \leq j \leq k\}$. The decision of $s = k$ suffers a potential loss when better channels occur in subsequent slots in the window; whereas the decision of $s \neq k$ risks the probability that a better channel never occurs subsequently. The stopping problem can be viewed as a classic Secretary Problem [63]. A necessary condition for stopping at slot s is that $h_{[s]} > h_{[j]}, \forall j = 1, \ldots, L, j < s$, i.e., slot s causally dominates all its previous slots in the window; otherwise, the probability P_{r} becomes zero. Hence, the optimal stopping rule lies in a class of policies, which are described as follows: Define the cutoff slot $f(L)$, which is a parameter that can be optimized, and $1 \leq f(L) \leq L$. The first $f(L)-1$ slots are for observation. During the remaining $L-f(L)+1$ slots, the first slot (if any) that causally dominates all its previous slots, is selected as s; if no slot is selected until the last slot, then $s = L$. The probability P_{r} is given by [63]

$$P_{\mathrm{r}} = \begin{cases} \frac{1}{L}, & f(L) = 1, \\ \frac{f(L)-1}{L} \sum\limits_{l=f(L)}^{L} \frac{1}{l-1}, & 1 < f(L) \leq L. \end{cases} \tag{4.32}$$

The optimal cutoff slot $f^*(L)$ that maximizes P_{r} is thus obtained as $f^*(L) = \arg\max\limits_{1 \leq f(L) \leq L} P_{\mathrm{r}}$. The above SC selection scheme is referred to as *dynamic SC with observe-then-transmit (OTT)*.

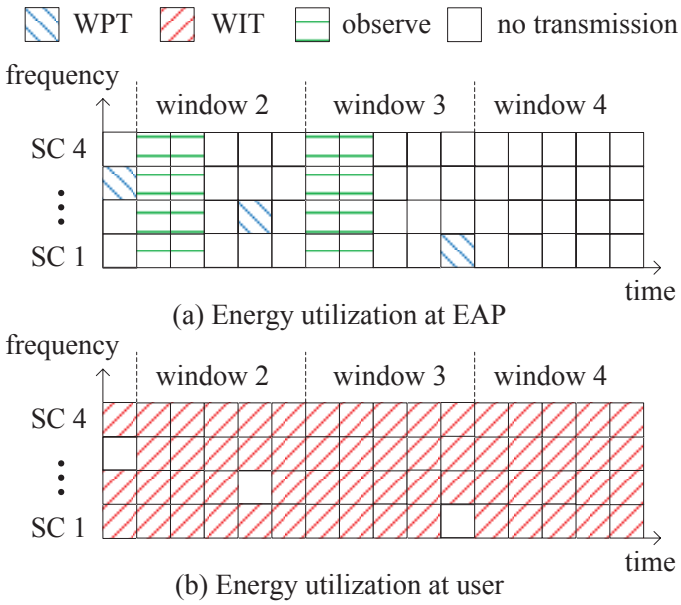

Figure 4.2: Energy utilization for the scheme of dynamic SC with OTT, where $K = 16, N = 4$ and $L = 5$.

An example of the scheme of dynamic SC with OTT is illustrated in Fig. 4.2, where the total number of slots is $K = 16$, and the window size is $L = 5$. The windows are obtained as $\mathcal{W}_1 = \{1\}, \mathcal{W}_2 = \{2, \ldots, 6\}, \mathcal{W}_3 = \{7, \ldots, 11\}, \mathcal{W}_4 = \{12, \ldots, 16\}$. In $\mathcal{W}_1$, the best SC (SC 3) at WPT link in slot one is selected to transmit energy. From (4.32), the cutoff slot is obtained as $f^*(L) = 3$. Hence, for $\mathcal{W}_2$ and $\mathcal{W}_3$, in each window the first two slots are for observing $h_{k,n}, n \in \mathcal{N}$, and the first slot (if any) during the remaining three slots that causally dominates all its previous slots in the window is selected for WPT; otherwise, the last slot is scheduled for WPT. In $\mathcal{W}_4$, there is no energy transmission from EAP. In Fig. 4.2(a), WPT is performed at SC 3 during slot 1, SC 2 during slot 5, and SC 1 during slot 11; hence, in Fig. 4.2(b), the user transmits information at the remaining SCs.

4.7 Numerical Example

In this section, we provide numerical examples. We focus on the separated EAP/DAP case, where the distances from EAP to the user and from the user to DAP are assumed to be 5m and 15m, respectively. The total number of slots is set to be $K = 61$. The total bandwidth of the system is assumed to be 10MHz, centered at 900MHz, which is equally divided into $N = 16$ SCs, each with bandwidth 625kHz. The six-tap exponentially distributed power profile is used to generate the frequency-selective fading channel. The channels over slots are generated independently. In later simulations, all achievable rates are averaged over 10^4 independent channel realizations. Assuming the path-loss exponent is three, the signal power attenuation at transmission distance d (in meter) is then approximately $(-31.5-30\log_{10} d)$dB. The receiver noise power spectrum density at DAP is assumed to be -174dBm/Hz, and $\Gamma = 9$dB. The initial batter energy is set to be $B_1 = 0$.

4.7.1 Offline Algorithms

First, consider the full CSI case, in which we compare the performance by different offline schemes. As benchmark, we consider the system in [56, 57] with random energy arrivals at the EH user. In particular, the EAP in Fig. 4.1 is replaced by an ambient RF transmitter which is oblivious of the WPT link, and hence its transmit power over time is random to the user, since it is adapted to its own information transmission link (to another receiver). Throughout the whole transmission block, the ambient transmitter transmits over a fixed SC (e.g., the first SC), and the remaining $(N-1)$ SCs are for the information transmission at the EH user. In simulation, the transmit power at the ambient transmitter $q_{k,1}, k \in \mathcal{K}$ are randomly generated by the uniform distribution over $[0, 1]$, and then are normalized such that $1/K \sum_{k=1}^{K} q_{k,1} = Q$. Hence, during each slot $k, k \in \mathcal{K}$, a random energy $h_{k,1}q_{k,1}$ arrives at the user. Given $\{h_{k,1}q_{k,1}, k \in \mathcal{K}\}$, the achievable rates are obtained by optimizing $\{p_{k,n}, k \in \mathcal{K}, n \in \mathcal{N}\backslash\{1\}\}$ according to [56, 57]. The performance of this system is obtained by averaging the results from 10^4 realizations of random

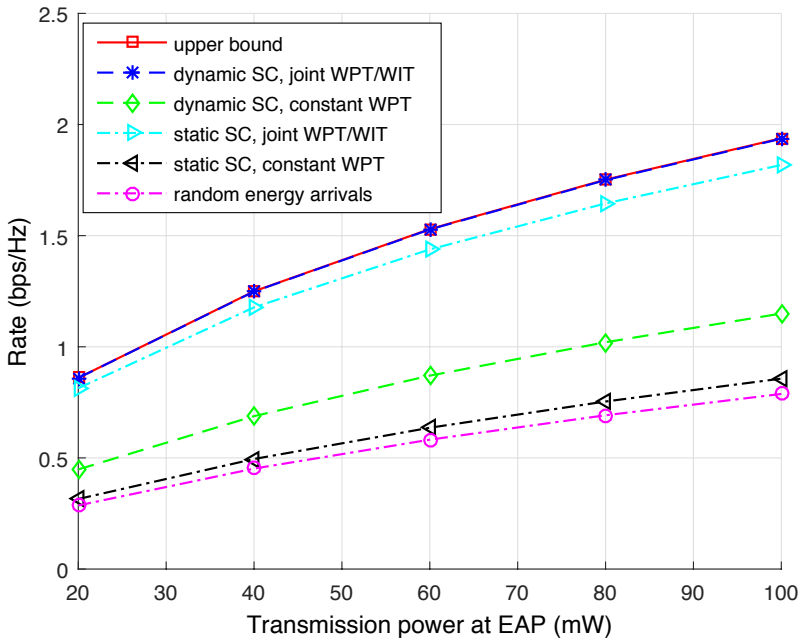

Figure 4.3: Performance comparison for offline algorithms when full CSI is available.

transmission power $\{q_{k,1}, k \in \mathcal{K}\}$. In addition, the performance upper bound obtained by the ideal DAP with perfect interference cancellation (refer to Remark 4.5.3) is also considered as benchmark. Besides the optimal joint WPT/WIT transmission, for comparison we also consider a sub-optimal WPT scheme referred to as constant WPT, where the EAP transmits constant power Q each slot at given SC (by dynamic/static SC schemes).

Fig. 4.3 shows the achievable rates at DAP versus transmission power at EAP by different offline schemes. In Fig. 4.3, it is observed that the achievable rates by the proposed dynamic SC scheme with joint WPT/WIT transmission are very close to that by the upper bound. Comparing the joint WPT/WIT with constant WPT transmission schemes, it is observed that for both dynamic and static SC, the joint WPT/WIT schemes achieve much larger rates than that by the constant WPT schemes, which demonstrates the importance of optimal energy allocation over time for the WPT link. Comparing the dynamic SC and the static SC schemes, it is observed that for either joint WPT/WIT or constant WPT transmission, the

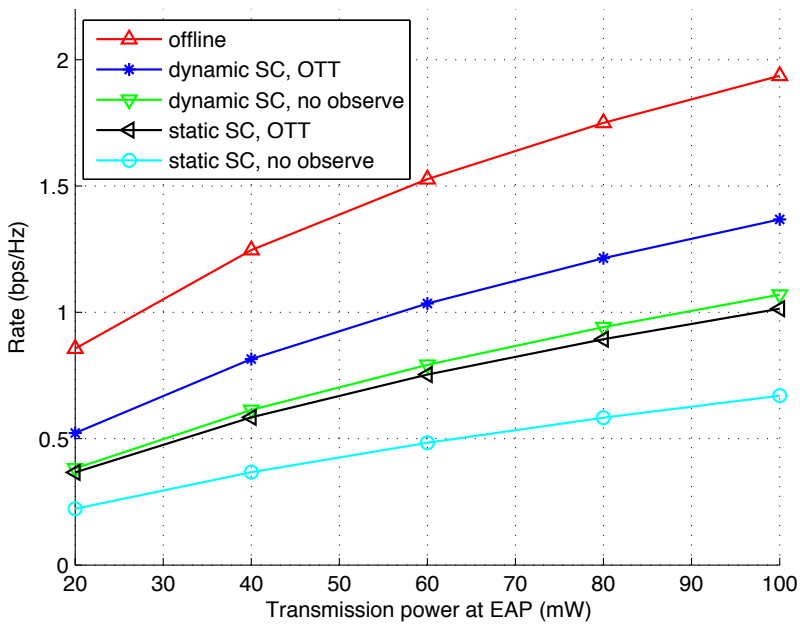

Figure 4.4: Performance comparison for online algorithms when casual CSI is available, where $L = 15$.

dynamic SC scheme is superior than the static SC scheme, and the performance gap is larger when EAP performs constant WPT transmission. This is because that the dynamic SC scheme exploits more frequency diversity for WPT; in contrast, the available channels for WPT are constrained on one SC over the whole transmission block. Hence, in general more energy can be harvested to support higher data rate by the dynamic SC scheme than by the static SC scheme. It implies that optimizing SC allocation is important to the performance, especially when EAP performs sub-optimal constant-power WPT. Last, comparing the achievable rates by the wireless powered communication system with dynamic SC, joint WPT/WIT and that by the system with random energy arrivals, a remarkable performance improvement is observed by the wireless powered system, which demonstrates the superiority of WPC with dedicated EAP over conventional EH system with random energy arrivals.

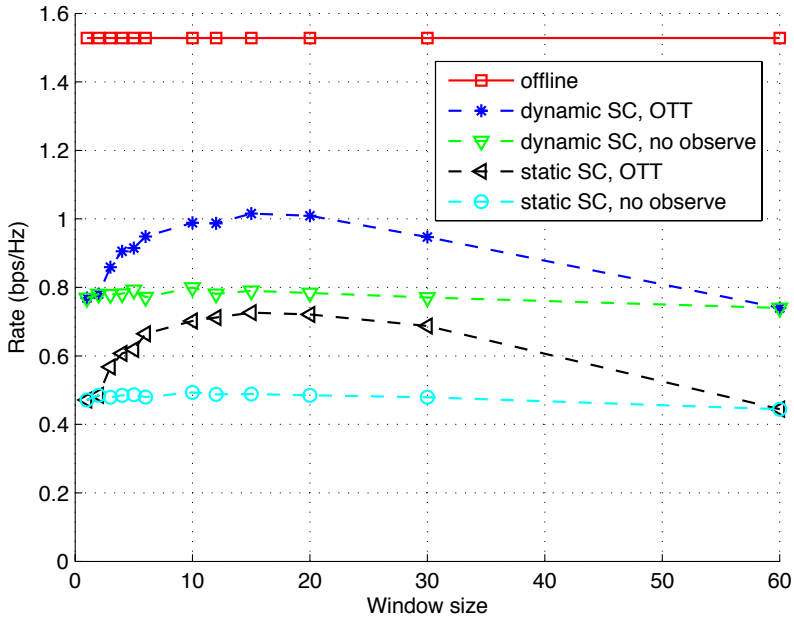

Figure 4.5: Performance comparison for online algorithms when casual CSI is available, where $Q = 60$mW.

4.7.2 Online Algorithms

Next, consider the causal CSI case, in which we compare the performance by different online schemes. Besides the scheme of dynamic SC with OTT proposed in Section 4.6, for comparison we also consider other window-based online schemes, where a static SC (e.g., the first SC) is fixed for WPT, or the EAP selects the first slot in each window (i.e., no channel observation) to perform WPT. In addition, the performance by the offline dynamic SC with joint WPT/WIT scheme is considered as a benchmark.

Fig. 4.4 shows the achievable rates by different window-based online schemes versus the transmission power at EAP Q. In Fig. 4.4, the window size L is set to be $L = 15$ with optimal cutoff slot $f^*(L) = 6$. It is observed in Fig. 4.4 that the achievable rates by online schemes are smaller than that by the offline scheme, due to lack of future information of channels for the WPT/WIT links. In Fig. 4.4, comparing the performance by the dynamic and static SC schemes, it is observed

that the dynamic SC schemes achieve larger rates. Comparing the performance by the OTT schemes and that by the no-observation schemes, it is observed that the OTT schemes are superior, as observation for the WPT link helps to employ more efficient energy transmission by transmitting on SC that is expected to have large channel power gain.

Fig. 4.5 further shows the achievable rates by different window-based online schemes versus the window size L. In Fig. 4.5, the transmission power at EAP is set to be $Q = 60$mW. Similar as in Fig. 4.4, it is observed in Fig. 4.5 that the dynamic SC scheme is superior than the static SC scheme, and the OTT scheme is better than the no-observation scheme. We notice that in Fig. 4.5 the performance by the OTT schemes degrade to that by the no-observation schemes when $L = 1, 2, 60$, as no observation is performed for these special cases. Furthermore, in Fig. 4.5, it is observed that as the window size increases, the achievable rates by the no-observation schemes are independent of the window size; whereas the achievable rates by the OTT schemes first increase and then decrease. Intuitively, this may be because that with larger window size more observation slots help to select SCs with large channel power gain to perform WPT. However, smaller window size results in more number of selected SCs, which helps to compensate the loss of selecting poor SCs (in the last slot of each window).

4.8 Chapter Summary

In this chapter, we studied an OFDM-based WPC system, where a user harvests energy from the EAP to power its information transmission to the DAP. The energy transmission by the EAP and the information transmission by the user is performed over orthogonal SCs. The achievable rate at the DAP was maximized by jointly optimizing the SC allocation over time and power allocation over time and SCs for both WPT and WIT links. Numerical results demonstrated that by dynamic SC allocation and joint power allocation, the performance is improved remarkably as compared to a conventional EH system where the information transmitter is powered

by random energy arrivals. Our results provide useful insights to the design for OFDM-based WPC system in practice.

Chapter 5

Conclusion and Future Work

5.1 Conclusion

This thesis has provided a unified study on wireless information and power transfer by comprehensive investigations on the system modeling, performance analysis, and resource allocation optimization for SWIPT and WPC. The main results of this thesis are summarized as follows.

In Chapter 2, we provided an in-depth modeling for the SWIPT system rooted on circuit analysis. This bottom-up circuit-based approach allows us to propose a novel integrated information and energy receiver, in which part of the information decoding implementation, i.e., the RF to baseband conversion, is integrated to the energy receiver via the rectifier. Taking circuit power consumption into account, we characterized the rate-energy performance and derived the optimal receiver strategies for both conventional separated receiver and the proposed integrated receiver. Performance comparison was also studied under a realistic system setup that employs practical modulation. Our proposed receiver provides an appealing new design for the implementation of SWIPT.

In Chapter 3, we studied a new resource allocation problem for the multiuser OFDM-based SWIPT system. We proposed two multiplexing and corresponding receiver schemes to coordinate the wireless information transmission and wireless energy transmission, namely, TDMA with TS receivers and OFDMA with PS receivers. We obtained the joint optimal transmission power allocation over time and

SCs, and the TS or PS ratios at the receivers for the two schemes. We compared the performances of the two schemes numerically, as well as analytically for the special case of a single user setup. Our results demonstrate that joint design for the resource allocation (power, bandwidth, time, etc.) and receiver strategy (TS/PS ratios) is essential to achieving near-optimal R-E performance in SWIPT systems. Our results also provide key insights for the optimal transmitter and receiver strategy design for OFDM-based SWIPT system. Specifically, the peak power constraint imposed on each OFDM SC as well as the number of users in the system play key roles in the R-E performance. Moreover, the TS receiver outperforms the PS receiver for moderate EH requirement at users.

In Chapter 4, we investigated a new resource allocation problem for the OFDM-based WPC system. We proposed a new energy and information transmissions scheme for WPC to support contiguous information transmission, by scheduling WPT and WIT over orthogonal SCs. Given availability of full CSI, we derived the structure of the optimal resource allocation strategy, based on which we proposed an offline algorithm to jointly optimize the SC allocation over time, and power allocation over time and SCs, for both WPT and WIT links. Given causal CSI, we proposed a low-complexity online algorithm. Our results demonstrate the advantage of using an optimized dedicated wireless power over relying on conventional opportunistic EH sources to supply energy to wireless devices. Our studies provide fundamental design principles for joint energy and information scheduling in OFDM-based WPC system. It is revealed that joint resource allocation (power, bandwidth, time, etc.) for both WPT and WIT links is essential to achieve the optimal system performance by balancing the energy supply and consumption at users. For the case of full CSI, energy transmissions may occur only during the so-called causally dominating slots. For the case of causal CSI, even utilizing partial information of the channels for the WPT link can be much beneficial to the throughput performance.

5.2 Future Work

In this section, we discuss possible extensions and future work directions that are worthy of further investigation.

For the receiver design for SWIPT, in Chapter 2 the achievable rate by the proposed integrated receiver is computed by the lower bound. From the information theoretical standpoint, it is worthy to derive the capacity of the new nonlinear channel and the corresponding optimal input distribution. Moreover, in the present work, we employ PEM with equispaced positive constellation points for energy and data modulation scheme. From the implementation standpoint, it will be useful to investigate the optimal constellation design for the modulation. Finally, there is still a performance gap between the performance achieved by the proposed integrated receiver and the optimistic upper bound achieved by an ideal receiver. How to close the gap with novel receiver architectures for SWIPT remains an open challenge, which is left for future work.

For the resource allocation optimization in SWIPT system, the proposed iterative algorithm for the PS receiver requires sufficient number of randomly generated initial points. In general, as the number of users increases, the number of initialization points needs to be increased to improve the robustness and near-optimality of the algorithm, which inevitably increases the computation complexity. Therefore, future work is needed to propose more efficient algorithm to reduce the complexity for the SWIPT system with large number of PS receivers. Moreover, in Chapter 3 we assume perfect CSI at the HAP. In practice, it may be difficult to obtain perfect CSI due to channel estimation error, feedback error, etc. Future work may consider the more practical scenario of imperfect CSI. The resource allocation will need to take into account the lack or uncertainty of the CSI. This leads to a very different problem involving the random nature of the feedback, and will call potentially for new tools such as stochastic programming.

For the resource allocation optimization in WPC system, in Chapter 4 only one single user is considered for the purpose of exposition. As an extension, future work

can investigate the more general scenario of multiple users co-existing in the system. For the multiuser case, the broadcast signals by the EAP may provide wireless power to supply all users simultaneously in DL. The UL information transmission from different users to the DAP may be coordinated by the OFDMA scheme. Hence, besides SC allocation between WPT and WIT links, the SCs for the WIT links need to be further allocated to multiple users. Moreover, in Chapter 4 we considered only average transmission power constraint at the EAP. It is of practical interests to extend the results in Chapter 4 to the more practical case when additional peak power constraint is imposed on the transmission power for each SC during any slot. Specifically, the structure of the optimal resource allocation may need to be adjusted to satisfy the peak power constraint. For example, intuitively, when the peak power constraint is very tight, instead of transferring energy only during the casually dominating slots, WPT may also occur on non-casually-dominating-slots. It will also be useful to extend the results in Chapter 4 to the case where the energy buffer at the user has limited storage capacity. Furthermore, in Chapter 4 we assumed that all harvested energy is utilized for information transmission. In practice, wireless users consume additional power for circuit operations, such as signal processing, and may lead to a change in the structure of the optimal resource allocation. Therefore, the inclusion of circuit power consumption in the problem formulation is worth further investigation.

Appendix A

Proof of Proposition 2.4.1

To show $\mathcal{C}_{\text{R-E}}^{\text{DPS}}(P) = \mathcal{C}_{\text{R-E}}^{\text{PS}}(P), P \geq 0$, it suffices for us to show that $\mathcal{C}_{\text{R-E}}^{\text{PS}}(P) \subseteq \mathcal{C}_{\text{R-E}}^{\text{DPS}}(P), P \geq 0$ and $\mathcal{C}_{\text{R-E}}^{\text{DPS}}(P) \subseteq \mathcal{C}_{\text{R-E}}^{\text{PS}}(P), P \geq 0$. The first part of proof is trivial, since PS is just a special case of DPS by letting $\rho_k = \rho, \forall k$ (c.f. (2.16)). Next, we prove the second part. Assuming that $f(\rho) = \log_2\left(1 + \frac{(1-\rho)hP}{(1-\rho)\sigma_{\text{A}}^2 + \sigma_{\text{cov}}^2}\right)$, it is easy to verify that $f(\rho)$ is concave in $\rho \in [0, 1]$. By Jensen's inequality, we have $\frac{1}{N}\sum_{k=1}^{N} f(\rho_k) \leq f\left(\frac{1}{N}\sum_{k=1}^{N}\rho_k\right)$. Thus, for $\forall \boldsymbol{\rho} = [\rho_1, \ldots, \rho_N]^T$, $\exists \rho = \frac{1}{N}\sum_{k=1}^{N}\rho_k$, so that $\frac{1}{N}\sum_{k=1}^{N}\rho_k \zeta hP = \rho\zeta hP$ and $\frac{1}{N}\sum_{k=1}^{N} f(\rho_k) \leq f(\rho)$. Since R-E region is defined as the union of rate-energy pairs (R, Q) under all possible $\boldsymbol{\rho}$, it follows immediately that $\mathcal{C}_{\text{R-E}}^{\text{DPS}}(P) \subseteq \mathcal{C}_{\text{R-E}}^{\text{PS}}(P), P \geq 0$, which completes the proof of Proposition 2.4.1.

Appendix B

Proof of Proposition 2.6.1

To show $\mathcal{C}_{\text{R-E}}^{\text{DPS}'}(P) = \mathcal{C}_{\text{R-E}}^{\text{OPS}'}(P), P \geq 0$, it suffices for us to show that $\mathcal{C}_{\text{R-E}}^{\text{OPS}'}(P) \subseteq \mathcal{C}_{\text{R-E}}^{\text{DPS}'}(P), P \geq 0$ and $\mathcal{C}_{\text{R-E}}^{\text{DPS}'}(P) \subseteq \mathcal{C}_{\text{R-E}}^{\text{OPS}'}(P), P \geq 0$. The first part of proof is trivial, since OPS is just a special case of DPS by letting $\rho_k = \rho, k = \alpha N, \ldots, N$ (c.f. (2.17)). Next, we prove the second part. By (2.36), ρ_k's are optimized at $\rho_k = 1$ for $k = 1, \ldots, \alpha N$; thus, we have $Q \leq \alpha\zeta hP + \frac{1}{N}\sum_{k=\alpha N+1}^{N} \rho_k \zeta hP - (1-\alpha)P_{\text{S}}$ for DPS. For any given α, by Jensen's inequality we have $\frac{1}{(1-\alpha)N}\sum_{k=\alpha N+1}^{N} f(\rho_k) \leq f\left(\frac{1}{(1-\alpha)N}\sum_{k=\alpha N+1}^{N} \rho_k\right)$. Thus, for $\forall\alpha$ and $\forall\boldsymbol{\rho} = [\rho_1, \ldots, \rho_N]^T$, $\exists\rho = \frac{1}{(1-\alpha)N}\sum_{k=\alpha N+1}^{N} \rho_k$, so that $\frac{1}{N}\sum_{k=\alpha N+1}^{N} \rho_k \zeta hP = (1-\alpha)\rho\zeta hP$ and $\frac{1}{N}\sum_{k=\alpha N+1}^{N} f(\rho_k) \leq (1-\alpha)f(\rho)$. Since R-E region is defined as the union of rate-energy pairs (R, Q) under all possible $\boldsymbol{\rho}$, it follows immediately that $\mathcal{C}_{\text{R-E}}^{\text{DPS}'}(P) \subseteq \mathcal{C}_{\text{R-E}}^{\text{OPS}'}(P), P \geq 0$, which completes the proof of Proposition 2.6.1.

Appendix C

Proof of Lemma 2.6.1

From (2.42), the first and second derivatives of $R(s)$ with respect of s are given by

$$\frac{dR}{ds} = \log_2\left(1 + \frac{cs+d}{as+b}\right) + \frac{s(bc-ad)}{((a+c)s+b+d)\,(as+b)\ln 2}, \tag{C.1}$$

$$\frac{d^2R}{ds^2} = \frac{(bc-ad)\,((b(a+c)+a(d+d))\,s+2b(d+d))}{((a+c)s+b+d)^2\,(as+b)^2\ln 2}. \tag{C.2}$$

From (C.2), the sign of $\frac{d^2R}{ds^2}$ is identical with the line $f_2(s) = (bc - ad)\,((b(a+c)+a(d+d))\,s+2b(d+d))$. Note that $bc-ad = -\sigma^2_{\mathrm{cov}}(hP-Q/\zeta) < 0$, $f_2(0) = 2b(b+d)(bc-ad) < 0$, and $f_2(-\frac{d}{c}) = \frac{(2b+d)(bc-ad)^2}{c} < 0$; thus, we have $\frac{d^2R}{ds^2} < 0$ for $s \in [0, -\frac{d}{c}]$. Since the set $[\frac{d}{hP-c}, \min\{-\frac{d}{c}, 1\}]$ is a subset of the set $[0, -\frac{d}{c}]$, we have $\frac{d^2R}{ds^2} < 0$ for $s \in [\frac{d}{hP-c}, \min\{-\frac{d}{c}, 1\}]$. Thus, $R(s)$ is concave in $s \in [\frac{d}{hP-c}, \min\{-\frac{d}{c}, 1\}]$, which completes the proof of Lemma 2.6.1.

Appendix D

Proof of Proposition 2.7.1

We first consider (P1) with $0 \leq Q_{\text{req}} \leq \zeta hP$ for the separated receiver. The optimal α for (P1) is given by $\alpha_1^* = \left(\frac{Q_{\text{req}} - \rho_1^* \zeta hP + P_{\text{S}}}{(1-\rho_1^*)\zeta hP + P_{\text{S}}}\right)^+$. Since $Q_{\text{req}} \leq \zeta hP$, α_1^* decreases as ρ_1^* increases. Thus, we have

$$\alpha_1^* \geq \left.\frac{Q_{\text{req}} - \rho_1^* \zeta hP + P_{\text{S}}}{(1-\rho_1^*)\zeta hP + P_{\text{S}}}\right|_{\rho_1^*=1} = \frac{Q_{\text{req}} - \zeta hP + P_{\text{S}}}{P_{\text{S}}}. \tag{D.1}$$

Next, for the integrated receiver with $0 \leq Q_{\text{req}} \leq \zeta hP$, the optimal α for (P2) is given by

$$\alpha_2^* = \left(\frac{Q_{\text{req}} - \zeta hP + P_{\text{I}}}{P_{\text{I}}}\right)^+ \tag{D.2}$$

From (D.1) and (D.2), we have $\alpha_1^* \geq \alpha_2^*$, given that $P_{\text{S}} > P_{\text{I}}$. Since $R = (1 - \alpha)\log_2 M$, we have $R_1^* \leq R_2^*$, given that $\alpha_1^* \geq \alpha_2^*$ and $M_1^* \leq M_2^*$. The proof of Proposition 2.7.1 thus follows.

Appendix E

Proof of Lemma 3.5.1

To prove the concavity of function $f(q_{k,n}, \alpha_k)$, it suffices to prove that for all $q_{k,n} \geq 0$, $\alpha_k \geq 0$, and the convex combination $(\hat{q}_{k,n}, \hat{\alpha}_k) = \theta(\dot{q}_{k,n}, \dot{\alpha}_k) + (1-\theta)(\ddot{q}_{k,n}, \ddot{\alpha}_k)$ with $\theta \in (0, 1)$, we have $f(\hat{q}_{k,n}, \hat{\alpha}_k) \geq \theta f(\dot{q}_{k,n}, \dot{\alpha}_k) + (1-\theta) f(\ddot{q}_{k,n}, \ddot{\alpha}_k)$. With $q_{k,n} \geq 0$, we consider the following four cases for α_k.

1) $\dot{\alpha}_k > 0$ and $\ddot{\alpha}_k > 0$: In this case, we have $\hat{\alpha}_k > 0$. Since $\log_2\left(1 + \frac{h_{k,n} q_{k,n}}{\Gamma \sigma^2}\right)$ is a concave function of $q_{k,n}$, it follows that its perspective $\alpha_k \log_2\left(1 + \frac{h_{k,n} q_{k,n}}{\Gamma \sigma^2 \alpha_k}\right)$ is jointly concave in $q_{k,n}$ and α_k for $\alpha_k > 0$ [43]. Therefore, we have $(\hat{q}_{k,n}, \hat{\alpha}_k) \geq \theta(\dot{q}_{k,n}, \dot{\alpha}_k) + (1-\theta)(\ddot{q}_{k,n}, \ddot{\alpha}_k)$.

2) $\dot{\alpha}_k > 0$ and $\ddot{\alpha}_k = 0$: In this case, we have $f(\ddot{q}_{k,n}, \ddot{\alpha}_k) = 0$, $\hat{\alpha}_k = \theta \dot{\alpha}_k$, and

$$
\begin{aligned}
f(\hat{q}_{k,n}, \hat{\alpha}_k) &= \theta \dot{\alpha}_k \log_2\left(1 + \frac{h_{k,n}(\theta \dot{q}_{k,n} + (1-\theta)\ddot{q}_{k,n})}{\Gamma \sigma^2 \theta \dot{\alpha}_k}\right) \\
&= \theta \dot{\alpha}_k \log_2\left(1 + \frac{h_{k,n} \dot{q}_{k,n}}{\Gamma \sigma^2 \dot{\alpha}_{k,n}} + \frac{(1-\theta) h_{k,n} \ddot{q}_{k,n}}{\Gamma \sigma^2 \theta \dot{\alpha}_k}\right)
\end{aligned}
$$

Thus, we have $f(\hat{q}_{k,n}, \hat{\alpha}_k) \geq \theta f(\dot{q}_{k,n}, \dot{\alpha}_k) + (1-\theta) f(\ddot{q}_{k,n}, \ddot{\alpha}_k)$.

3) $\dot{\alpha}_k = 0$ and $\ddot{\alpha}_k > 0$: Similar as case 2), we have $f(\hat{q}_{k,n}, \hat{\alpha}_k) \geq \theta f(\dot{q}_{k,n}, \dot{\alpha}_k) + (1-\theta) f(\ddot{q}_{k,n}, \ddot{\alpha}_k)$.

4) $\dot{\alpha}_k = 0$ and $\ddot{\alpha}_k = 0$: In this case, we have $f(\hat{q}_{k,n}, \hat{\alpha}_k) = f(\dot{q}_{k,n}, \dot{\alpha}_k) = f(\ddot{q}_{k,n}, \ddot{\alpha}_k) = 0$. Therefore, $f(\hat{q}_{k,n}, \hat{\alpha}_k) = \theta f(\dot{q}_{k,n}, \dot{\alpha}_k) + (1-\theta) f(\ddot{q}_{k,n}, \ddot{\alpha}_k)$.

From the above four cases, we have $f(\hat{q}_{k,n}, \hat{\alpha}_k) \geq \theta f(\dot{q}_{k,n}, \dot{\alpha}_k) + (1-\theta) f(\ddot{q}_{k,n}, \ddot{\alpha}_k)$ for all $q_{k,n} \geq 0$ and $\alpha_k \geq 0$, and thus $f(q_{k,n}, \alpha_k)$ is concave, which completes the proof.

Appendix F

Proof of Proposition 3.5.1

For any $\hat{\lambda}_i \geq 0, i = 1, \ldots, K, \hat{\mu} \geq 0, \hat{\nu} \geq 0$, we have

$$\begin{aligned} g\left(\hat{\lambda}_i, \hat{\mu}, \hat{\nu}\right) &\geq \mathcal{L}\left(\{\dot{q}_{k,n}\}, \{\dot{\alpha}_k\}, \{\hat{\lambda}_i\}, \hat{\mu}, \hat{\nu}\right) \\ &= g\left(\{\lambda_i\}, \mu, \nu\right) + \sum_{i=1}^{K} (\hat{\lambda}_i - \lambda_i) \left(\zeta \sum_{k \neq i}^{K+1} \sum_{n=1}^{N} h_{i,n} \dot{q}_{k,n} - \overline{E}_i\right) \\ &\quad + (\hat{\mu} - \mu) \left(P - \sum_{k=1}^{K+1} \sum_{n=1}^{N} \dot{q}_{k,n}\right) + (\hat{\nu} - \nu) \left(1 - \sum_{k=1}^{K+1} \dot{\alpha}_k\right) \end{aligned}$$

By the definition of subgradient, the choice of $\boldsymbol{d}$ as given in (3.22) is indeed a subgradient for $g\left(\{\lambda_i\}, \mu, \nu\right)$.

Appendix G

Proof of Proposition 4.5.1

Since no WPT is performed at the last slot K, we prove Proposition 4.5.1 for $1 \leq k \leq K-1$. For optimal $q^*_{k,n}, k \in \mathcal{K}, n \in \mathcal{N}^{\mathrm{E}}_k$, assume there exists a slot $j, 1 \leq j \leq K-1$ and SC $l \in \mathcal{N}^{\mathrm{E}}_j, l \neq m(j)$, such that $q^*_{j,l} > 0$. We construct a different power allocation for the WPT link as follows:

$$\hat{q}_{k,n} = \begin{cases} \sum\limits_{u \in \mathcal{N}^{\mathrm{E}}_k} q^*_{j,u}, & k = j, n = m(j), \\ 0, & k = j, n \neq m(j), \\ q^*_{k,n}, & k \neq j, n \in \mathcal{N}^{\mathrm{E}}_k. \end{cases} \tag{G.1}$$

From (G.1), $\hat{q}_{k,n}, k \in \mathcal{K}, n \in \mathcal{N}^{\mathrm{E}}_k$ satisfies (4.6a). Since $q^*_{j,l} > 0$, we have

$$\sum_{n \in \mathcal{N}^{\mathrm{E}}_j} h_{j,n}(\hat{q}_{j,n} - q^*_{j,n}) = \sum_{n \in \mathcal{N}^{\mathrm{E}}_j} \left(h_{j,m(j)} - h_{j,n}\right) q^*_{j,n} > 0. \tag{G.2}$$

From (G.2), by $\hat{q}_{k,n}, k \in \mathcal{K}, n \in \mathcal{N}^{\mathrm{E}}_k$, a larger feasible region for $p_{k,n}, k \in \mathcal{K}, n \in \mathcal{N}^{\mathrm{I}}_k$ is obtained than that by $q^*_{k,n}, k \in \mathcal{K}, n \in \mathcal{N}^{\mathrm{E}}_k$, thus a larger achievable rate can be obtained by increasing some $p_{K,n}, n \in \mathcal{N}$, which contradicts the assumption that $q^*_{k,n}, k \in \mathcal{K}, n \in \mathcal{N}^{\mathrm{E}}_k$ is optimal. Hence, $q^*_{k,n} = 0$ for $n \neq m(k)$. Proposition 4.5.1 is thus proved.

Appendix H

Proof of Proposition 4.5.2

Given SC allocation $\Pi(k), k \in \mathcal{K}$, there are two possible cases for slots in set $\mathcal{D}^{\mathrm{c}}$, i.e., $\Pi(k) = 0$ or $\Pi(k) \in \mathcal{N}$. For $k \in \mathcal{D}^{\mathrm{c}}, \Pi(k) = 0$, we have $q_k^* = 0$, since no SC is available for WPT during the slot k. Next, we prove that $q_k^* = 0$ for $k \in \mathcal{D}^{\mathrm{c}}, \Pi(k) \in \mathcal{N}$. For any power allocation $\{q_k\}$, $\{p_{k,n}\}$ that satisfy the constraints (4.8a) and (4.8b), assume there exists a slot $i \in \mathcal{D}^{\mathrm{c}}$ with $\Pi(i) \in \mathcal{N}$ and $q_i > 0$. By the definition of set $\mathcal{D}$, there exists a slot $1 \leq j < i$ such that $h_j > h_i > 0, \Pi(j) \in \mathcal{N}$. We construct a power allocation strategy $\{\hat{q}_k\}$, $\{\hat{p}_{k,n}\}$ given by

$$\hat{q}_k = \begin{cases} q_j + q_i, & k = j, \\ 0, & k = i, \\ q_k, & \text{otherwise.} \end{cases}$$

$$\hat{p}_{k,n} = \begin{cases} p_{k,n} + \frac{(h_j - h_i) q_i}{N}, & k = i, n \in \mathcal{N}_k^{\mathrm{I}}, \\ p_{k,n}, & \text{otherwise.} \end{cases}$$

It can be verified that $\{\hat{q}_k\}$ and $\{\hat{p}_{k,n}\}$ satisfy the constraints (4.8a) and (4.8b). Since $h_j > h_i$ and $q_i > 0$, the achievable rate by $\{\hat{q}_k\}$, $\{\hat{p}_{k,n}\}$ is larger than that by $\{q_k\}$, $\{p_{k,n}\}$, i.e., $\{q_k\}$, $\{p_{k,n}\}$ is not optimal. Hence, the optimal solution satisfies that $q_k^* = 0$ for $k \in \mathcal{D}^{\mathrm{c}}$. The proof of Proposition 4.5.2 is thus completed.

Appendix I

Proof of Proposition 4.5.3

We prove that if $\{q_k^*\}$ and $\{p_{k,n}^*\}$ satisfy (4.8b) with equality at $i = d_j$, where $1 \leq j \leq |\mathcal{D}|$, then they satisfy (4.8b) with equality at $i = d_{j+1}$, i.e.,

$$\sum_{k=1}^{d_{j+1}} \sum_{n \in \mathcal{N}_k^{\mathrm{I}}} p_{k,n}^* = \sum_{k=1}^{d_{j+1}-1} h_k q_k^* + B_1. \tag{I.1}$$

Note that (I.1) is satisfied for $j = |\mathcal{D}|$; otherwise, the objective function in Problem (4.8) can be increased by increasing some $p_{K,n}$.

Next, we prove (I.1) for the case $1 \leq j \leq |\mathcal{D}| - 1$ by contradiction. The optimal solutions $\{q_k^*\}$ and $\{p_{k,n}^*\}$ satisfy the constraints (4.8a) and (4.8b). Assume $\{q_k^*\}$ and $\{p_{k,n}^*\}$ do not satisfy (I.1), i.e., $\Delta \triangleq \sum_{k=1}^{d_{j+1}-1} h_k q_k^* + B_1 - \sum_{k=1}^{d_{j+1}} \sum_{n \in \mathcal{N}_k^{\mathrm{I}}} p_{k,n}^* > 0$. From (4.10) and Proposition 4.5.2, we have

$$\Delta = h_{d_j} q_{d_j}^* - \sum_{k=d_j+1}^{d_{j+1}} \sum_{n \in \mathcal{N}_k^{\mathrm{I}}} p_{k,n}^*. \tag{I.2}$$

Now, we construct a power allocation strategy $\{\hat{q}_k\}$, $\{\hat{p}_{k,n}\}$ given by

$$\hat{q}_k = \begin{cases} q_{d_j}^* - \frac{\Delta}{h_{d_j}}, & k = d_j, \\ q_{d_{j+1}}^* + \frac{\Delta}{h_{d_j}}, & k = d_{j+1}, \\ q_k^*, & \text{otherwise.} \end{cases} \tag{I.3}$$

$$\hat{p}_{k,n} = \begin{cases} p_{k,n}^*, & k = 1, \ldots, d_{j+1}, n \in \mathcal{N}_k^{\mathrm{I}}, \\ p_{k,n}^* + \frac{(h_{d_{j+1}} - h_{d_j})\Delta}{h_{d_j}(K - d_{j+1})N}, & k = d_{j+1} + 1, \ldots, K, n \in \mathcal{N}_k^{\mathrm{I}}. \end{cases} \tag{I.4}$$

It can be verified that $\{\hat{q}_k\}$ and $\{\hat{p}_{k,n}\}$ satisfy the constraints (4.8a) and (4.8b). Since $\Delta > 0$ and $h_{d_{j+1}} > h_{d_j}$, the power allocation $\{\hat{q}_k\}$ and $\{\hat{p}_{k,n}\}$ achieve larger rate than $\{q_k^*\}$ and $\{p_{k,n}^*\}$, which contradicts the assumption that $\{q_k^*\}$ and $\{p_{k,n}^*\}$ are optimal for (4.8). Therefore, $\{q_k^*\}$ and $\{p_{k,n}^*\}$ satisfy (I.1). By induction,

$$\sum_{k=1}^{d_{l+1}} \sum_{n \in \mathcal{N}_k^{\mathrm{I}}} p_{k,n}^* = \sum_{k=1}^{d_{l+1}-1} h_k q_k^* + B_1, \quad l = j, \ldots, |\mathcal{D}|. \tag{I.5}$$

It follows from (I.5) that, for $l = j, \ldots, |\mathcal{D}|$,

$$\sum_{k \in \mathcal{D}_{l+1}} \sum_{n \in \mathcal{N}_k^{\mathrm{I}}} p_{k,n}^* = \sum_{k=d_l}^{d_{l+1}-1} h_k q_k^* = h_{d_l} q_{d_l}^* \tag{I.6}$$

which completes the proof of Proposition 4.5.3.

Appendix J

Proof of Lemma 4.5.1

For the case $1 \leq x \leq 2$, from (4.22), (4.23) is satisfied. For the case $2 < x \leq |\mathcal{D}|+1$, we first prove $q^*_{d_k} = 0$ for $1 \leq k \leq x-2$ by contradiction. Assume there exists $q^*_{d_j} > 0$ for $1 \leq j \leq x-2$. Define $\Delta \triangleq \min\limits_{i=j+1,\ldots,x-1} \left(\sum\limits_{k=1}^{i-1} h_{d_k} q_{d_k} + B_1 - \sum\limits_{k=1}^{d_i} \sum\limits_{n \in \mathcal{N}_k^{\mathrm{I}}} p_{k,n} \right)$. From (4.21), we have $\Delta > 0$. We construct a power allocation strategy $\{\hat{q}_k\}$ and $\{\hat{p}_{k,n}\}$ given by

$$\hat{q}_k = \begin{cases} q^*_{d_j} - \min\left(q^*_{d_j}, \frac{\Delta}{h_{d_j}}\right), & k = d_j, \\ q^*_{d_{x-1}} + \min\left(q^*_{d_j}, \frac{\Delta}{h_{d_j}}\right), & k = d_{x-1}, \\ q^*_k, & \text{otherwise.} \end{cases}$$

$$\hat{p}_{k,n} = \begin{cases} p^*_{k,n} + \frac{h_{d_{x-1}} - h_{d_j}}{N} \min\left(q^*_{d_j}, \frac{\Delta}{h_{d_j}}\right), & k = d_x, n \in \mathcal{N}_k^{\mathrm{I}}, \\ p^*_{k,n}, & \text{otherwise.} \end{cases}$$

It can be verified that $\{\hat{q}_k\}$ and $\{\hat{p}_{k,n}\}$ satisfy the constraints (4.8a) and (4.8b). Since $h_{d_{x-1}} > h_{d_j}$, $q^*_{d_j} > 0$, and $\Delta > 0$, the power allocation $\{\hat{q}_k\}$ and $\{\hat{p}_{k,n}\}$ achieve larger rate than $\{q^*_k\}$ and $\{p^*_{k,n}\}$, which contradicts the assumption that $\{q^*_k\}$ and $\{p^*_{k,n}\}$ are optimal for (4.8). Therefore, $q^*_{d_k} = 0$ for $1 \leq k \leq x-2$. Then (4.23) follows from (4.22). The proof of Lemma 4.5.1 then completes.

Appendix K

Proof of Lemma 4.5.2

Given $\{\Pi(k)\}$, we prove the equivalence between Problems (4.8) and (4.26). It is sufficient for us to prove that given optimal solution $\{q_{k,n}\}$, $\{p_{k,n}\}$ for Problem (4.8), $\{p'_{k,n}\}$ obtained by (4.25) is optimal for Problem (4.26); given optimal solution $\{p'_{k,n}\}$ for Problem (4.26), $\{q_k\}$, $\{p_{k,n}\}$ obtained by (4.27) and (4.25) is optimal for Problem (4.8). For convenience, the optimal value of Problems (4.8) and (4.26) are denoted by R^* and R', respectively.

Given optimal solution $\{q_{k,n}\}$, $\{p_{k,n}\}$ for Problem (4.8), then $\{q_{k,n}\}$, $\{p_{k,n}\}$ satisfy constraints (4.8a) and (4.8b). We obtain $\{p'_{k,n}\}$ by (4.25). Since $g_{k,n}p_{k,n} = g'_{k,n}p'_{k,n}$, the average rate achieved by $\{p'_{k,n}\}$ equals to R^*. Next, we prove that $\{p'_{k,n}\}$ is a feasible solution for Problem (4.26). From Lemma 4.5.1, (4.25), and (4.21), $\{p'_{k,n}\}$ satisfy constraints (4.26b) and (4.26c). From Proposition (4.22), and 4.5.3, $\{q_{k,n}\}$, $\{p_{k,n}\}$ satisfy

$$\sum_{k\in\mathcal{D}_{l+1}}\sum_{n\in\mathcal{N}_k^{\mathrm{I}}} p^*_{k,n} = h_{d_l}q^*_{d_l}, \quad l = x,\ldots,|\mathcal{D}|. \tag{K.1}$$

From Proposition 4.5.2, (4.23), and (4.25), it follows that

$$\sum_{k=1}^{K}\sum_{n\in\mathcal{N}_k^{\mathrm{I}}} p'_{k,n} \le \sum_{i=x-1}^{|\mathcal{D}|} q_{d_i} + \frac{B_1}{h_{d_{x-1}}} \le KQ + \frac{B_1}{h_{d_{x-1}}}. \tag{K.2}$$

It follows that $\{p'_{k,n}\}$ satisfy constraint (4.26a); thus, $\{p'_{k,n}\}$ is a feasible solution for Problem (4.8). Therefore, the average rate achieved by $\{p'_{k,n}\}$ is no larger than R'; i.e., $R^* \le R'$, where the equality holds if and only if $\{p'_{k,n}\}$ is optimal for Problem (4.26).

Appendix K. Proof of Lemma 4.5.2

Given optimal solution $\{p'_{k,n}\}$ for Problem (4.26), then $\{p'_{k,n}\}$ satisfy constraints (4.26a), (4.26b), and (4.26c). We obtain q_k and $p_{k,n}$ by (4.27) and (4.25). Since $g_{k,n}p_{k,n} = g'_{k,n}p'_{k,n}$, the average rate achieved by $\{q_k\}$, $\{p_{k,n}\}$ equals to R'. Next, we prove that $\{q_k\}$, $\{p_{k,n}\}$ is a feasible solution for Problem (4.8). From (4.26a) and (4.27), $\{q_k\}$ satisfy constraint (4.8a). From (4.25), (4.26b), and (4.27), $\{q_k\}$ and $\{p_{k,n}\}$ satisfy constraints (4.8a) and (4.8a). Therefore, $\{q_k\}$, $\{p_{k,n}\}$ is a feasible solution for Problem (4.8). It follows that the average rate achieved by $\{q_k\}$, $\{p_{k,n}\}$ is no larger than R^*; thus, $R' \leq R^*$, where the equality holds if and only if $\{q_k\}$, $\{p_{k,n}\}$ is optimal for Problem (4.8).

From $R^* \leq R'$ and $R' \leq R^*$, we have $R^* = R'$. Therefore, given optimal solution $\{q_{k,n}\}$, $\{p_{k,n}\}$ for Problem (4.8), $\{p'_{k,n}\}$ obtained by (4.25) is optimal for Problem (4.26); given optimal solution $\{p'_{k,n}\}$ for Problem (4.26), $\{q_k\}$, $\{p_{k,n}\}$ obtained by (4.27) and (4.25) is optimal for Problem (4.8). The proof of Lemma 4.5.2 completes.

Appendix L

Proof of Proposition 4.5.4

Problem (4.26) is a convex optimization problem, and thus can be optimally solved by applying the Lagrange duality method. The Lagrangian of Problem (4.26), denoted by $\mathcal{L}\left(\{p'_{k,n}\}, \lambda, \delta, \mu\right)$, is given by

$$\frac{1}{KN}\sum_{k=1}^{K}\sum_{n\in\mathcal{N}_k^{\mathrm{I}}}\log_2\left(1+\frac{g'_{k,n}p'_{k,n}}{\Gamma\sigma^2}\right)+\lambda\left(KQ+\frac{B_1}{h_{d_{x-1}}}-\sum_{k=1}^{K}\sum_{n\in\mathcal{N}_k^{\mathrm{I}}}p'_{k,n}\right)$$
$$+\delta\left(\frac{B_1}{h_{d_{x-1}}}-\sum_{k=1}^{d_{x-1}}\sum_{n\in\mathcal{N}_k^{\mathrm{I}}}p'_{k,n}\right)+\mu\left(\sum_{k=1}^{d_x}\sum_{n\in\mathcal{N}_k^{\mathrm{I}}}p'_{k,n}-\frac{B_1}{h_{d_{x-1}}}\right) \tag{L.1}$$

where $\lambda, \delta,$ and μ are the non-negative dual variables associated with the corresponding constraints in Problem (4.26). The necessary and sufficient conditions for $\{p'_{k,n}\}$ and λ, δ, μ to be both primal and dual optimal are given by the Karush-Kuhn-Tucker (KKT) optimality conditions: $\{p'_{k,n}\}$ satisfy all the constraints in Problem (4.26), and

$$\lambda\left(KQ+\frac{B_1}{h_{d_{x-1}}}-\sum_{k=1}^{K}\sum_{n\in\mathcal{N}_k^{\mathrm{I}}}p'_{k,n}\right)=0, \tag{L.2a}$$

$$\delta\left(\frac{B_1}{h_{d_{x-1}}}-\sum_{k=1}^{d_{x-1}}\sum_{n\in\mathcal{N}_k^{\mathrm{I}}}p'_{k,n}\right)=0, \tag{L.2b}$$

$$\mu\left(\sum_{k=1}^{d_x}\sum_{n\in\mathcal{N}_k^{\mathrm{I}}}p'_{k,n}-\frac{B_1}{h_{d_{x-1}}}\right)=0, \tag{L.2c}$$

$$\frac{\partial\mathcal{L}\left(\{p'_{k,n}\}, \lambda, \delta, \mu\right)}{\partial p'_{k,n}}=0. \tag{L.2d}$$

From (4.21) and Lemma 4.5.1, $\sum_{k=1}^{d_{x-1}} \sum_{n\in\mathcal{N}_k^{\mathrm{I}}} p_{k,n}^* < B_1$; therefore, the optimal $\{p'_{k,n}\}$ satisfies $\sum_{k=1}^{d_{x-1}} \sum_{n\in\mathcal{N}_k^{\mathrm{I}}} p'_{k,n} < B_1/h_{d_{x-1}}$. It follows that the optimal $\delta = 0$ by (L.2b). From (L.2d) and $\delta = 0$, the optimal $p'_{k,n}$ is given by

$$p'_{k,n} = \begin{cases} \left(\frac{1}{(\lambda-\mu)KN\ln 2} - \frac{\Gamma\sigma^2}{g'_{k,n}}\right)^+, & k = 1,\ldots,d_x, n \in \mathcal{N}_k^{\mathrm{I}}, \\ \left(\frac{1}{\lambda KN\ln 2} - \frac{\Gamma\sigma^2}{g'_{k,n}}\right)^+, & k = d_x+1,\ldots,K, n \in \mathcal{N}_k^{\mathrm{I}}. \end{cases} \tag{L.3}$$

If the optimal $\mu > 0$, from (L.2a) and (L.2c), we have $\sum_{k=1}^{d_x} \sum_{n\in\mathcal{N}_k^{\mathrm{I}}} p'_{k,n} = B_1/h_{d_{x-1}}$ and $\sum_{k=d_x+1}^{K} \sum_{n\in\mathcal{N}_k^{\mathrm{I}}} p'_{k,n} = KQ$. If the optimal $\mu = 0$, then

$$p'_{k,n} = \left(\frac{1}{\lambda KN\ln 2} - \frac{\Gamma\sigma^2}{g'_{k,n}}\right)^+, k \in \mathcal{K}, n \in \mathcal{N}_k^{\mathrm{I}} \tag{L.4}$$

where λ satisfies $\sum_{k=1}^{K} \sum_{n\in\mathcal{N}_k^{\mathrm{I}}} p'_{k,n} = KQ + B_1/h_{d_{x-1}}$ by (L.2a). Proposition 4.5.4 is thus proved.

Appendix M

Proof of Lemma 4.5.3

Consider Problem (4.6) with $\mathcal{N}_k^{\mathrm{E}} = \mathcal{N}_k^{\mathrm{I}} = \mathcal{N}', k \in \mathcal{K}$. Since $\mathcal{N}_k^{\mathrm{E}} = \mathcal{N}'$, from (4.7) and (4.30), $m(k) = \tilde{\Pi}(k), k \in \mathcal{K}$. By Proposition 4.5.1, we have $q_{k,n}^* = 0, n \neq \tilde{\Pi}(k), k \in \mathcal{K}$ for Problem (4.6) with $\mathcal{N}_k^{\mathrm{E}} = \mathcal{N}_k^{\mathrm{I}} = \mathcal{N}', k \in \mathcal{K}$. It follows that Problem (4.6) with $\mathcal{N}_k^{\mathrm{E}} = \mathcal{N}_k^{\mathrm{I}} = \mathcal{N}', k \in \mathcal{K}$ achieves same rate as Problem (4.8) with $\Pi(k) = \tilde{\Pi}(k), \mathcal{N}_k^{\mathrm{I}} = \mathcal{N}', k \in \mathcal{K}$. From Proposition 4.5.2, $q_k^* = 0, k \in \tilde{D}^{\mathrm{c}}$ for Problem (4.8) with $\Pi(k) = \tilde{\Pi}(k), \mathcal{N}_k^{\mathrm{I}} = \mathcal{N}', k \in \mathcal{K}$. It follows that Problem (4.8) with $\Pi(k) = \tilde{\Pi}(k), \mathcal{N}_k^{\mathrm{I}} = \mathcal{N}', k \in \mathcal{K}$ achieves same rate as Problem (4.8) with $\Pi(k)$ given in (4.31) and $\mathcal{N}_k^{\mathrm{I}} = \mathcal{N}', k \in \mathcal{K}$. Therefore, Problem (4.6) with $\mathcal{N}_k^{\mathrm{E}} = \mathcal{N}_k^{\mathrm{I}} = \mathcal{N}', k \in \mathcal{K}$ achieves same rate as Problem (4.8) with $\Pi(k)$ given in (4.31) and $\mathcal{N}_k^{\mathrm{I}} = \mathcal{N}', k \in \mathcal{K}$. This thus completes the proof of Lemma 4.5.3.

References

[1] N. Shinohara, "Power without wires," *IEEE Microwave Mag.*, vol. 12, no. 7, pp. 564–573, Dec. 2011.

[2] J. Murakami, F. Sato, T. Watanabe, H. Matsuki, S. Kikuchi, K. Harakawa, and T. Satoh, "Consideration on cordless power station-contactless power transmission system," *IEEE Trans. Mag.*, vol. 32, no. 5, pp. 5037–5039, Sep. 1996.

[3] A. Kurs, A. Karalis, R. Moffatt, J. D. Joannopoulos, P. Fisher, and M. Soljacic, "Wireless power transfer via strongly coupled magnetic resonances," *Science*, vol. 317, no. 83, pp. 83–86, July 2007.

[4] Powercast Documentation, Powercast Corporation. [Online]. Available: http://www.powercastco.com/power-calculator/.

[5] M. Stoopman, S. Keyrouz, H. J. Visser, K. Philips, and W. A. Serdijn, "Co-design of a CMOS rectifier and small loop antenna for highly sensitive RF energy harvesters," *IEEE Journal of Solid-State Circuits*, vol. 49, no. 3, pp. 622–634, Mar. 2014.

[6] L. R. Varshney, "Transporting information and energy simultaneously," in *Proc. IEEE Int. Symp. Inf. Theory (ISIT)*, July 2008.

[7] P. Grover and A. Sahai, "Shannon meets Tesla: wireless information and power transfer," in *Proc. IEEE Int. Symp. Inf. Theory (ISIT)*, June 2010.

[8] A. Goldsmith, *Wireless communications*. Cambridge university press, 2005.

[9] R. Zhang and C. K. Ho, "MIMO broadcasting for simultaneous wireless information and power transfer," *IEEE Trans. Wireless Commun.*, vol. 12, no. 5, pp. 1989–2001, June 2013.

[10] H. Ju and R. Zhang, "Throughput maximization in wireless powered communication networks," *IEEE Trans. Wireless Commun.*, vol. 13, no. 1, pp. 418–428, Jan. 2014.

[11] L. Liu, R. Zhang, and K. C. Chua, "Multi-antenna wireless powered communication with energy beamforming," *IEEE Trans. Commun.*, vol. 62, no. 12, pp. 4349–4361, Dec. 2014.

[12] T. Cover and J. Thomas, *Elements of information theory.* New York: Wiley, 1991.

[13] T. Paing, J. Shin, R. Zane, and Z. Popovic, "Resistor emulation approach to low-power RF energy harvesting," *IEEE Trans. Power Electronics*, vol. 23, no. 3, pp. 1494–1501, May 2008.

[14] J. A. G. Akkermans, M. C. van Beurden, G. J. N. Doodeman, and H. J. Visser, "Analytical models for low-power rectenna design," *IEEE Antennas Wireless Propag. Letters*, vol. 4, pp. 187–190, June 2005.

[15] Product Datasheet, P2110-915MHz RF Powerharvester Receiver, Powercast Corporation.

[16] Y. Wu, Y. Liu, Q. Xue, S. Li, and C. Yu, "Analytical design method of multiway dual-band planar power dividers with arbitrary power division," *IEEE Trans. Microwave Theory and Techniques*, vol. 58, no. 12, pp. 3832–3841, Dec. 2010.

[17] Product Datasheet, 11667A Power Splitter, Agilent Technologies.

[18] H. Urkowitz, "Energy detection of unknown deterministic signals," *Proc. IEEE*, vol. 55, pp. 523–231, Apr. 1967.

[19] I. Abou-Faycal and J. Fahs, "On the capacity of some deterministic non-linear channels subject to additive white Gaussian noise," in *Proc. IEEE Int. Conf. on Telecommunications (ICT)*, Apr. 2010.

[20] A. Lapidoth, S. M. Moser, and M. A. Wigger, "On the capacity of free-space optical intensity channels," *IEEE Trans. Inf. Theory*, vol. 55, no. 10, pp. 4449–4461, Oct. 2009.

[21] M. Katz and S. Shamai (Shitz), "On the capacity-achieving distribution of the discrete-time noncoherent and partially coherent AWGN channels," *IEEE Trans. Inf. Theory*, vol. 50, no. 10, pp. 2257–2270, Oct. 2004.

[22] A. Lapidoth, "On phase noise channels at high SNR," in *Proc. IEEE Inf. Theory Workshop (ITW)*, Oct. 2002.

[23] P. Carbone and D. Petri, "Noise sensitivity of the ADC histogram test," *IEEE Trans. Instrum. Meas.*, vol. 47, no. 4, pp. 1001–1004, Aug. 1998.

[24] S. Ruscak and L. Singer, "Using histogram techniques to measure A/D converter noise," *Analog Dialogue*, vol. 29, no. 2, 1995.

[25] M. Loy, "Understanding and enhancing sensitivity in receivers for wireless applications," Technical brief SWRA030, Texas Instruments [Online]. Available: http://www.ti.com/lit/an/swra030/swra030.pdf.

[26] L. Liu, R. Zhang, and K. C. Chua, "Wireless information transfer with opportunistic energy harvesting," *IEEE Trans. Wireless Commun.*, vol. 12, no. 1, pp. 288–300, Jan. 2013.

[27] ——, "Wireless information and power transfer: a dynamic power splitting approach," *IEEE Trans. Commun.*, vol. 61, no. 9, pp. 3990–4001, Sep. 2013.

[28] S. Timotheou, I. Krikidis, and B. Ottersten, "MISO interference channel with QoS and RF energy harvesting constraints," in *Proc. IEEE Int. Conf. on Commun. (ICC)*, June 2013.

[29] J. Park and B. Clerckx, "Joint wireless information and energy transfer in a two-user MIMO interference channel," *IEEE Trans. Wireless Commun.*, vol. 12, no. 8, pp. 4210–4221, Aug. 2013.

[30] C. Shen, W. Li, and T. Chang, "Wireless information and energy transfer in multi-antenna interference channel," *IEEE Trans. Signal Process.*, vol. 62, no. 23, pp. 6249–6264, Dec. 2014.

[31] A. A. Nasir, X. Zhou, S. Durrani, and R. A. Kennedy, "Relaying protocols for wireless energy harvesting and information processing," *IEEE Trans. Wireless Commun.*, vol. 12, no. 7, pp. 3622–3636, July 2013.

[32] Z. Ding, S. M. Perlaza, I. Esnaola, and H. V. Poor, "Power allocation strategies in energy harvesting wireless cooperative networks," *IEEE Trans. Wireless Commun.*, vol. 13, no. 2, pp. 846–860, Feb. 2014.

[33] Z. Ding, I. Krikidis, B. Sharif, and H. V. Poor, "Wireless information and power transfer in cooperative networks with spatially random relays," *IEEE Trans. Wireless Commun.*, vol. 13, no. 8, pp. 4440–4453, Aug. 2014.

[34] I. Krikidis, "Simultaneous information and energy transfer in large-scale networks with/without relaying," *IEEE Trans. Commun.*, vol. 62, no. 3, pp. 900–912, Mar. 2014.

[35] H. Chen, Y. Li, Y. Jiang, Y. Ma, and B. Vucetic, "Distributed power splitting for SWIPT in relay interference channels using game theory," *IEEE Trans. Wireless Commun.*, vol. 14, no. 1, pp. 410–420, Jan. 2015.

[36] L. Liu, R. Zhang, and K. C. Chua, "Secrecy wireless information and power transfer with MISO beamforming," *IEEE Trans. Signal Process.*, vol. 62, no. 7, pp. 1850–1863, Apr. 2014.

[37] D. W. K. Ng, E. S. Lo, and R. Schober, "Robust beamforming for secure communication in systems with wireless information and power transfer," *IEEE Trans. Wireless Commun.*, vol. 13, no. 8, pp. 4599–4615, Aug. 2014.

[38] Q. Shi, W. Xu, J. Wu, E. Song, and Y. Wang, "Secure beamforming for MIMO broadcasting with wireless information and power transfer," *IEEE Trans. Wireless Commun.*, vol. 14, no. 5, pp. 2841–2853, May 2015.

[39] K. Huang and E. G. Larsson, "Simultaneous information and power transfer for broadband wireless systems," *IEEE Trans. Signal Process.*, vol. 61, no. 23, pp. 5972–5986, Dec. 2013.

[40] D. W. K. Ng, E. S. Lo, and R. Schober, "Wireless information and power transfer: energy efficiency optimization in OFDMA systems," *IEEE Trans. Wireless Commun.*, vol. 12, no. 12, pp. 6352–6370, Dec. 2013.

[41] P. Richtarik and M. Takac, "Iteration complexity of randomized block-coordinate descent methods for minimizing a composite function," *Mathematical Programming, Series A*, Dec. 2012.

[42] S. Boyd, "Convex optimization II." [Online]. Available: http://www.stanford.edu/class/ee364b/lectures.html

[43] S. Boyd and L. Vandenberghe, *Convex Optimization.* Cambridge, U.K., Cambidge Univ. Press, 2004.

[44] K. Seong, M. Mohseni, and J. M. Cioffi, "Optimal resource allocation for OFDMA downlink systems," in *Proc. IEEE Int. Symp. Inf. Theory (ISIT)*, July 2006.

[45] W. Yu and R. Liu, "Dual methods for nonconvex spectrum optimization of multicarrier systems," *IEEE Trans. Commun.*, vol. 54, no. 7, pp. 1310–1322, July 2006.

[46] H. Ju and R. Zhang, "Optimal resource allocation in full-duplex wireless powered communication network," *IEEE Trans. Commun.*, vol. 62, no. 10, pp. 3528–3540, Oct. 2014.

[47] X. Kang, C. K. Ho, and S. Sun, "Full-duplex wireless powered communication network with energy causality," to appear in *IEEE Trans. Wireless Commun.* (Available online at arXiv:1404.0471).

[48] Q. Sun, G. Zhu, C. Shen, X. Li, and Z. Zhong, "Joint beamforming design and time allocation for wireless powered communication networks," *IEEE Commun. Letters*, vol. 18, no. 10, pp. 1783–1786, Oct. 2014.

[49] G. Yang, C. K. Ho, R. Zhang, and Y. L. Guan, "Throughput optimization for massive MIMO systems powered by wireless energy transfer," *IEEE J. Sel. Areas Commun.*, vol. 33, no. 8, pp. 1640–1650, Aug. 2015.

[50] H. Ju and R. Zhang, "User cooperation in wireless powered communication networks," in *Proc. IEEE Global Commun. Conf. (Globecom)*, Dec. 2014.

[51] H. Chen, Y. Li, J. L. Rebelatto, B. F. Uchoa-Filho, and B. Vucetic, "Harvest-then-cooperate: wireless-powered cooperative communications," *IEEE Trans. Signal Process.*, vol. 63, no. 7, pp. 1700–1711, Apr. 2015.

[52] R. Morsi, D. S. Michalopoulos, and R. Schober, "On-off transmission policy for wireless powered communication with energy storage," in *IEEE Asilomar Conference on Signals, Systems, and Computers*, Nov. 2014.

[53] K. Huang and V. K. N. Lau, "Enabling wireless power transfer in cellular networks: architecture, modeling and deployment," *IEEE Trans. Wireless Commun.*, vol. 13, no. 2, pp. 902–912, Feb. 2014.

[54] S. Lee, R. Zhang, and K. B. Huang, "Opportunistic wireless energy harvesting in cognitive radio networks," *IEEE Trans. Wireless Commun.*, vol. 12, no. 9, pp. 4788–4799, Sep. 2013.

[55] Y. Che, L. Duan, and R. Zhang, "Spatial throughput maximization of wireless powered communication networks," *IEEE J. Sel. Areas Commun.*, vol. 33, no. 8, pp. 1534–1548, Aug. 2015.

[56] C. K. Ho and R. Zhang, "Optimal energy allocation for wireless communications with energy harvesting constraints," *IEEE Trans. Signal Process.*, vol. 60, no. 9, pp. 4808–4818, Sep. 2012.

[57] O. Ozel, K. Tutuncuoglu, J. Yang, S. Ulukus, and A. Yener, "Transmission with energy harvesting nodes in fading wireless channels: optimal policies," *IEEE J. Sel. Areas Commun.*, vol. 29, no. 8, pp. 1732–1743, Sep. 2011.

[58] C. Huang, R. Zhang, and S. Cui, "Throughput maximization for the Gaussian relay channel with energy harvesting constraints," *IEEE J. Sel. Areas Commun.*, vol. 31, no. 8, pp. 1469–1479, Aug. 2013.

[59] D. Gunduz and B. Devillers, "Two-hop communication with energy harvesting," in *IEEE International Workshop on Computational Advances in Multi-Sensor Adaptive Processing (CAMSAP)*, Dec. 2011.

[60] B. Gurakan, O. Ozel, J. Yang, and S. Ulukus, "Energy cooperation in energy harvesting wireless communications," in *Proc. IEEE Int. Symp. Inf. Theory (ISIT)*, June 2012.

[61] ——, "Throughput maximization for energy harvesting two-hop networks," in *Proc. IEEE Int. Symp. Inf. Theory (ISIT)*, June 2013.

[62] M. Y. Naderi, K. R. Chowdhury, S. Basagni, W. Heinzelman, S. De, and S. Jana, "Experimental study of concurrent data and wireless energy transfer for sensor networks," in *Proc. IEEE Global Commun. Conf. (Globecom)*, Dec. 2014.

[63] T. S. Ferguson, "Who solved the secretary problem," *Statistical Science*, vol. 4, no. 3, pp. 282–296, Dec. 1989.

List of Publications

Journal Publications

1. X. Zhou, R. Zhang, and C. K. Ho, "Wireless information and power transfer: architecture design and rate-energy tradeoff," *IEEE Trans. Commun.*, vol. 61, no. 11, pp. 4754-4767, Nov. 2013.

2. X. Zhou, R. Zhang, and C. K. Ho, "Wireless information and power transfer in multiuser OFDM systems," *IEEE Trans. Wireless Commun.*, vol. 13, no. 4, pp. 2282-2294, Apr. 2014.

3. X. Zhou, C. K. Ho, and R. Zhang, "Wireless power meets energy harvesting: a joint energy allocation approach in OFDM-based system," submitted to *IEEE Trans. Wireless Commun.*.

Conference Publications

1. X. Zhou, R. Zhang, and C. K. Ho, "Wireless information and power transfer: architecture design and rate-energy tradeoff," in *Proc. IEEE Global Communications Conference (Globecom)*, Dec. 2012.

2. X. Zhou, R. Zhang, and C. K. Ho, "Wireless information and power transfer in multiuser OFDM systems," in *Proc. IEEE Global Communications Conference (Globecom)*, Dec. 2013.

3. X. Zhou, C. K. Ho, and R. Zhang, "Wireless power meets energy harvesting: a joint energy allocation approach," in *Proc. IEEE Global Conference on Signal and Information Processing (GlobalSIP)*, Dec. 2014.